

“Aerosol Thiol-ene Photopolymerization for the Synthesis of Nanostructures and their Biofunctionalization “

Zur Erlangung des akademischen Grades einer
DOKTORIN DER NATURWISSENSCHAFTEN (Dr. rer. nat)

von der KIT-Fakultät für Chemieingenieurwesen und Verfahrenstechnik des
Karlsruher Instituts für Technologie (KIT)

genehmigte

DISSERTATION

von

Narmin Suvarli, M.Sc.

aus Baku, Aserbaidshan

Tag der mündlichen Prüfung:

11.03.2022

Erstgutachter:

Prof. Dr. Jürgen Hubbuch

Zweitgutachter:

Prof. Dr. Michael Türk

Acknowledgements

Many people who supported me during the course of my doctoral dissertation deserve to be acknowledged as direct and indirect contributors to the success of my work.

First and foremost I would like to express my gratitude to my first and second reviewers Prof. Dr. Jürgen Hubbuch and Prof. Dr. Michael Türk for their contribution and effort in evaluating my thesis. I also thank the rest of the defense board, Prof. Matthias Franzreb and Prof. Hermann Nirschl for their participation.

To my project supervisors, Dr. Michael Wörner and Dr. Iris Perner-Nochta I send my gratitude for the work they put into my Ph.D. for the past three years, for supporting me throughout my project, for their contribution to my scientific career and for the care and kindness they showed towards me throughout my stay in Karlsruhe.

I would also like to thank all of the contributors (consortium, advisors, supervisors, fellows) of the “Photo-Emulsion” project, as well as the following funding source: Horizon 2020 Marie Skłodowska-Curie Actions “Towards Next-generation Eco-efficient PHOTO and EMULSION Polymerizations Imparting Synergy to Process, Products and Applications” (Grant Agreement ID: 765341).

As part of my project I collaborated with many institutions within and outside KIT. I would like to thank Prof. Dr. Christophe Serra for hosting me at Institute Charles Sadron at the University of Strasbourg and contributing to one of my papers. Also, I would like to thank Alexander Peschl for hosting me at PESCHL Ultraviolet GmbH and helping me to design and assemble the *Photo-Capsule*.

I express sincere gratitude to all of my colleagues at MAB, especially, David Grijalva, Polina Mednikova, Jan Müller and Dr. Sarah Gretzinger, who have helped me through the first months of my life in Germany and, subsequently, became close and dear friends of mine. Special thanks also go to all of my Profilfach students and my Master student Max Frentzel for doing his Master Thesis and HiWi under my supervision.

During my doctoral dissertation which was majorly influenced by the COVID-19 pandemic, I have received a lot of support from friends and family. I would like to thank my mother Shahla Suvorova and my father Nizam Suvorov, my brothers Parviz and Fariz and their wives Arzu and Nora for providing remote moral support throughout this enterprise. I especially thank my dearest friends Olga Kuzminskaya, Tatiana Kunsmann and Brahim Bessif for always being there when I needed them and helping me through the difficulties I faced while in Germany.

Finally, I would like to thank the dearest and closest friend Lukas Wenger, who co-authored one of my publications and assisted me through the years of my doctoral dissertation. His immense contribution to my life and work deserves more than just a thank you. I look forward to whatever future is holding for you and wish you all the best on your journey.

Ich versichere, dass die hier vorliegende Dissertation mit dem eingereichten und genehmigten Prüfungsexemplar der Doktorarbeit übereinstimmt.

Narmin Suvarli

20.03.2022

Table of Contents

Abstract.....	i
Zusammenfassung	vii
1. Introduction	14
1.1. Aerosol Photopolymerization	16
1.1.1. Concept	16
1.1.2. Polymer particles	17
1.1.3. Organic-inorganic spherical nanocomposites.....	18
1.2. Thiol-ene chemistry	19
1.2.1. Mechanism of thiol-ene photopolymerization	20
1.2.2. Thiol-ene miniemulsion photopolymerization for polymer nanomaterials synthesis.....	21
1.3. Hybrid nanoparticles.....	22
1.3.1. Properties and applications of hybrid nanomaterials.....	22
1.3.2. Polymer hybrid nanomaterials.....	22
1.4. Bioconjugation techniques	23
1.5. Immobilization of enzymes.....	25
1.6. Emulsion photopolymerization via microfluidic devices	27
2. Thesis outline	29
2.1. Research proposal.....	29
2.2. Comprehensive overview of publications.....	32
3. Thiol-functional polymer nanoparticles via aerosol photopolymerization	36
3.1. Introduction	36
3.2. Materials and methods	38
3.2.1. Chemicals	38
3.2.3. Experiments	40
3.2.4. Analysis methods	41
3.3. Results and Discussion	42
3.3.1. Polymer nanoparticles from aerosol thiol-ene photopolymerization	42
3.3.2. Ellman's test.....	44
3.3.3. Size distribution studies	45
3.4. Conclusion.....	46

4. Synthesis of spherical nanoparticle hybrids via aerosol thiol-ene photopoly-merization and their bioconjugation	49
4.1. Introduction	50
4.2. Experimental	51
4.2.1. Chemicals	51
4.2.2. Aerosol photopolymerization	52
4.2.3. Experimental methods.....	52
4.2.4. Analytical methods	55
4.3. Results and discussion	56
4.3.1. Silver@poly(thio-ether) nanoparticle hybrids	56
4.3.2. Nanoparticle binding sites	60
4.3.3. Bioconjugation of silver@poly(thio-ether) nanoparticle hybrids.....	60
5. Immobilization of β -galactosidase by encapsulation of enzyme-conjugated polymer nanoparticles inside hydrogel microparticles.....	65
5.1. Introduction	66
5.2. Materials and Methods.....	68
5.2.1. Chemicals	68
5.2.2. Experimental methods.....	68
5.2.3. Analysis methods	72
5.3. Results and Discussion	74
5.3.1. Conjugation of enzymes on the surface of polymer nanoparticles	74
5.3.2. Encapsulation of enzyme-conjugated nanoparticles inside the hydrogel microparticles ..	75
5.3.3. Storage studies.....	79
5.3.4. Further remarks	81
5.4. Conclusion.....	82
6. Aerosol photopolymerization reactor with LED light sources	85
6.1. Introduction	85
6.2. Materials and Methods.....	86
6.2.1. Photo-Capsule design.....	86
6.2.2. Materials	88
6.2.3. Chemicals	89
6.3. Results and Discussion	90
6.3.1. Technical characteristics	90
6.3.2. Experimental performance	92
6.4. Conclusion.....	93

7. Conclusion and outlook	95
Bibliography	98
Abbreviations	112
Appendix A. Supplementary data for Chapter 3	116
Appendix B. Supplementary data for chapter 4.	123

Abstract

The work presented in this thesis corresponds to the research of polymer particles produced employing aerosol photopolymerization process. Various types of highly pure and dry micro and nanoparticles can be obtained from aerosol photopolymerization: spherical polymer micro- and nanoparticles, porous nanoparticles, micro- and nanocapsules, organic-inorganic nanocomposites, etc. The produced materials may find applications in biosensors, biomedicine and nanotechnology. Aerosol photopolymerization is an integrated and continuous gas-phase process that does not require surfactants, use of heating and hazardous solvents. A typical aerosol photopolymerization setup consists of an aerosol generator and an irradiation device. The solution of monomers and a photoinitiator (altogether named spray solution) is placed inside the aerosol generator connected to the stream of pressurized nitrogen. The produced droplet aerosol is transferred to the irradiation device, where the photopolymerization reaction takes place converting the monomer droplets into solid polymer particles. The particles produced via aerosol photopolymerization are ready for further modifications. Nevertheless, the aerosol photopolymerization method has a few limitations: to produce nanoparticles of a specific size additional equipment must be introduced into the setup, the irradiation process is usually carried out with UV-fluorescence lamps which have a limited shelf life and are difficult to dispose of. In addition, the mechanism of the aerosol photopolymerization process requires fast polymerization kinetics and is not suitable for the polymerization of monomers with low propagation rates. The thiol-ene chemistry can be applied with the aerosol photopolymerization process to produce highly cross-linked spherical polymer nanoparticles with available thiol functional groups. Thiol-ene chemistry has gained attention over recent years because it is an easy, straightforward reaction that results in biocompatible materials. Thiol-ene “click” reaction is one of the well-known and often used bioconjugation methods. Thiol-ene photopolymerization is a rapid process uninhibited by oxygen exhibiting delayed gelation. Miniemulsion photopolymerization using thiol-ene monomers often results in submicrometer polymer particles comprising cross-linked or linear chains. A combination of aerosol photopolymerization and thiol-ene chemistry can be beneficial when thiol-functional polymer nanoparticles of sizes 30-700 nm are in demand. These nanoparticles can be modified to serve as biosensors, drug carriers and nanoimmobilization agents for enzymes. In this dissertation, the synthesis of polymer nanoparticles with reactive -SH groups on the surface is accomplished, and 1) this accomplishment is used to produce hybrid nanoparticles with silver and poly(thio-ether) components which can be functionalized with various biological molecules; 2) these polymer nanoparticles are used to immobilize β -galactosidase via affinity binding and, subsequently, encapsulate the enzyme-conjugated nanoparticles inside the hydrogel microparticles using microfluidic devices. A new aerosol photoreactor was designed and constructed to overcome some limitations of the setup used in this thesis (unpublished work).

Polymer nanoparticles produced via aerosol photopolymerization of various thiol-ene monomer combinations possess functional -SH groups, confirmed with Ellman's assay. Di-, tri- and tetrafunctional thiols were introduced into reactions with acrylates, allyl or vinyl ethers. All combinations (with appropriate organic solvents) result in homogeneous spray solutions. The polymerization of the atomized spray solutions leads to the formation of agglomerated and non-agglomerated polymer nanoparticles. The type of monomers influences the tendency of polymer nanoparticles to agglomerate after the aerosol photopolymerization process. To compare, all alkene monomers were introduced into an aerosol photopolymerization reaction (homopolymerization) individually. Allyl and vinyl ethers do not polymerize in the process of free-radical (aerosol photo)polymerization, acrylates do. The residence time of the aerosol in the photoreactor (28 seconds) is too short for the polymerization of allyl and vinyl ethers. However, allyl and vinyl ethers can produce spherical polymer nanoparticles employing aerosol photopolymerization when cationic chain-growth reaction (and not free radical initiation) is used. When thiol monomers are introduced as cross-linking agents in the reactions with the diallyl and divinyl ethers, the thiol-ene photopolymerization results in polymer nanoparticles. This work concluded that the photopolymerization of trifunctional alkenes and trifunctional thiols in the equal stoichiometry of functional groups results in polymer nanoparticles with the most desirable morphology (spherical, non-agglomerated polymer nanoparticles).

Various combinations (with 1:1 stoichiometry of functional groups (-SH and -C=C)) of thiols and alkenes were examined and a few combinations subsequently formed spherical poly(thio-ether) nanoparticles with a low tendency for agglomeration. As mentioned above, only acrylate monomers successfully formed polymer nanoparticles in absence of thiol monomers. The SEM analysis reveals that the combinations of trifunctional acrylate with trifunctional thiol and trifunctional acrylate with tetrafunctional thiol have resulted in non-agglomerated polymer nanoparticles. The nanoparticles produced from different thiols and difunctional acrylate were showing different levels of agglomeration on the SEM micrographs. In the case of acrylates thiol-ene (step-growth) polymerization is not the only reaction that takes place during the aerosol photopolymerization process. The homopolymerization (chain-growth) reaction of acrylates takes place at the same time and both reactions (step-growth + chain-growth) result in a so-called mixed-mode polymerization. The result of a mixed-mode polymerization with multifunctional monomers is the formation of highly cross-linked material.

Diallyl, triallyl and divinyl ethers did not result in any polymer product in the process of free radical aerosol photopolymerization. The combinations with thiol monomers of higher functionalities (3 or 4 SH groups) lead to the formation of polymer nanoparticles. It is proposed that these alkene monomers participate in a "pure" thiol-ene photopolymerization, where thiol acts as a cross-linker. The combinations of difunctional allyl and vinyl ethers with thiols resulted in agglomerated nanoparticles, in some cases, the agglomeration was so advanced that individual nanoparticles were not identifiable. In the case of a trifunctional allyl monomer combined with tri and tetrafunctional thiol monomers, no agglomeration of the produced nanoparticles was observed. Trifunctional thiols with trifunctional alkene monomers in an equal stoichiometry of functional

groups are the best tool in producing cross-linked and individual polymer nanoparticles. The nuclear magnetic resonance (NMR) and infrared spectroscopy (FTIR) revealed that the heteropolymers of trifunctional thiol and trifunctional acrylate monomers produce polymers with residual -SH groups and fully consumed double bonds, whereas the triacrylate homopolymers still possess unreacted double bonds.

The studies of the size distribution of produced polymer nanoparticles showed that increasing the solvent ratio (by weight, in relation to monomers) from 1:1 to 1:20 in the spray solution significantly narrows the size distribution and lowers the mean nanoparticle diameter. This showcases the possibility to obtain nanoparticles of narrower size by varying the solvent ratio of the spray solution. Ellman's test was used to evaluate the presence of reactive -SH groups within the polymer matrix of the nanoparticles. The polymer nanoparticles produced from triacrylate-trithiol and triacrylate-tetrathiol combinations showed the highest concentration of -SH groups after the colorimetric Ellman's assay. Very low concentration of -SH groups was observed for other thiol-ene combinations.

The acquired knowledge about suitable monomer combinations for aerosol thiol-ene photopolymerization (that can produce polymer nanoparticles with a high concentration of -SH groups) was applied to produce hybrid nanoparticles with silver nanospheres incorporated into poly(thio-ether) particles. The monomers (with the photoinitiator) were introduced into a stabilized dispersion of silver nanoparticles and atomized employing an aerosol photopolymerization setup used to produce polymer nanoparticles. The synthesized silver-poly(thiol-ether) nanoparticle hybrids were analyzed using transmission and scanning electron microscopy (TEM and SEM) and tested for the presence of -SH groups using Ellman's reaction. Subsequently, a bioconjugation method was developed in order to test the functionality of residual -SH groups. A two-step bioconjugation process was implemented: the first step was based on the conjugation of maleimide on the surface of polymer nanoparticles through -SH groups via a thiol-ene "click" reaction mechanism; the second step was based on high-affinity non-covalent binding of biotin by streptavidin. Nanoparticle hybrids were introduced into the reactions with fluorescence-labeled biomolecules and the fluorescence of conjugated polymer nanoparticles was observed via Fluorescence Microscopy and Fluorescence Spectroscopy. Various applications can be considered for the designed products, they can be modified to be used in biosensors and biomedicine. Properties of silver nanoparticles e. g., surface plasmon resonance, make them a desirable tool for cancer treatment and diagnostics.

The stabilization of silver nanoparticles was an essential step carried out before the aerosol photopolymerization process. Different stabilization techniques were applied in order to prevent the premature aggregation of the silver nanoparticles (mostly, taking place inside the spray solution during atomization) and different grades of silver nanoparticles were used (coated nanoparticles, nanoparticle ink). Without stabilizer silver nanoparticles usually appeared aggregated on TEM images of synthesized hybrids. Only silver nanoparticles that were coated with polyvinylpyrrolidone (PVP) (by the supplier) have resulted in low aggregation. α -Lipoic acid is one of the most suitable stabilizers for silver nanoparticles. Solution of α -lipoic acid (10 mM) has

demonstrated superb stabilization of silver nanoparticles in ink and resulted in the formation of silver-poly(thio-ether) nanoparticle hybrids with non-aggregated silver and non-agglomerated polymer particles.

The produced nanoparticle hybrids were examined for the presence of -SH groups applying Ellman's assay for quantitative analysis of sulfhydryl groups. Quantitative analysis was conducted to establish the mean concentration of -SH groups within the polymer matrix. The abundance of available -SH groups was fundamental to carry out thiol-maleimide bioconjugation. Bioconjugation to maleimide via thiol-ene "click" reactions is a widely used technique in many biological applications. Maleimide-fluorophore was introduced into the reaction with nanoparticle hybrids and the conjugated product was analyzed using Fluorescence spectroscopy and Fluorescence microscopy. A two-step bioconjugation of biotin-maleimide and streptavidin-fluorophore was carried out and the produced nanoparticles were analyzed for the presence of fluorescence. The TEM and Fluorescence analyses confirm the efficiency of the bioconjugation procedure which can be used to conjugate various biomolecules on the surface of polymer nanoparticles.

The produced thiol-functional polymer nanoparticles and the established working bioconjugation technique were combined into an approach to immobilize enzyme on the surface of the nanoparticles and then encapsulate the product inside hydrogel microparticles. The immobilization of enzymes is a prominent topic in biotechnology. Immobilization provides prolongation of the shelf life, reusability, and structural stability of the enzyme. Affinity binding provides excellent selectivity and high retention of enzyme activity. Thus, this method of immobilization was used with polymer nanoparticles produced from aerosol photopolymerization and a commercially available streptavidin- β -galactosidase. The established two-step bioconjugation technique was used to 1) bind biotin-maleimide onto the surface of polymer nanoparticles through accessible -SH groups, and, subsequently, 2) non-covalently bind streptavidin- β -galactosidase onto the biotin-functionalized polymer nanoparticles.

The motivation behind the encapsulation of nanoimmobilized enzyme inside the hydrogel microparticles was two-fold: enzyme is prone to retain its native confirmation in a hydrogel network, and microparticles are easier to reuse. Two types of hydrogel – poly(ethylene glycol)-diacrylate (PEG-DA) and acrylamide (with cross-linker) – were tested. An axisymmetric needle/tubing microfluidic device with a set of UV-LED spots was employed to produce microdroplets and polymerize them resulting in hydrogel microparticles.

The samples of hydrogel microparticles with enzyme were stored in a specialized buffer at different temperatures (22, 8 and -26 °C) for 1, 7 and 28 days. The encapsulation within acrylamide-based hydrogels resulted in particles with no relevant residual activity, whereas the PEG-DA microparticles preserved a residual activity of 25 % (compared to the free unconjugated enzyme of the same concentration). The photopolymerization process (during encapsulation) resulted in a significant reduction of activity which might have occurred due to the formation of free radicals from the photoinitiator exposed to UV irradiation. Storage studies show a slight decline in activity over time for the unbound enzyme (94 % after 28 days) at room temperature,

while the activity of the conjugated enzyme increased to 115 %. All tested samples were stable at 8 °C and lost most of their activity when stored in a frozen state at -26 °C. Freezing of the buffer can result in pH shift and subsequent lowering of enzyme activity. Encapsulating enzyme-conjugated nanoparticles inside hydrogel microparticles can enable the reusability, however, an improvement of the encapsulation technique is necessary to address the loss of enzymatic activity.

A part of this thesis was aimed at improving the aerosol photopolymerization setup by constructing a safe and low-maintenance photoreactor. A computer-aided design (CAD) software was used to design individual parts and run a simulation of assembling the reactor. To establish homogeneous irradiation conditions, the light has to be delivered to all sides of the reaction tube evenly. This specific requirement was the main idea behind the *Photo-Capsule*: a tube-in-tube setup with the light sources located in the circle around the reaction tube. To redirect the scattered light towards the reaction tube and for the safety of the experimenter, the *Photo-Capsule* has to be covered in aluminum foil.

In conclusion, the present thesis unfolds the potentials of the combination of aerosol photopolymerization with thiol-ene technology for the synthesis of polymer nanoparticles with thiol functionalities. This method motivated two coherent objectives of this work: production of biofunctionalized nanoparticle hybrids and nanoimmobilization of enzymes followed by encapsulation inside hydrogel microparticles. In addition, an improved aerosol photopolymerization reactor was designed and constructed to overcome the drawbacks of the current setup.

Zusammenfassung

Die in dieser Dissertation vorgestellten Arbeiten beschäftigen sich mit der Erforschung von Polymerpartikeln, die durch Aerosol-Photopolymerisation hergestellt werden. Durch Aerosol-Photopolymerisation können verschiedene Arten von hochreinen, trockenen Mikro- und Nanopartikeln gewonnen werden: kugelförmige Polymermikro- und -nanopartikeln, poröse Nanopartikeln, Mikro- und Nanokapseln, organisch-anorganische Nanokomposite usw. Die hergestellten Materialien können in der Biosensorik, Biomedizin und Nanotechnologie Anwendung finden. Die Aerosol-Photopolymerisation ist ein integrierter und kontinuierlicher Gasphasenprozess, der ohne Tenside, Erhitzung und gefährliche Lösungsmittel auskommt. Ein typischer Versuchsaufbau zur Durchführung einer Aerosol-Photopolymerisation besteht aus einem Aerosolgenerator und einer Lichtquelle zur Bestrahlung. Die Lösung aus Monomeren, organischem Lösungsmittel und einem Photoinitiator (insgesamt als Sprühhlösung bezeichnet) wird in den Aerosolgenerator vorgelegt, der mit Stickstoff aus Druckgasflaschen betrieben wird. Das erzeugte Tröpfchenaerosol wird in die Bestrahlungsvorrichtung geleitet, wo die Photopolymerisationsreaktion stattfindet und die Tröpfchen in feste Polymerpartikel umgewandelt werden. Die hergestellten Partikel sind trocken und für weitere Modifikationen geeignet. Die herkömmliche Aerosol-Photopolymerisation hat jedoch auch Nachteile: Zur Herstellung von Nanopartikeln einer bestimmten Größe müssten zusätzliche Geräte in die Anlage eingebaut werden und der Bestrahlungsprozess wird in der Regel mit UV-Fluoreszenzlampen durchgeführt, die eine begrenzte Haltbarkeit haben und schwer zu entsorgen sind. Darüber hinaus erfordert der Prozess der Aerosol-Photopolymerisation eine rasche Initiierung der radikalischen Reaktion und eine schnelle Polymerisationskinetik. Für die Polymerisation von Monomeren mit geringen Wachstumsraten ist der Prozess hingegen nicht geeignet. Die Thiol-Ene-Chemie kann mit einem Aerosol-Photopolymerisationsprozess angewendet werden, um hochvernetzte kugelförmige Polymer-Nanopartikel mit verfügbaren Thiol-funktionellen Gruppen herzustellen. Dieser Bereich der Chemie hat in den letzten Jahren an Aufmerksamkeit gewonnen, da es sich um eine einfache, unkomplizierte Reaktion handelt, mit der auch biokompatible Materialien erzeugt werden können. Die Thiol-Ene-“Click“-Reaktion ist eine bekannte und häufig verwendete Biokonjugationsmethode. Die Thiol-Ene-Photopolymerisation ist ein sehr schneller Prozess, der auch nicht durch Sauerstoff gehemmt wird. Die Miniemulsions-Photopolymerisation mit Thiol-Ene-Monomeren wird zur Synthese von Submikrometer-Polymerpartikeln (*Latex*) eingesetzt, die aus vernetzten oder linearen Ketten bestehen. Eine Kombination aus Aerosol-Photopolymerisation und Thiol-Ene-Chemie kann vorteilhaft sein, wenn Thiol-funktionelle Polymernanopartikeln der Größe 50-1000 nm gefragt sind. Diese Nanopartikeln können so modifiziert werden, dass sie als Biosensoren, Wirkstoffträger oder zur Nanoimmobilisierung von Enzymen Verwendung finden könnten.

In dieser Dissertation wurde die Synthese von Polymer-Nanopartikeln mit reaktiven -SH-Gruppen ausgearbeitet. Dabei wurde 1) eine methodische Grundlage geschaffen, um

Hybridnanopartikeln mit Silber- und Poly(thioether)-Komponenten herzustellen, die mit verschiedenen biologischen Molekülen funktionalisiert werden können. 2) wurden diese Polymernanopartikeln verwendet, um β -Galactosidase durch Affinitätsbindung zu immobilisieren und die Enzym-konjugierten Nanopartikel im Inneren von Hydrogel-Mikropartikeln mit Hilfe einer mikrofluidischen Methode zu verkapseln. Darüber hinaus wurde ein neuer Aerosol-Photopolymerisationsreaktor (*Photo-Capsule*) entworfen und konstruiert, um einige Nachteile des alten Aufbaus zu überwinden (unveröffentlichte Arbeit).

Polymernanopartikel, die durch Aerosol-Photopolymerisation verschiedener Kombinationen von Thiol-Ene-Monomeren hergestellt wurden, besitzen funktionelle -SH-Gruppen, was mit dem Test nach Ellman nachgewiesen wurde. Di-, tri- und tetrafunktionelle Thiole wurden in Reaktion mit Acrylaten, Allyl- oder Vinylethern gebracht. Alle Kombinationen (mit geeigneten Lösungsmitteln) führten zu homogenen Sprühlösungen. Die Polymerisation der zerstäubten Sprühlösungen führte zur Bildung von agglomerierten und auch nicht agglomerierten Polymernanopartikeln. Es wurde festgestellt, dass das Agglomerationsverhalten von der Art der gewählten Monomere und Monomerkombinationen abhängt. Zum Vergleich wurden alle Alkenmonomere einzeln in eine Aerosol-Photopolymerisationsprozess unterzogen (Homopolymerisation). Allyl- und Vinylether polymerisierten bei der radikalisch initiierten Aerosol-Photopolymerisation im Gegensatz zu Acrylaten nicht. Dies ist auf die kurze Verweilzeit des Aerosols im Photoreaktor (etwa 28 Sekunden) zurückzuführen. Allerdings können Allyl- und Vinylether zur Synthese von kugelförmigen Polymer-Nanopartikeln verwendet werden, wenn eine kationische Kettenwachstumsreaktion (und nicht die Initiierung durch freie Radikale) angewendet wird. Wenn Thiolmonomere in die Reaktionen mit den Allyl- und Vinylethern eingeführt werden, findet die Thiol-Ene-Photopolymerisation statt, was zu polymeren Produkten führen kann. Hierbei wurde festgestellt, dass die Photopolymerisation von trifunktionalen Alkenen und trifunktionalen Thiolen bei gleicher Stöchiometrie der funktionellen Gruppen zu Polymer-Nanopartikeln mit der angestrebten Morphologie führt (kugelförmige, nicht agglomerierte Polymer-Nanopartikel).

Es wurden verschiedene Kombinationen (mit einer 1:1-Stöchiometrie der funktionellen Gruppen (-SH und -C=C)) der Thiole und Alkene untersucht und einige Kombinationen bildeten anschließend sphärische Poly(thioether)nanopartikel mit geringer Tendenz zur Agglomeration. Wie bereits erwähnt, bildeten nur Acrylatmonomere erfolgreich Polymernanopartikel in Abwesenheit von Thiolmonomeren. Die Analyse mittels Rasterelektronenmikroskopie (REM) zeigte auf, dass die Kombinationen von trifunktionalem Acrylat mit trifunktionalem Thiol und trifunktionalem Acrylat mit tetrafunktionalem Thiol zu nicht-agglomerierten Polymer-Nanopartikeln geführt haben. Die aus verschiedenen Thiolen und difunktionellem Acrylat hergestellten Nanopartikel wiesen auf den REM-Aufnahmen unterschiedliche Agglomerationsgrade auf. Die Kombination von difunktionellem Acrylat mit tetrafunktionellem Thiol war die Einzige, die nicht-agglomerierte Polymernanopartikeln ergab. Bei der Verwendung von Acrylaten ist die Thiol-Ene-Polymerisation (Stufenwachstum) nicht die einzige Reaktion, die während des Aerosol-Photopolymerisationsprozesses stattfinden kann, sondern es kann auch zu einer Homopolymerisationsreaktion (Kettenwachstum) von Acrylaten kommen. Beim

gleichzeitigen Stattfinden beider Reaktionen spricht man von einer sogenannten Mixed-Mode-Polymerisation. Wie bereits in der Literatur beschrieben, findet eine Mixed-Mode-Polymerisation statt, wenn unter bestimmten Bedingungen sowohl Stufen- als auch Kettenwachstumsreaktionen ablaufen können. Das Ergebnis einer Mixed-Mode-Polymerisation mit multifunktionellen Monomeren ist die Bildung von stark vernetztem Material.

Allyl- und Vinylether führten bei der freien radikalischen Aerosol-Photopolymerisation zu keinem Polymerprodukt. Die Kombinationen mit Thiol führten zur Bildung von Polymer-Nanopartikeln. Es wird vermutet, dass diese Alkenmonomere an einer "reinen" Thiol-Ene-Photopolymerisation teilnehmen, wobei Thiolgruppen im Falle von difunktionellen Allylverbindungen und bei Verbindungen mit mindestens drei Thiolgruppen als Vernetzer wirken. Die Kombinationen von bifunktionellen Allyl- und Vinylethern mit Thiolen führten zu agglomerierten Nanopartikeln. In einigen Fällen war die Agglomeration so weit fortgeschritten, dass die einzelnen Nanopartikel nicht mehr identifizierbar waren. Bei der Kombination eines trifunktionellen Allylmonomers (TATT) mit einem tri- und tetrafunktionellen Thiolmonomer wurde keine Agglomeration der hergestellten Nanopartikel beobachtet. Trifunktionelle Thiole mit trifunktionellen Allylmonomeren in gleicher Stöchiometrie der funktionellen Gruppen sind am besten geeignet zur Herstellung von individuellen Polymernanopartikeln, die ein poly(thioether)-Netzwerk aufweisen. Die kernmagnetische Resonanz (NMR) und die Infrarotspektroskopie (FTIR) zeigten auf, dass die Heteropolymere aus trifunktionellen Thiolen und trifunktionellen Acrylatmonomeren Polymere mit nachweisbaren -SH-Gruppen und vollständig abreagierten Doppelbindungen ergeben, während die Triacrylat-Homopolymere noch nicht umgesetzte Doppelbindungen besitzen.

Die Untersuchungen zur Größenverteilung der hergestellten Polymernanopartikel zeigten, dass eine Erhöhung des Lösungsmittelverhältnisses (nach Gewicht, im Verhältnis zu den Monomeren) in der Sprühlösung von 1:1 auf 1:20 zu einer deutlich engeren und in Richtung kleinerer Partikel verschobenen Größenverteilung führte. Folglich ist es möglich, durch Variation des Lösungsmittelverhältnisses in der Sprühlösung Nanopartikel mit einer engeren Größenverteilung und geringerer Durchschnittsgröße zu erhalten. Mit Ellmans Reagenz wurde das Vorhandensein von reaktiven -SH-Gruppen in der Polymermatrix der Nanopartikel untersucht. Die aus Triacrylat-Trithiol- und Triacrylat-Tetrathiol-Kombinationen hergestellten Polymer-Nanopartikel zeigten nach dem kolorimetrischen Ellman-Assay die höchste Konzentration an -SH-Gruppen. Bei anderen Thiol-En-Kombinationen wurde eine sehr niedrige Konzentration von -SH-Gruppen beobachtet.

Das erworbene Wissen über geeignete Monomerkombinationen für die Aerosol-Thiol-Ene-Photopolymerisation wurde zur Herstellung von Hybrid-Nanopartikeln mit Silber- und Poly(thioether)-Komponenten eingesetzt. Eine stabilisierte Dispersion von Silbernanopartikeln wurde in eine Monomerlösung mit Photoinitiator eingebracht und in demselben Versuchsaufbau der Aerosol-Photopolymerisation prozessiert. Die synthetisierten Silber-Poly(thioether)nanopartikel-Hybride wurden anschließend mit Hilfe der Transmissions- und Rasterelektronenmikroskopie (TEM und REM) analysiert und mit Ellmans Reagenz auf das

Vorhandensein von -SH-Gruppen untersucht. Anschließend wurde eine Biokonjugationsmethode entwickelt, um die Funktionalität der -SH-Gruppen zu untersuchen. Es wurde ein zweistufiger Biokonjugationsprozess entwickelt: Der erste Schritt basiert auf der Konjugation von Maleimid-Derivaten auf der Oberfläche von Polymer-Nanopartikeln durch -SH-Gruppen über einen Thiol-Ene-"Click"-Reaktionsmechanismus; der zweite Schritt basiert auf der hochaffinen nicht-kovalenten Bindung von Biotin mit Streptavidin. Die Nanopartikel-Hybride wurden in die Reaktionen mit fluoreszenzmarkierten Biomolekülen eingebracht und die Ergebnisse dieser Reaktionen wurden mittels Fluoreszenzmikroskopie und Fluoreszenzspektroskopie analysiert. Für so hergestellte Konjugate kommen prinzipiell verschiedene Anwendungen in Frage, sie können so modifiziert werden, dass sie in Biosensoren und in der Biomedizin eingesetzt werden könnten. Die Eigenschaften von Silbernanopartikeln, z. B. die Oberflächenplasmonenresonanz, machen sie zu einem vielversprechenden Werkzeug für die Krebsbehandlung und -diagnostik.

Die Stabilisierung von Silber-Nanopartikeln war ein wesentlicher Schritt. Hierzu wurden verschiedene Stabilisierungstechniken angewandt, um die vorzeitige Aggregation der Silber-Nanopartikel zu verhindern (die meist in der Sprühh Lösung vor/während der Zerstäubung stattfand), und es wurden verschiedene Qualitäten von Silber-Nanopartikeln verwendet (beschichtete Nanopartikel, Nanopartikelintinen). Ohne den Zusatz eines Stabilisators erschienen die Silbernanopartikel auf den TEM-Bildern meist aggregiert. Nur Silbernanopartikel, die mit Polyvinylpyrrolidon (PVP) beschichtet waren (vom Lieferanten), führten zu einer deutlich geringen Aggregation. α -Liponsäure erwies sich als geeigneter Stabilisator für Silbernanopartikel-Tinten. Eine Lösung von α -Liponsäure (10 mM) zeigte eine hervorragende Stabilisierung von Silber-Nanopartikeln und führte zur Bildung von Silber-Poly(thioether)-Nanopartikel-Hybriden mit nicht aggregierten Silber-Nanopartikeln und nicht agglomerierten Polymerpartikeln.

Die hergestellten Nanopartikel-Hybride wurden nach dem gleichen Protokoll auf das Vorhandensein von -SH-Gruppen untersucht. Es wurde auch versucht, eine quantitative Analyse durchzuführen, um die durchschnittliche Konzentration von -SH-Gruppen in der Polymermatrix zu ermitteln. Das Vorhandensein von -SH-Gruppen war für die Durchführung der Thiol-Maleimid-Biokonjugation von grundlegender Bedeutung. Die kovalente Anknüpfung von Maleimid-Derivaten über Thiol-Ene-"Click"-Reaktionen ist eine weit verbreitete Technik in vielen biologischen Anwendungen. Maleimid-Fluorophor wurde mit Nanopartikel-Hybriden konjugiert und das konjugierte Produkt wurde mittels Fluoreszenzspektroskopie und Fluoreszenzmikroskopie analysiert. Nach der erfolgreichen Bestätigung der Verfügbarkeit von reaktiven -SH-Gruppen wurde eine zweistufige Biokonjugation von Biotin-Maleimid und Streptavidin-Fluorophor auf die gleiche Weise analysiert. Die Fluoreszenzmessungen bestätigen, dass die Biokonjugation ein effizientes Verfahren ist, mit dem sich prinzipiell verschiedene Biomoleküle an die Oberfläche von Polymer-Nanopartikeln konjugieren lassen.

Die hergestellten Thiol-funktionellen Polymer-Nanopartikel und die etablierte Biokonjugationstechnik wurden in einem Projekt zusammengeführt, bei dem ein Enzym auf der Oberfläche der Nanopartikel immobilisiert und das Produkt in Hydrogel-Mikropartikel eingekapselt wurde. Die Immobilisierung von Enzymen ist ein wichtiges Thema in der

Biotechnologie. Durch die Immobilisierung können die Haltbarkeit, die Wiederverwendbarkeit und die strukturelle Stabilität des Enzyms verlängert werden. Im Laufe der Jahre wurden verschiedene Immobilisierungstechniken eingeführt: Adsorption, Affinitätsbindung, kovalente Bindung, chemische Aggregation, Einschluss und Verkapselung. Diese Techniken beruhen auf chemischen (kovalente Bindung, chemische Aggregation) und physikalischen Wechselwirkungen (Verkapselung, Einschluss, Adsorption, Affinitätsbindung), wobei jede Methode ihre Vor- und Nachteile hat. Die Affinitätsbindung bietet eine ausgezeichnete Selektivität und eine hohe Retention der Enzymaktivität. Daher wurde diese Immobilisierungsmethode mit durch Aerosol-Photopolymerisation hergestellten Polymer-Nanopartikeln und einer handelsüblichen Streptavidin- β -Galactosidase angewendet. Die zuvor etablierte zweistufige Biokonjugationstechnik wurde verwendet, um 1) Biotin-Maleimid über zugängliche -SH-Gruppen an die Oberfläche von Polymer-Nanopartikeln zu binden und anschließend 2) Streptavidin- β -Galactosidase nicht-kovalent an die Biotin-funktionalisierten Polymernanopartikel zu binden.

Für die Verkapselung des nanoimmobilisierten Enzyms in Hydrogel-Mikropartikeln gab es zwei Gründe: Das Hydrogelnetzwerk kann durch eine stabilisierende Wirkung zum Erhalt der nativen Konformation des Enzyms beitragen und Mikropartikel können leicht abgetrennt und wiederverwendet werden. Zwei Arten von Hydrogelen – Poly(ethylenglycol)-diacrylat (PEG-DA) und Acrylamid – wurden zu diesem Zweck getestet. Ein achsensymmetrisches Mikrofluidiksystem, bestehend aus einer Kapillare innerhalb eines Schlauchs und einer Reihe von UV-LED-Spots, wurde verwendet, um Mikrotropfen zu erzeugen und diese zu polymerisieren, um auf diese Weise Hydrogel-Mikropartikel herzustellen.

Die Proben der Hydrogel-Mikropartikel mit Enzym wurden bei verschiedenen Temperaturen (22, 8 und -26 °C) für 1, 7 und 28 Tage in einem Phosphatpuffer gelagert. Die Ergebnisse der Lagerungsstudien zeigten, dass die Verkapselung in Acrylamid-Hydrogelen zu Partikeln ohne relevante Restaktivität des Enzyms führte, während die PEG-DA-Mikropartikel eine Restaktivität von 25 % aufwiesen. Der Photopolymerisationsprozess (während der Verkapselung) führte zu einer signifikanten Verringerung der Enzym-Aktivität, was möglicherweise auf die Bildung freier Radikale aus dem Photoinitiator bei UV-Bestrahlung zurückzuführen ist. Die Lagerungsstudien zeigten einen leichten Rückgang der Aktivität des ungebundenen Enzyms (94 % nach 28 Tagen) bei Raumtemperatur, während die Aktivität des konjugierten Enzyms auf 115 % anstieg. Alle getesteten Proben waren bei 8 °C stabil und verloren den größten Teil ihrer Aktivität, wenn sie in gefrorenem Zustand bei -26 °C gelagert wurden. Dies kann vermutlich auf die durch den verwendeten Phosphatpuffer verursachte pH-Verschiebung andere relevante Faktoren zurückgeführt werden. Die Verkapselung von Enzym-konjugierten Nanopartikeln in Hydrogel-Mikropartikeln ermöglicht prinzipiell eine einfachere Wiederverwendbarkeit, jedoch sollte vorerst das Verfahren optimiert werden, um eine höhere Enzymaktivität zu erreichen.

Ein Teil dieser Arbeit zielte darauf ab, den Versuchsaufbau der Aerosol-Photopolymerisation durch Konstruktion eines sicheren und wartungsarmen Photoreaktors zu verbessern. Eine CAD-Software wurde verwendet, um die einzelnen Teile zu entwerfen und eine

Simulation des Reaktorzusammenbaus durchzuführen. Um homogene Bestrahlungsbedingungen zu schaffen, sollte das Licht gleichmäßig zu allen Seiten des Reaktionsrohrs geleitet werden. Diese spezielle Anforderung war die Hauptidee zu einer sogenannten Photo-Capsule: ein Rohr-in-Rohr-Aufbau, bei dem die Lichtquellen im Kreis um das Reaktionsrohr angeordnet sind. Ein weiteres wichtiges Ziel war das einfache Auswechseln des Reaktionsrohrs, was wiederum zum Innendurchmesser der Photo-Capsule beitrug. Die Abmessungen der Photo-Capsule wurden so gewählt, dass sie die Anforderungen für die Aerosol-Photopolymerisation erfüllen. Die Länge des Reaktionsrohres wurde dabei so gewählt, dass Verweilzeiten zwischen 10 und 30 Sekunden realisierbar waren, die auf Grundlage von Erfahrungswerten für eine erfolgreiche Aerosol-Photopolymerisation als geeignet befunden wurden. Um das gestreute Licht auf das Reaktionsrohr zu lenken und zur Sicherheit des Experimentators muss die Fotokapsel mit Aluminiumfolie abgedeckt werden.

Zusammenfassend legt die vorliegende Arbeit die Möglichkeiten zur Kombination der Aerosol-Photopolymerisation mit der Thiol-Ene-Reaktionschemie dar. Diese Kombination diene zwei zusammenhängenden Zielen dieser Arbeit: der Herstellung von biofunktionalisierten Nanopartikel-Hybriden und der Nanoimmobilisierung von Enzymen mit anschließender Verkapselung in Hydrogel-Mikropartikeln. Darüber hinaus wurde ein verbesserter Aerosol-Photopolymerisationsreaktor entworfen und gebaut, um die Nachteile des zuvor eingesetzten Photoreaktors zu überwinden.

1. Introduction

Unique properties of polymer nanoparticles have a wide range of applications: electronics, photonics, sensors, medicine, biotechnology and environmental technology [1]. One of the largest areas of application of polymer nanoparticles is smart drug delivery, a technique that enhances the therapeutic effect of the drug allowing it to selectively accumulate in the diseased area, therefore minimizing the side effects [2, 3]. Chemotherapy is currently considered the most effective treatment for cancer [4], however, many side effects of this method leave the world of science in an urge to find advancements or alternatives. Anticancer drug delivery systems target one of the main issues of chemotherapeutics – selectivity [5]. Therapeutic drugs can be linked to the polymer backbone for controlled drug release specifically in the cancer tissue. For these purposes, polymers can be designed to be biocompatible, nonimmunogenic and biodegradable [6]. As an example, one of the most studied polymers in drug carriers is poly(l-glutamic acid); poly(l-glutamic acid)-drug conjugates possess more favorable pharmacokinetic properties than the individual drug. As a polymer they have multiple conjugation sites, as a polypeptide they are biodegradable and as a polyelectrolyte they can “solubilize” hydrophobic molecules in aqueous media [7]. Many polymer nanoparticle-drug conjugates have entered clinical trials and some are already used for the treatment of breast cancer [8].

Polymer nanoparticles can be designed as multifunctional therapeutic tools for not only targeting but also imaging and therapeutics. Organic-inorganic nanoparticle hybrids combine the functions of their two (or more) components into a single system that can, for example, be both imaging [9] and therapeutic [10] tools. Nanoparticle hybrids have demonstrated compatibility with magnetic resonance imaging (MRI), computed X-ray tomography (CT) and other medical diagnostics methods [9, 11], where they act as contrast agents and can be useful in detecting early stages of cancer growth. The therapeutic component of the hybrid nanoparticles often regulates the biodistribution of the materials to reduce the potential side effects to the healthy tissues [12]. One of the applications of nanomaterials in bioengineering is their implications in the immobilization of enzymes, because nanoparticles possess the necessary characteristics for ensuring effective enzyme loading, mass transfer resistance and specific surface area [13]. Nanoimmobilized enzymes show exceptional stability at different temperatures and pH [14].

Nanoparticles are defined by IUPAC as particles of any shape with dimensions in the 1-100 nm range, although the term “nano” is accepted for dimensions below 500 nm [15]. For continuous and controlled drug release applications, the nanoparticles must be smaller than 250 nm in order to avoid negative interactions with the reticulo-endothelial system (RES) in the bloodstream [16]. Polymer nanoparticles can be produced either from the preformed polymer or by polymerization of monomers [1]. When the nanoparticles are produced from preformed polymers, the need for certain organic solvents can cause issues with toxicity and the purification procedure might be in demand [17]. Polymerization procedure, however, presents higher efficacy

usually in a single reaction. A number of emulsion polymerization techniques that produce polymer nanoparticles of different sizes have been introduced through the years: conventional emulsion polymerization, miniemulsion and microemulsion polymerizations. In a miniemulsion polymerization process, a polymerization reaction takes place within emulsified droplets producing latex particles of nanometer size [18]. Often these droplets can only be formed when a high-energy emulsification process is employed: sonication, rotor-stator systems or high-pressure homogenizers [19]. To obtain dry nanoparticles, e.g., for future functionalization, the produced mixture must be purified after the miniemulsion polymerization to remove unreacted monomers and other components of the reaction (surfactants, costabilizers).

The aerosol photopolymerization technique has been introduced in the late 90s as a method to produce highly monodisperse polymer microparticles [20, 21]. This polymerization technique was later modified to produce various polymer particles in the nanometer range: nanospheres, nanocapsules, porous nanoparticles, nanocomposite particles and drug-loaded nanoparticles [22-24]. The aerosol photopolymerization process involves the atomization of liquid monomers and subsequent photopolymerization of the aerosol droplets. Monomers, photoinitiator and other appropriate compounds are atomized in an aerosol generation system forming nanoscale droplets. The droplets pass through the photoreactor, where the photopolymerization process takes place and polymer nanoparticles are formed. The size and shape of the produced nanoparticles can be toggled by changing the components in the initial monomer mixture [23]. Aerosol photopolymerization offers a number of advantages: it is a continuous process that does not require heating or the use of surfactants or hazardous solvents, and it produces dry nanoparticles of exceptional purity from cross-linked polymers. This method has a great potential to obtain biocompatible and biodegradable polymer nanostructures with possible applications in bioengineering, drug delivery and biomedicine. Moreover, aerosol photopolymerization can be used to synthesize polymer-based nanocomposites with inorganic nanoparticles [24].

Synthesis of polymer nanoparticles brings us only one step closer to systems that can be applied for biomedical applications. The polymer nanoparticles have to be functionalized with biomolecules using various bioconjugation techniques to be biocompatible with cell systems [25]. Functionalization of polymer nanoparticles is a challenge for many researchers worldwide because the drug molecules often lose their cell-binding properties during the conjugation process [26]. Functionalization of ligands (e.g., drug molecules) on the surface of polymer nanoparticles can be achieved through the interactions of the reactive groups on the surface of the nanocarrier and the ligand. There are many covalent coupling techniques: thiol-thiol interaction, maleimide-thiol interaction, the reaction between a primary amine and a carboxylic acid, etc. [27]. Maleimide-thiol interactions have been well studied for maleimide and its derivatives; it is one of many applications of thiol-ene chemistry [28].

1.1. Aerosol Photopolymerization

1.1.1. Concept

Aerosol photopolymerization is an integrated continuous process that takes place at room temperature under the stream of pressurized nitrogen. Many different versions of the process and equipment have been introduced through the years with different aerosol generators and irradiation sources. One of the most recently modeled systems [29] consists of two units: aerosol generation and photopolymerization. The aerosol generation unit often employs an aerosol generator that can produce droplets from liquid under the stream of pressurized nitrogen. This atomization process is usually carried out under the pressure of 1 bar or more. The droplet aerosol then passes inside the photoreactor unit where the polymerization process occurs, and polymer nanoparticles are produced. The stream of nitrogen carries the produced nanoparticles out of the reactor where they can be collected manually using different collection concepts (glass slides, filter membranes, solution). The schematic representation of the process is depicted in *Figure 1.1*.

To obtain particles in the nanometer range a collision-type atomizer with a two-component nozzle was employed. The photopolymerization reaction took place under irradiation of two UV-fluorescent lamp devices facing the reactor tube. The concept of this specific system was adapted by *Akgün et al.* [29] from a previous design of the reactor where a XeCl excimer irradiation source was employed [22].

A homogeneous solution of liquid monomers, organic solvent and dissolved photoinitiator is placed inside the aerosol generator. The spray solution is often set to be homogeneous to ensure continuous aerosol generation and to obtain nanoparticles of standard size and composition. Flow rate and residence time of the aerosol inside the photoreactor can be easily adjusted by varying the pressure of nitrogen. Depending on the type of the monomer, an appropriate polymerization mechanism has to be adapted. For example, spray solution of methyl methacrylate (MMA) and radical photoinitiator did not produce any polymer nanoparticles in the process of aerosol

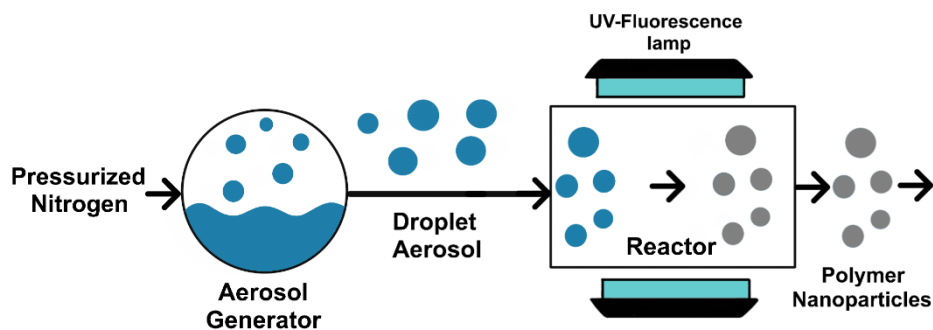


Figure 1. 1. Schematic representation of the aerosol photopolymerization process. Arrows follow the stream of nitrogen.

photopolymerization [22], due to low residence time inside the reactor of about half a minute. The presence of a cross-linker or a comonomer is required for the process to speed up. Polymerization of vinyl ethers conducted in presence of a cationic initiator and a cross-linker produced spherical polymer nanoparticles [29].

Although the system is versatile and can offer many possibilities of producing different polymer nanostructures, several limitations of the technique have to be addressed. The photoreactor utilizes UV-fluorescence lamps, which contain mercury vapor and are potentially dangerous to utilize and difficult to dispose of. A large portion of the irradiated light is scattered in the surroundings of the system, which requires the use of UV-protection equipment. Another limitation of the system is the relatively large particle size distribution: 50-500 nm [22], which can be toggled by introducing additional devices into the system, e.g. a differential mobility analyzer that can classify the aerosol particles by size [30].

1.1.2. *Polymer particles*

The illustration of the different kinds of polymer nanoparticles that can be obtained by aerosol photopolymerization is shown in **Figure 1. 2**. Highly monodisperse spherical microscale polymer particles (5-100 μm) were produced from multiacrylate monomers via aerosol photopolymerization [20, 31]. The diameter of the polymer particles can be predetermined by adjusting the diameter of the aerosol droplets (depending on the system's parameters). The produced particles are highly pure without surfactants, nevertheless, multicomponent polymer structures can be produced. Photopolymerization reaction of multifunctional monomers usually results in cross-linked macromolecules but the use of a photoinitiator is necessary to start the polymerization process. Raman spectroscopy was applied continuously to observe the polymerization of the monomer droplets and the change in the composition of the droplets was evaluated on-line and *in situ* [32], and the changes in size and mass of the dynamic particles were measured [33]. The changes in the size of the monomer droplets during the photopolymerization process depend on shrinkage, which occurs due to an increase in density from the conversion of double bonds to single bonds [20]. Polymer microcapsules can also be produced using aerosol photopolymerization by introducing a hydrophilic component into the monomer solution [34].

Nanoscale polymer particles were produced from aerosol photopolymerization by modifying the system introduced by *Essen* and *Schweiger* [20], specifically changing the aerosol generation unit from a vibrating-orifice generator to a collision-type generator [22]. This modification was aimed to increase the droplet generation rate and, subsequently, produce a higher concentration of polymer nanoparticles. When a highly reactive butyl acrylate (BA) was chosen as the monomer, cross-linker was unnecessary and spherical submicron polymer particles free of additives were produced. On-line scanning mobility particles sizer was employed to measure and compare the droplet and the particle size distributions. Aerosol photopolymerization permits a 1-to-1 copy of the monomer droplets to polymer particles [22].

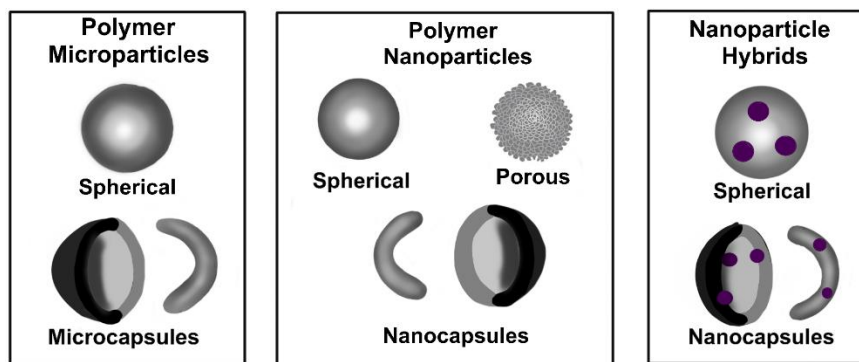


Figure 1. 2. Polymer materials that can be synthesized via different aerosol photopolymerization techniques.

Other polymer nanostructures can also be produced using aerosol photopolymerization technology [23, 35]. Non-spherical capsules and porous polymer nanoparticles can be produced, when additional compounds are introduced into the monomer solution. The addition of glycerol and a volatile solvent to the monomer solution results in polymer nanocaps named according to their shape (**Figure 1. 2.**). The mechanism of the synthesis of these types of structures was proposed. The atomized droplets are spherical and contain all components of the solution, during the photoreactor passage, the volatile solvent is evaporated leading to oversaturation of glycerol (subsequently, delayed gelation) and phase separation (due to the polymer formation). Softening agent glycerol leads to the controlled collapse of the preformed polymer shell before the gelation during the photopolymerization. When glycerol was extracted from polymer nanocaps, their unique shape remained. A volatile solvent in combination with a softening agent is necessary to produce nanocaps, its absence leads to regular spherical polymer nanoparticles [23]. The release of biomolecules/drugs (*e.g.*, caffeine) from these types of particles was also studied, and results show slower release of caffeine in particles with higher amounts of cross-linker. In addition, spherical nanoparticles show a faster release of caffeine, compared to nanocaps.

Porous or cauliflower-like polymer nanoparticles (**Figure 1. 2.**) can also be produced, when a non-volatile solvent is introduced into the mixture of monomers and the photoinitiator. *Akgün et al.* used 2-ethylhexanol (or hexadecane) as a porogen, which forms a homogeneous solution with the monomer and photoinitiator [23]. However, a later developed mixture containing only monomers photoinitiator and ethanol resulted in the formation of cauliflower-like polymer particles [35]. They produced amphiphilic copolymer (from the combination of hydrophilic and hydrophobic monomers) porous nanoparticles of different sizes.

1.1.3. Organic-inorganic spherical nanocomposites

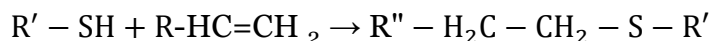
The aerosol photopolymerization technique allows the production of organic-inorganic polymer matrix nanocomposites (PMNC) (**Figure 1. 2.**) by introducing un-agglomerated inorganic nanoparticles into the monomer solution [23, 24, 36, 37]. The previously described methods to produce nanocaps were used to produce ZnO-loaded polymer nanocaps. ZnO nanoparticles were

incorporated into the monomer formulation and sprayed in an aerosol generator, produced nanocaps were analyzed via transmission electron microscopy to observe the encapsulated ZnO nanoparticles [23]. Subsequently, spherical polymer nanoparticles were produced with incorporated ZnO and Fe₂O₃ nanoparticles [24]. In these systems, the content of inorganic nanoparticles can be varied up to 40 wt.% in regard to the entire system. Nevertheless, the concentration of ZnO must be selected carefully to maintain the low viscosity of the monomer solution for successful atomization. The use of ZnO nanoparticles always has to be supported by stabilization, to avoid aggregation of the ZnO nanoparticles with each other. Infrared spectroscopy results reveal no residual monomers in the PMNC obtained via aerosol photopolymerization, suggesting all monomers were consumed during the reaction.

Submicrometer carbon nitride-based polymer composites were also produced via aerosol photopolymerization [37]. Initially prepared mesoporous carbon nitride nanoparticles act as both photoinitiators and fillers. Aerosol photopolymerization offers a considerable advantage over conventional methods of preparation of carbon nitride-based polymer nanocomposites (solution blending). The most recent work focused on coating de-agglomerated TiO₂ polymer nanoparticles with a thin PMMA-like film employing aerosol photopolymerization with a jet-impactor-assisted fluidized bed [36].

1.2. Thiol-ene chemistry

Thiol-ene reactions are often referred to as thiol-ene “click” reactions due to the resulting carbon-sulfur bond, which is present in many drug molecule conjugates, and the speed of the reaction. The process was first reported in the early years of the 20th century [38] but dates further back to the discovery of the vulcanization of rubber [39]. Thiol-ene chemistry was extensively used in the past as a method to produce cross-linked networks, which showed remarkable properties for their time [40]. Thiol-ene technology has made a comeback over the past decades due to its many benefits for polymer synthesis: high efficiency, orthogonality, known and well-studied chemistry, tolerance to many reaction conditions, etc. Polymer networks produced from thiol-ene monomers have more regular structures compared to polymers obtained from the polymerization of acrylate monomers [41]. Thiol-ene chemistry is also famous for being a great functionalization mechanism [42] [43]. A simplified mechanism of the reaction between thiol and alkene can be predicted as follows:



The reaction is initiated via thiol-ene free radical addition or thiol-Michael addition. In free radical thiol-ene reactions, a chain process takes place with initiation, propagation, and termination steps. In an initiation process, the thiol is exposed to the initiator, followed by the formation of the thiyl radical function. In a propagation step, the formed radical “adds” to the double bond of the alkene and forms an intermediate product with radical centered on one of the two carbons of the

double bond. Chain transfer proceeds with the transfer of radical function onto another thiol generating a new thiyl radical. The termination step takes place during the coupling of two radicals. Thiol-ene (photo)polymerization processes usually proceed through a step-growth reaction mechanism [38, 44]. In thiol-Michael addition reactions, thiols act as nucleophiles that react with electron-deficient enes. Thiol-Michael additions can be utilized for a variety of applications when appropriate catalyzer, monomers and solvents are used. Well-known applications involve thiol-maleimide reactions in biochemistry, thiol-polymer reactions, tissue engineering and polymerization [45].

Among many advantages of using thiol-ene reactions most notable are: availability of the compounds, only a small concentration of benign catalysts required, rapid reaction rates, insensitivity to oxygen, quantitative yields, no requirements for purification [46]. Thiol-ene reactions are often used in peptide and protein science as post-translational modification agents that produce homogeneously modified peptides and proteins [47]. Arrangement of complex molecular structures can be achieved using thiyl radicals in intramolecular cyclization [48]. Thiol-ene click reactions are also used in a variety of bioconjugation techniques [49, 50]. One of the major applications of free radical thiol-ene addition reactions is polymerization and, more specifically, photopolymerization [46, 51].

Despite its numerous advantages and wide range of applications, thiol-ene reactions present a major issue due to the utilization of thiols that possess a distinctive sulfur odor. Researchers worldwide face difficulties in working with some volatile thiol compounds [45].

1.2.1. Mechanism of thiol-ene photopolymerization

Thiol-ene photopolymerization offers a number of desirable features absent in the polymerization of acrylic monomers: oxygen inert, rapid polymerization with little or no added photoinitiator, synthesis of a variety of linear and cross-linked polymer networks, spatial and temporal control of the reaction [46, 51]. As studied by *Cramer et al*, the thiol-ene photopolymerization process proceeds via a step-growth mechanism depicted in **Figure 1.3**. [52]. During thiol-ene photopolymerization of stoichiometric quantities of thiols and acrylates, only

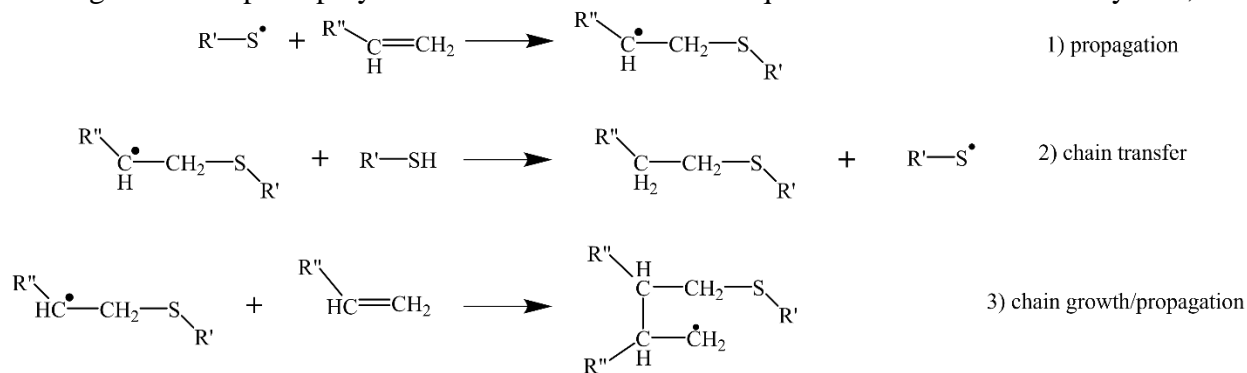


Figure 1.3. Mechanism of the thiol-ene photopolymerization reaction (initiation and termination steps are not depicted).

50% of thiol monomer was consumed, whereas almost no residual acrylate monomers remained in the system. The homopolymerization of acrylates and the heteropolymerization of thiols and acrylates are two reactions that are somewhat competing, resulting in lower consumption of the thiol. In theory, as soon as the thiyl radical propagates through -C=C- bond (1), the new thio-alkyl radical can either transfer the radical onto another thiol (2) or propagate through acrylate in a chain-growth step (3) (**Figure 1.3.**). The pathway of the thio-alkyl radical is usually defined by the nature of the alkene monomer: the chain transfer pathway is a result of the prevalence of the heteropolymerization of thiol and alkene monomers, and the chain growth pathway is a result of the prevalence of the homopolymerization of alkene monomer. In thiol-acrylate reactions, for example, with 1,6-hexanediacylate, the kinetic constant of the chain growth step is higher than the constant of the chain transfer step, due to the prevalence of the acrylate homopolymerization [52]. The changes in rates of a specific functional group, e.g. thiols, solely depend on the function of the kinetic constants of the chain transfer and chain-growth steps and are independent of the concentration of the secondary functional group, e.g. alkenes [51]. This phenomenon is also observed for allyl ethers: highest ratio of propagation to chain transfer kinetics with the first order in thiol functional group concentration. Norbornene and vinyl ether systems have roughly equivalent ratios resulting in half order of both thiol and ene functional groups. The ratio of propagation to chain transfer kinetics is below 1 in vinyl silyl systems and the polymerization rate is first order in the concentration of ene functional groups [53].

Linear polymer chains can be obtained via thiol-ene photopolymerization using difunctional alkene and thiol monomers when the possibility of homopolymerization is low. Higher functionalities lead to cross-linked polymers. For a number of thiol-ene monomers, kinetic constants of propagation and chain transfer reactions are high ensuring a fast process. A great variety of polymer structures, for example, polysulfide nanoparticles, films and coatings, can be produced [54-56].

1.2.2. Thiol-ene miniemulsion photopolymerization for polymer nanomaterials synthesis

Polymerization of thiol-ene miniemulsions produces linear and cross-linked polymer micro and nanoparticles of a variety of shapes and sizes [57-59]. First reports of thiol-ene miniemulsion photopolymerization for the synthesis of latex nanoparticles triggered many following investigations due to many advantages of the method: applications of continuous flow reactors (instead of batch reactors), chain characterization for linear polymerization defining the chemical and physical properties of the polymer [54]. Cross-linked thiol-ene latexes with narrow particle size distribution were obtained from a semi-batch emulsion copolymerization of trifunctional allyl and tetrafunctional thiol monomers [59]. The compounds used in miniemulsion photopolymerization, i.e. surfactant and initiator, affect the size of the produced polymer nanoparticles. The increase of the surfactant concentration leads to the formation of nanoparticles of smaller sizes. A similar trend was observed for the variation of initiator concentrations. The

linear polymers obtained using thiol-ene emulsion polymerization had relatively low molecular weights [59].

Thiol-Michael addition miniemulsion polymerizations were investigated to produce functional nanoparticles and latex materials. When the stoichiometry of the thiol-ene monomer concentrations was shifted favoring thiols, alkene monomer was fully consumed and excess of unreacted thiol groups within the latex films was detected. The excess of ene monomer concentration produces latex films with unreacted double bonds [60]. These films have demonstrated substantial properties as lithographic impression materials, shape memory polymers and optical materials [61].

1.3. Hybrid nanoparticles

1.3.1. Properties and applications of hybrid nanomaterials

The synthesis of multifunctional materials with tailored physicochemical properties is of great interest for many different fields of research. These hybrid nanomaterials contain two or more components, each with its own properties, can offer a variety of attractive features: high thermal stability, mechanical strength, light emission, electron conductivity, biocompatibility, etc. [62]. Hybrid nanomaterials where various types of nanoparticles (gold, silver, zinc oxide, titanium oxide, magnetic iron oxide) are introduced into the graphene sheets or coated with graphene have found applications in biosensors [63]. Silica-based hybrid nanomaterials, for example, mesoporous silica nanoparticles, have tunable pore sizes and large pore volumes allowing the therapeutics to be incorporated inside or grafted onto the outer surface for biomedical applications, such as cysteine delivery to cells [64]. Nanoscale metal-organic frameworks, or coordination polymers, are materials containing transition metal ions and polydentate bridging ligands. The metal-organic frameworks containing gadolinium have found applications in magnetic resonance imaging and computer tomography, where they enhance the image contrast leading to more precise detection of diseased cells [65].

1.3.2. Polymer hybrid nanomaterials

The method of synthesis of hybrid nanomaterials depends on the nature of the targeted components. Polymer nanocomposites usually refer to systems where polymers are considered the support materials and inorganic nanomaterials (size below 100 nm) are fillers [66]. A great variety of materials with specific properties can be produced, thus, there is always demand to conduct research aimed at understanding the physical and chemical properties and new synthesis pathways

of the polymer nanocomposite [67]. The first practically used polymer nanocomposites (nylon 6 clay hybrid) were introduced in 1990 by *Usuki* and his colleagues [68]. They synthesized the nanocomposites by incorporating monomers in between the clay silicate layers, followed by polymerization. In fact, most of the synthesis methods of polymer nanocomposites consider polymerization procedures in order to obtain materials of a specific shape, size and morphology, and to incorporate the fillers [69-72].

Silver and gold nanoparticles possess a great potential for applications in cancer treatment and diagnostics [73]. The insufficient selectivity of current cancer therapies calls for less harmful alternatives. Coated or conjugated gold and silver nanoparticles in combination with various drug molecules have been investigated for selective cancer therapy applications. Size, charge, shape, optical and electrical properties, multifunctionality (and, more importantly, well-studied properties and behavior) of gold and silver nanoparticles are contributing factors to their extensive use in modern cancer research. Unique properties of gold nanoparticles have been investigated in *in vitro* assays, *in vitro* and *in vivo* imaging, cancer therapy and drug delivery [74]. Many gold nanoparticle therapeutics have already reached the level of clinical trials [75] and some are already on the market [76]. However, the remaining issues with *in vivo* toxicity and difficulties reaching complex tumor tissue require more studies to be carried out before gold nanoparticles can be effectively introduced as cancer treatment systems [77]. Gold nanorod polymer nanocomposites were fabricated by *Chen* and colleagues [78] and a clinical anticancer drug was loaded into the nanocomposite through electrostatic interactions. These systems exhibit minimal cytotoxicity and high biocompatibility in cells, showing promising potentials of the nanocomposites for cancer therapy.

Similar to gold nanoparticles, silver nanoparticles possess exceptional optical properties that were already applied in cancer diagnostics and treatment studies [79, 80]. Silver nanoparticles also show cytotoxic and genotoxic behavior when introduced into living cells [81]. Silver polymer nanocomposites can be designed to eliminate this issue in various possible medicinal applications. Recently produced silver nanoparticles/polymer nanocomposites were intended to be used in electronics, due to their electromagnetic interference shielding [82, 83]. Different polymer stabilizers have been shown to reduce the cytotoxicity of silver nanoparticles [84].

1.4. Bioconjugation techniques

The term bioconjugation usually refers to the process of attachment of a biomolecule to another (synthetic compound or material), typically through a covalent bond. The produced complex exhibits the combined properties of both constituents and can, therefore, find a broader range of applications than each constituent individually. Some of the commonly used bioconjugates include fluorescent-labeled molecules, antibody-enzyme and antibody-drug conjugates, affinity ligands on particles. There are a few routine reactions used in bioconjugation

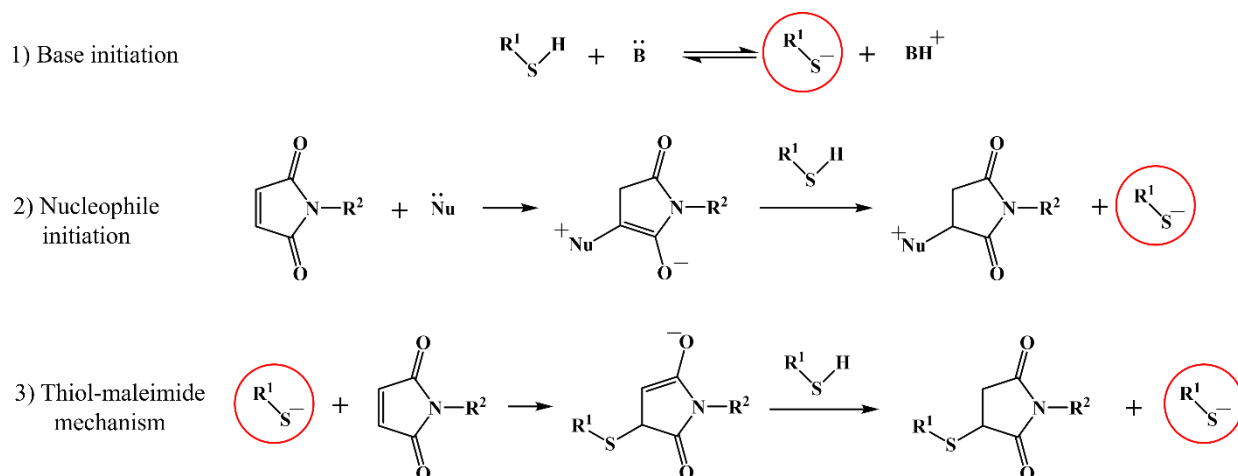


Figure 1. 4. Initiation of a thiolate-anion through 1) base and 2) nucleophile. The mechanism of thiol-maleimide reaction with thiolate-anion initiator (3).

chemistry that usually include either of the following functionalities: amine, thiol, carboxylate, hydroxylate, aldehyde, ketone, etc. [85].

Thiol-based bioconjugation reactions are dominated by thiol-ene reactions, which are commonly initiated by radicals [50]. Alternative thiol-based bioconjugation pathways, such as Michael addition and enzymatic synthesis are also used [86, 87], but are very rare in bioconjugation chemistry. Polymer-protein, polymer-siRNA conjugates are among many bioconjugates that are produced using radically initiated thiol-ene reaction [88-90]. Although thiol-ene reactions usually require the presence of radicals or catalyzers, thiol-maleimide reactions can often proceed at room temperature without any additives [50], and are recognized as one of the most efficient Michael-type additions [91].

The mechanism of the thiol-maleimide reaction is presented in **Figure 1. 4**. The reaction between thiol and maleimide proceeds with the generation of thiolate anion either from a base (1) or a nucleophile (2) [92]. The thiolate anion then reacts with the π -bond of the maleimide forming an intermediate thiol-maleimide anion which deprotonates another thiol, forming a new thiolate anion and a thiol-maleimide conjugate. The kinetics of the thiol-maleimide reaction depend on the specific combination of base/nucleophile, Michael acceptor and thiol [93]. Thiol-maleimide reactions can also be carried out in presence of a radical (photo)initiator, however, these reactions are slower than nucleophile and base-initiated processes [91]. Radically initiated thiol-ene reactions usually favor electron-rich alkenes [46].

Thiol-maleimide reaction was applied to functionalize polymer materials, such as poly(lactic acid) to avoid the degradation of polymer backbone [94]. Functionalization of polymer nanoparticles with peptides by using maleimide conjugation to thiols resulted in high conjugation efficiency between 50 and 90%, depending on the used peptide and other relatable parameters of the conjugation reaction [95]. The bioconjugation chemistry of nanoparticle-based drug delivery systems usually depends on the nature of the chosen components [27] and the intended means of application.

1.5. Immobilization of enzymes

Enzymes are complex biological molecules that catalyze a multitude of chemical reactions occurring in living systems. They were used by humans way before the origins of their properties were discovered [96]. A diagram of the typical enzyme-catalyzed reaction is presented in **Figure 1. 5**. The ability to react under mild conditions without being altered or consumed by reactions and without changing the equilibrium between the reactants and the products, enzymes have raised considerable interest in many fields of research and industry [97]. However, the limitations concerning high cost, instability, challenging recovery, and reuse require optimization of enzymes for industrial applications [98]. One main strategy towards obtaining cost-effective stable and reusable systems is enzyme immobilization. The ‘immobilized enzymes’ are referred to as ‘enzymes physically confined or localized in a certain defined region of space with retention of

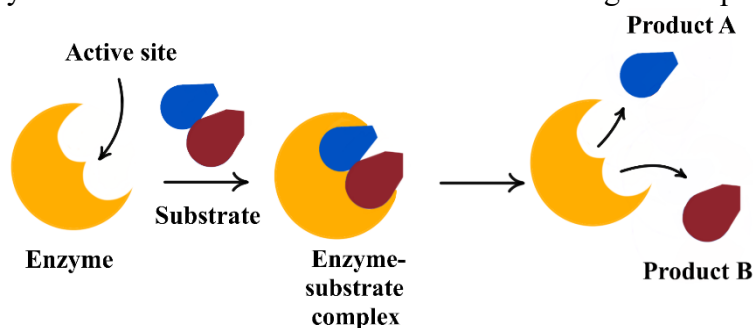


Figure 1. 5. The reaction catalyzed by an enzyme.

their catalytic activities, and which can be used repeatedly and continuously [99]. Throughout history, a number of versatile immobilization techniques were introduced: reversible physical adsorption, ionic linkages and affinity binding, as well as irreversible but exceptionally stable covalent bonding [98]. These techniques can be divided into two categories: immobilization by physical (Van Der Waals, ionic and hydrogen binding) and chemical (covalent binding) interactions[100]. The immobilization technology not only offers stability and reusability but also facilitates the separation of the enzyme from the reaction mixture, subsequently stopping the reaction at any given time. Moreover, the immobilization minimizes the product contamination by the protein and improves the enzyme’s stability at different temperatures, solvents and pH [101]. However, the immobilization process itself can change conformation of the enzyme, therefore altering its kinetic behavior [102].

Difficulties with the digestion of lactose occur with approximately 70% of the world’s adult population. Therefore, the need for lactose-free nutritional products is a prominent topic in the food processing industry. β -Galactosidase is an enzyme that is largely applied in large-scale processes to perform lactose hydrolysis and galacto-oligosaccharide production (**Figure 1. 6.**) [103-105]. β -Galactosidase can be produced by microorganisms or derived from plants and animals, and every source defines the properties of the enzyme. The enzyme produced from bacteria

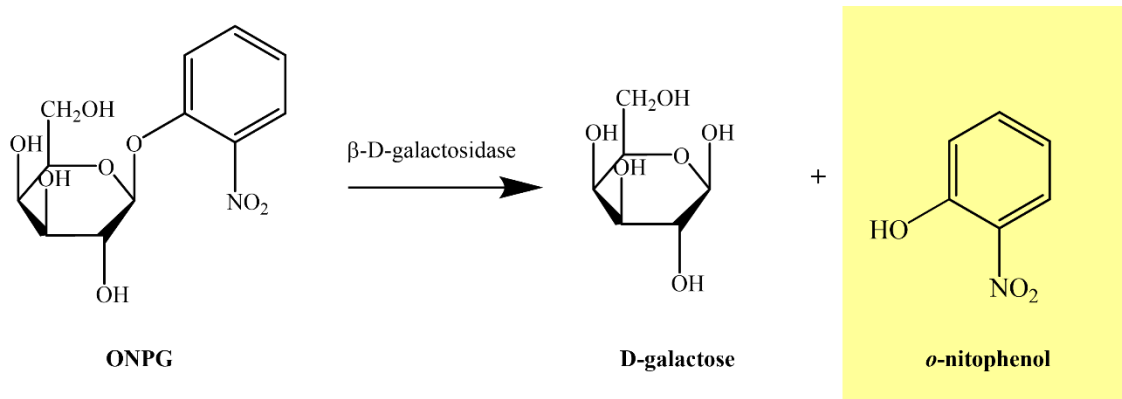


Figure 1. 6. Hydrolysis of ortho-nitrophenyl-β-galactoside (ONPG) in presence of β-D-galactosidase. The products of the reaction are D-galactose (colorless) and ortho-nitrophenol (yellow, absorption $\lambda_{max} = 420 \text{ nm}$).

Escherichia coli is widely applied in science to understand the behavior of the enzyme, but not used in the food industry. Instead, β-galactosidase produced from yeast is very promising in this application [103]. Due to the high demand for this enzyme, various immobilization techniques were established: entrapment in alginate, covalent attachment onto chitosan, gelatin, alginate, etc. and adsorption onto phenol-formaldehyde resin and bone powder [104, 106-109].

The products of hydrolysis of ortho-nitrophenyl-β-galactoside (ONPG) in presence of β-D-galactosidase are D-galactose and yellow-colored o-nitrophenol. In this reaction, the change in absorption of the mixture can be evaluated, for example via UV-Vis spectrophotometry and the rate of the reaction can be determined. The reaction rate assists determination of the activity of β-D-galactosidase. Many studies on the mechanism of this reaction provide good knowledge on the properties of the enzyme: deactivation rate constants, kinetic constants and deactivation energy [103].

Using nanomaterials for immobilization of enzymes offers a series of benefits: miniature size, large surface area for effective enzyme loading, mass transfer resistance, tolerance to temperature and pH variations, etc. [13]. Moreover, the immobilization on nanoparticles lowers the chance of protein unfolding, subsequently increasing the stability of the enzyme [110]. To date silica nanoparticles [111, 112], metal oxide nanoparticles [113], polymer nanofibers [114], magnetic Fe₃O₄ chitosan nanoparticles [115] and many more nanomaterials have been used to immobilize β-galactosidase.

The unique and variable water content makes hydrogels similar to natural tissues, opening potentials for many applications with bio-based systems. They have been used for enzyme immobilization for a long time and show minimal loss of enzyme activity upon immobilization [116]. Since then, many groups have reported immobilization of β-galactosidase via biocompatible, stimuli-responsive, synthetic, and composite hydrogels [108, 116-119].

1.6. Emulsion photopolymerization via microfluidic devices

Polymer particles of a variety of sizes can be produced employing emulsion polymerization reactions [120]. However, the polymerization technique should be chosen appropriate to the desired size and properties of the polymer particles. Continuous flow microfluidic devices can produce droplets of narrow size distribution and, when coupled with polymerization source, polymer particles of different shapes, morphology and composition [121]. In these systems, the viscosity of the fluids is directly related to the size of the synthesized particles [122]. There are two main categories of microfluidic devices: 1) both continuous and dispersed phase flow inside microchannels, 2) continuous phase flows inside the tube and the dispersed phase flows inside the capillary of narrower diameter. Both types of microfluidic devices have considerable benefits, however, in capillary-based systems dispersed phase is not in direct contact with the wall of the device before the emulsification [123]. In addition, the chances of clogging of capillary-based systems are much lower than in microchannel-based devices [122, 124]. A great variety of particles (toroidal polymer particles, Janus microparticles, clustered particles, non-spherical colloidosomes) can be obtained due to controlled droplet production mechanism of the microfluidic devices [125]. These devices can also be used to encapsulate various materials, micro- and nanoparticles inside polymer microparticles [126].

Oakey and coworkers have encapsulated cells within hydrogel microparticles employing photopolymerization of poly(ethyl glycol) diacrylate water solutions. Their results demonstrate that cell viability is not affected by exposure to UV light, but rather influenced by a generation of reactive oxygen species, which can be avoided under nitrogen [127]. In a review by *Kumacheva* and colleagues, several successful cell encapsulations within microgels derived from synthetic and biopolymers and proteins were discussed [128]. The viability of cells was different for each type of microgels, proving the dependency on components of the hydrogel. Several other teams also successfully encapsulated biomolecules inside the polymer particles using microfluidic devices [129, 130].

2. Thesis outline

2.1. Research proposal

The interest in polymer nanoparticles has grown over the past few decades, while new advances in the preparation and characterization of polymer nanoparticles emerge. The development of polymer nanoparticles in the 1970s paved the way for multipurpose applications, such as drug delivery and imaging. Drug delivery systems are designed to selectively deliver a drug to a specific location in an organism to not only increase the therapeutic efficiency of the drug but also minimize the side effects. Rising requirements for safe and efficient polymer-based nanotherapeutics, e.g., biocompatibility, biodegradability, sufficient residence time in the body, effective drug release, hold off the clinical translation of polymer nanoparticles. A lot depends on the choice of the polymer and the polymerization procedure for the synthesis of the polymer nanoparticles.

Various synthesis methods have been introduced over the years, with some using hazardous solvents, surfactants and/or heating. A more eco-efficient synthesis of highly pure polymer nanoparticles can be achieved using aerosol photopolymerization. It is an integrated continuous process with instantaneous formation of radicals and has already demonstrated various advantages in the synthesis of polymer nanoparticles of different shapes (capsules, porous structures) and compositions (organic-inorganic nanoparticle hybrids). While the aerosol photopolymerization process offers a set of advantages and has already been used to prepare different types of polymer materials, improvements are necessary to produce functional polymer nanoparticles for future applications in biomedicine. Conjugated polymer nanoparticles can be designed to be compatible, stable and tunable for various applications. One of the methods to produce conjugated polymer nanoparticles is to first produce polymer nanoparticles with functional groups and then bioconjugate molecules on the surface of the nanoparticles. Thiol-ene photopolymerization reaction can be used in combination with aerosol photopolymerization to produce polymer nanoparticles with thiol functional groups. A bioconjugation of these functional groups can produce conjugated polymer nanoparticles. Thiol-based bioconjugation methods are well known and have been used for a long time in biotechnology.

This dissertation aims to produce thiol-functional polymer nanoparticles (of size 50-500 nm) via aerosol photopolymerization utilizing thiol-ene monomers. These polymer nanoparticles are further modified for two possible applications: as enzyme immobilization agents, and as drug-delivery systems. On one hand, spherical polymer nanoparticle hybrids are produced with silver nanoparticles (of diameter 25-100 nm) trapped inside the polymer matrix (from thiol and alkene monomers). These spherical polymer nanocomposites are then conjugated with various,

fluorescent-labeled biomolecules. On the other hand, the polymer nanoparticles are functionalized with enzyme molecules and encapsulated inside the hydrogel microparticles.

The work presented in the first part of this thesis is focused on the investigation of a series of thiol and alkene monomers that are compatible with aerosol photopolymerization and that can produce polymer nanoparticles with reactive -SH groups on the surface. The evaluation of suitable thiol-ene combinations was necessary to produce spherical polymer nanoparticles with low agglomeration (analyzed via electron microscopy) and abundance of reactive -SH groups on the surface. It was also important to determine which thiol and alkene combinations produce polymer nanoparticles following thiol-ene photopolymerization and alkene homopolymerization. The size of polymer nanoparticles had to be determined and the possibilities of lowering the size distribution were attempted to produce particles suitable for future applications as drug delivery systems. The qualitative analysis of -SH groups on the polymer nanoparticles assisted the possibility of bioconjugation in further works.

The second part of this work was focused on producing spherical nanoparticle hybrids with polymer and silver components employing the same aerosol photopolymerization process. The silver nanoparticles were stabilized and introduced into the aerosol photopolymerization process with thiol-ene monomers from previous work. The produced hybrid nanoparticles were then tested for the presence of -SH groups and then conjugated with various fluorescence-labeled biomolecules. A new two-step bioconjugation procedure was introduced for the polymer nanoparticle hybrids with thiol functionalities. Various biomolecules can be conjugated onto the surface of these nanoparticles applying this method.

The immobilization of enzyme by conjugation on the surface of thiol-functional polymer nanoparticles and their subsequent encapsulation inside hydrogel microparticles (diameter 400-500 μm) was the focus of the third part of this thesis. The same two-step bioconjugation method was applied to produce enzyme-conjugated polymer nanoparticles. The change in activity of these nanoparticles was observed and compared to the activity of the unbound enzyme. The enzyme-conjugated nanoparticles were subsequently encapsulated inside the hydrogel microparticles using a microfluidic device coupled with UV-irradiation sources. This process can ensure the reusability of the enzyme for multiple reactions. The activity of the enzyme entrapped in hydrogel microparticles was compared to the activity of the unbound enzyme and the activity of the enzyme-conjugated nanoparticles.

The last part of this thesis represents work that is currently in preparation and is not yet submitted for publishing. The current aerosol photopolymerization reactor has a number of disadvantages. A new aerosol photopolymerization setup was designed and constructed in collaboration with PESCHL Ultraviolet GmbH. In the “Photo-Capsule” reactor six sets of LED irradiation sources are located in the capsule facing the reaction tube.

This thesis is a part of Horizon 2020 Marie Skłodowska-Curie Innovative Training Network (ITN) “Towards next-generation eco-efficient photo and emulsion polymerizations imparting synergy to process products and applications” program. Using thiol-ene chemistry with photopolymerization was one of the essential topics of the project. Other teams within the project

were focused on optimizing (mini)emulsion photopolymerization in combination with thiol-ene chemistry and/or other methods.

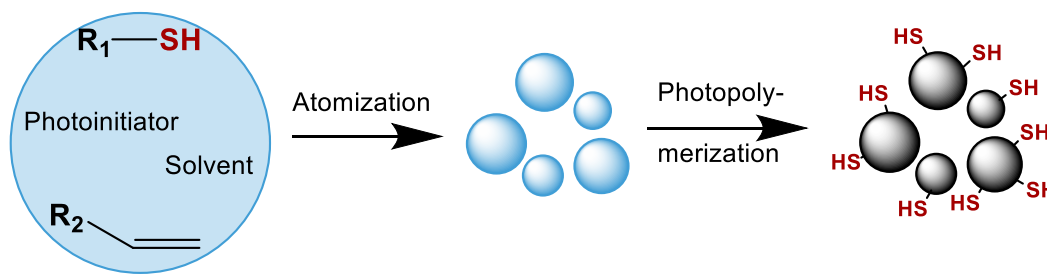
2.2. Comprehensive overview of publications

The manuscript presented in Chapter 5 was co-authored with my colleague Lukas Wenger, as he provided a great contribution to finalizing this research. The work was carried out at the intersection of polymer science and bioengineering, therefore a contribution of expertise in enzymes was necessary. However, the majority of writing, experiments, and analytics was carried out by me. The work presented in Chapter 6 is currently in preparation and is not yet submitted for publishing.

Chapter 3. Thiol-functional polymer nanoparticles via aerosol photopolymerization

N. Suvarli, I. Perner-Nochta, J. Hubbuch, M. Wörner

Polymers **2021** 13(24), 4363

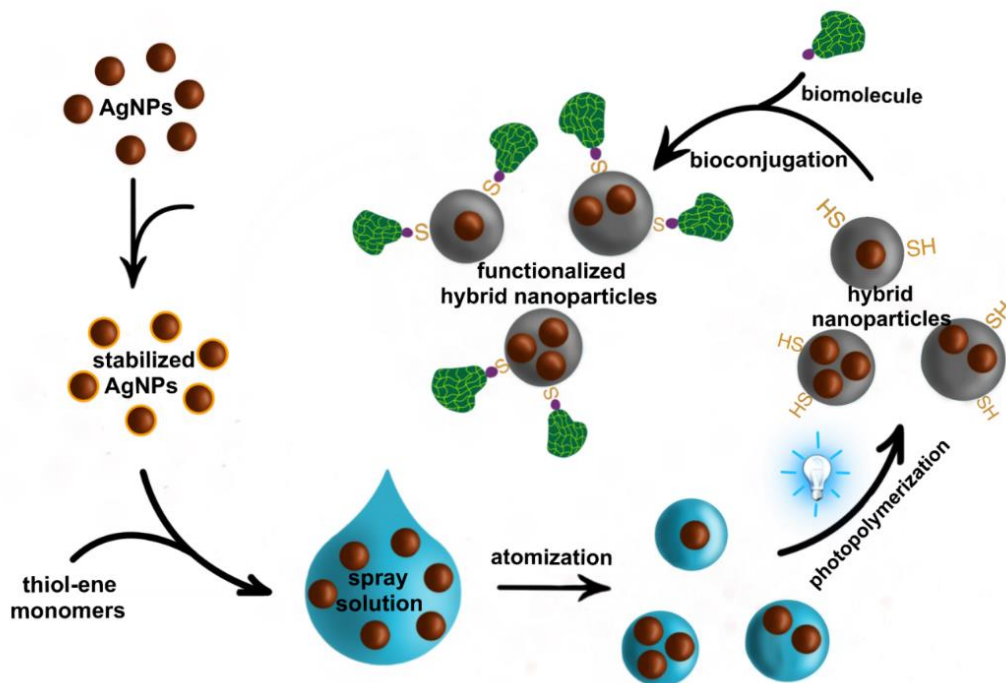


In Chapter 3, the aerosol photopolymerization technique was combined with thiol-ene chemistry to produce thiol-functional polymer nanoparticles for future possible applications as drug delivery systems, biosensors, etc. Synthesis of polymer nanoparticles often requires the use of hazardous solvents, heating, or surfactants. Aerosol photopolymerization provides an integrated, continuous, eco-efficient method for the synthesis of dry and highly pure polymer nanoparticles of 50-500 nm in diameter. Thiol-ene chemistry offers fast kinetics and delayed gelation and can be carried out at room temperature. The proposed combination of the two methods produces polymer nanoparticles with reactive $-SH$ groups on the surface. This functionality of the nanoparticles is used in publications in Chapters 4 and 5 for bioconjugation.

Chapter 4. Synthesis of spherical polymer nanoparticle hybrids via aerosol thiol-ene photopolymerization and their bioconjugation.

N. Suvarli, M. Frentzel, I. Perner-Nochta, J. Hubbuch, M. Wörner

Nanomaterials **2022** 12(3), 577



In this article, silver poly(thio-ether) nanoparticle hybrids are produced using aerosol thiol-ene photopolymerization presented in Chapter 3. The produced materials are subsequently functionalized with fluorescence-labeled biomolecules. Stabilization of silver nanoparticles was necessary to prevent their aggregation during the atomization process in the aerosol generator. The silver-polymer nanoparticle hybrids are biofunctionalized using a two-step conjugation process. The first step follows the thiol-maleimide reaction of maleimide-biotin and thiol groups on the surface of the polymer component of the hybrids. The second step considers the affinity binding of streptavidin on biotin. The outcome of bioconjugation was analyzed via Fluorescence spectroscopy and microscopy. This two-step bioconjugation method is used in Chapter 5 for the immobilization of enzymes via conjugation.

Chapter 5. Immobilization of β -galactosidase by encapsulation of enzyme-conjugated polymer nanoparticles inside hydrogel microparticles.

N. Suvarli, L. Wenger, I. Perner-Nochta, J. Hubbuch, C. Serra, M. Wörner

Frontiers in Bioengineering and Biotechnology **2022** 9:818053

In Chapter 5 β -galactosidase was immobilized on the surface of polymer nanoparticles produced in Chapter 3 through a two-step bioconjugation process as presented in Chapter 4. The enzyme-conjugated nanoparticles are encapsulated inside the hydrogel microparticles via microfluidic devices for reusability purposes. The activity of the produced enzyme-conjugated nanoparticles and enzyme-conjugated nanoparticles encapsulated inside hydrogel microparticles is then compared to the activity of the unbound enzyme at different storage temperatures throughout one month. The effect of the encapsulation process of the enzyme and enzyme-conjugated particles inside the hydrogel microparticles is investigated.

Chapter 6. Aerosol photopolymerization reactor with LED light sources.

N. Suvarli, A. Peschl, M. Wörner

In preparation

The aerosol photopolymerization setup employed in Chapters 3, 4 and 5 is not the most optimal technique to produce polymer nanoparticles. The UV-fluorescence irradiation setup (photoreactor) has a number of disadvantages that have to be addressed in order to obtain a more eco-friendly, long-lasting and efficient procedure. The new Photo-Capsule was designed and constructed with LED irradiation sources, the properties of which can be easily toggled. The reactor is now more compact and directs all of the irradiated light onto the reaction tube.

3. Thiol-functional polymer nanoparticles via aerosol photopolymerization

N. Suvarli, I. Perner-Nochta, J. Hubbuch, M. Wörner*

Karlsruhe Institute of Technology (KIT), Institute of Process Engineering in Life Sciences,
Section IV: Biomolecular Separation Engineering, Karlsruhe, Germany

*Corresponding author

Abstract

Spherical, individual polymer nanoparticles with functional -SH groups were synthesized via aerosol photopolymerization (APP) employing radically initiated thiol-ene chemistry. A series of various thiol and alkene monomer combinations were investigated based on di-, tri- and tetrafunctional thiols, reacted with difunctional allyl and vinyl ethers, di- and trifunctional acrylates. Only thiol and alkene monomer combinations able to build cross-linked poly(thio-ether) networks were compatible with APP, which requires fast polymerization of the generated droplet aerosol during the photoreactor passage within a residence time of half-minute. Higher monomer functionalities and equal overall stoichiometry of functional groups resulted in the best nanoparticles being spherical and individual, proven by Scanning Electron Microscopy (SEM). The presence of reactive -SH groups in the synthesized nanoparticles as a basis for post-polymerization modifications was verified by Ellman's test.

Keywords: thiol-ene polymerization, aerosol photopolymerization, polymer nanoparticles, thiol-functional nanoparticles

3.1. Introduction

Polymer nanomaterials have found applications in many fields of science and technology, e.g. drug delivery [2, 5], tissue engineering [131], biophotonics [132, 133], water treatment [134, 135], food processing [136, 137]. The synthesis of polymer nanoparticles via liquid routes can be achieved using either preformed polymers or by polymerization of monomers [1]. Concerning preformed polymers, several techniques have been reported. Among these, solvent evaporation is widely used, in particular, for the formation of nanoparticles for drug delivery applications [138, 139]. A drawback of this technique is the requirement for high amounts of hazardous organic solvents. Other methods that use preformed polymers, such as dialysis [140], nanoprecipitation [141], and salting-out [142], usually do not involve the use of hazardous materials. Polymerization of monomers in aqueous dispersed reaction systems, such as conventional emulsion [143], miniemulsion [144], microemulsion [145] polymerizations, result in polymer micro- and nanoparticles. These methods are used, when a polymer is designed for a specific range of

applications [1]. Emulsion polymerization is one of the most often employed techniques in industry, where the use of surfactants is required and mostly thermal initiation is applied, consuming energy for the emulsification process as well. Different emulsification procedures can be also combined with photochemical techniques, where photons are used to initiate the polymerization reaction, in order to produce polymer particles. Photopolymerization of multifunctional monomers is an effective method to produce cross-linked polymers/coatings within a very short time and has been applied, for example, in curing technologies [146].

Aerosol-based polymerization methods can be applied for the synthesis of nanomaterials as an alternative to liquid-based processes. Integrated and continuous gas-phase processes synthesize nanostructures of higher purity compared to the liquid-phase methods. Nanoparticles can be produced via either evaporation and crystallization of atomized droplets, or condensation and coagulation from nucleation and growth of gas particles [147]. Microscale polymer particles (5-100 μm) have been produced via atomization of monomer solutions with a vibrating-orifice aerosol generator and subsequent photopolymerization to accomplish droplet-to-particle conversion with UV-irradiation [20, 31]. To overcome the drawbacks of low droplet generation rate and size limitations within the μm -scale, a modified technique using a collision-type aerosol device was established which permits the generation of highly concentrated monomer droplet aerosols ($>10^8$ droplets/ cm^3) in the nano-size domain (0.1 – 0.5 μm) [22]. The produced droplet aerosol is exposed to UV-irradiation in a flow-through reactor, where the droplets polymerize in a continuous process. In contrast to other methods that produce polymer nanoparticles, aerosol photopolymerization (APP) does not require the presence of surfactants, use of heating and hazardous solvents, resulting in highly pure polymer particles. The residence time of the aerosol inside the photoreactor is short, which requires fast polymerization kinetics that can be accomplished by various combinations of initiation and propagation rates [148]. For monomers with low propagation rates, APP is not a suitable method, but the addition of a small amount of an appropriate cross-linker can lead to faster polymerization and APP can be applied [22]. Various types of nanomaterials can be produced via APP: organic-inorganic hybrid nanoparticles [24], *in-situ* drug-loaded polymer nanocarriers [23], porous spherical nanoparticles, and nanocapsules [149, 150].

Research in the field of thiol-ene chemistry has widened in recent years due to numerous benefits of the method: it is an easy, straightforward reaction that results in biocompatible materials [51, 58, 151-154]. The highly efficient thiol-ene “click” reaction is one of the well-known methods in biochemistry [46]. Thiol-ene photopolymerization is a rapid process [155] uninhibited by oxygen that does not require the use of solvents [53] and exhibits delayed gelation [156]. The step-growth mechanism of the thiol-ene photopolymerization reaction is based on alternating propagation and chain-transfer steps [157] [53]. Studies of thiol-ene photopolymerization reaction systems in solutions have shown that changes in the rate of thiol and ene functional group concentrations depend on the ratio of kinetic constants of propagation and chain transfer [51]. When the chain-transfer is the limiting step, the polymerization kinetics of the thiol-ene photopolymerization does not depend on the concentration of ene functional groups, it is rather

first-order kinetics depending on the concentration of thiol groups, and, *vice versa*, when the propagation is the rate limiting step [51, 157]. Combination of thiol-ene chemistry with photochemistry in miniemulsion polymerization process produces semicrystalline poly(thioether ester) latex nanoparticles. This facile and environmentally friendly route utilizes efficient thyl radical addition on unsaturated monomers ensuring fast polymerization at room temperature that can be applied in continuous photoreactors [54].

The use of thiol-ene photopolymerization in combination with miniemulsification that produces polymer nanoparticles was reported [58, 158-160]. To date, no application of APP technique with thiol-ene chemistry was reported. In this paper, we present aerosol thiol-ene photopolymerization as a method to produce cross-linked, narrow-size, spherical individual polymer nanoparticles with active -SH groups. We studied a variety of thiol and alkene monomers to discover the most suitable set of combinations. Regarding future applications of the particles, *e.g.*, by biofunctionalization, the availability of -SH groups was determined.

3.2. Materials and methods

3.2.1. Chemicals

The following thiols and alkenes were used as monomers (**Figure 3. 1**): diallyl adipate (**DAA**, TCI chemicals, Tokyo, Japan), tri(ethylene glycol) divinyl ether (**TEG-DVE**, Merck Group, Darmstadt, Germany), trimethylolpropane triacrylate (**TMPTA**, Sigma-Aldrich, St. Louis, MO, USA contains 600 ppm monomethyl ether hydroquinone as inhibitor), neopentyl glycol diacrylate (**NPG**, Sigma-Aldrich, St. Louis, MO, USA), 1,3,5-triallyl-1,3,5-triazin-2,4,6-(1H,3H,5H)-trion (**TATT**, Sigma-Aldrich, St. Louis, MO, USA), trimethylolpropane tris (3-mercaptopropionate) (**Trithiol**, 95%, Sigma-Aldrich St. Louis, MO, USA), tris(2-(3-mercaptopropionyloxy)ethyl) isocyanurate (**TMPIC**, Bruno Bock, Marschacht, Germany), ethylenbis(3-mercaptopropionat) (**Dithiol**, Bruno Bock, Marschacht, Germany), pentaerythrit-tetrakis-(3-mercaptopropionat) (**Tetrathiol**, Bruno Bock, Marschacht, Germany). 2-methyl-4'-(methylthio)-2 morpholinopropiophenone (**MMP**) purchased from Sigma-Aldrich (St. Louis, MO, USA) was used as a photoinitiator. Ellman's test was performed with 5,5'-dithiobis(2-nitrobenzoic acid) (**DTNB**, ReagentPlus[®], 99%) purchased from Sigma Aldrich (St. Louis, MO, USA).

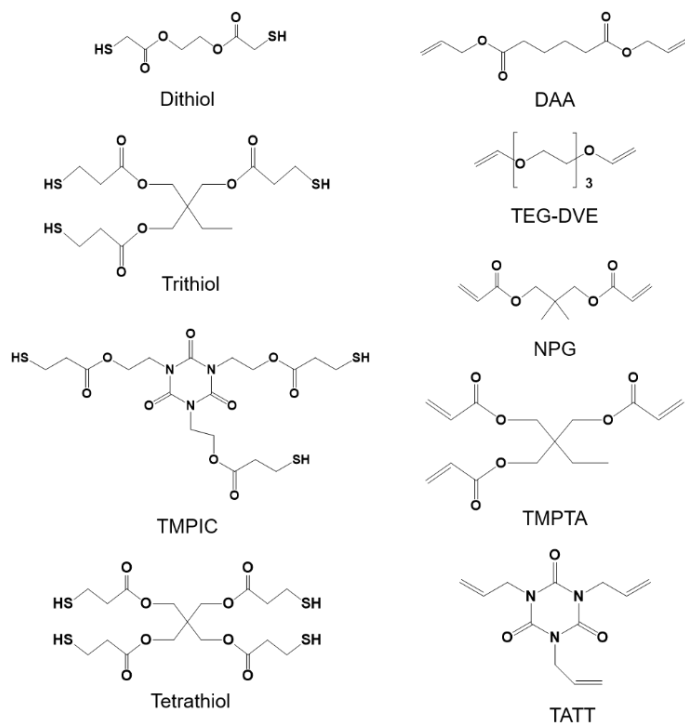


Figure 3. 1. Thiol (left) and ene (right) monomers used for synthesis of polymer nanoparticles via APP.

3.2.2. Aerosol photopolymerization setup

The aerosol photopolymerization setup (**Figure 3. 2.**) consists of a collision-type atomizer (TOPAS[®] ATM220), a photoreactor and a collection unit. The spray solution (1) placed in the aerosol generator is atomized with the stream of nitrogen inside the nozzle (2) forming a droplet aerosol. Droplets pass into the UV-irradiated reaction chamber (3), which consists of five 14 mm inner diameter fluorinated ethylene propylene (FEP) tubes connected to form a cycle inside the reactor. UV irradiation is provided by two irradiation devices, each equipped with three UV-fluorescent tubes (T-15.C, Vilber Lourmat, $\lambda_{max} = 312 \text{ nm}$ – incident irradiance $E = 15.4 \text{ mW/cm}^2$ (measured via UV-Pad-E from Opsytec Dr. Gröbel GmbH)) (4) facing the reactor. Polymerized nanoparticles are collected inside a BOLA[®] flow filtration housing on 0,1 μm hydrophobic PVDF membrane filters (Durapore[®]) (5). The nanoparticles are then left to dry on the filter overnight. An aerosol photopolymerization reaction can yield between 50 and 200 mg of nanoparticles per hour of operation, depending on the concentration of monomers in the spray solution and pressure of nitrogen. At 1 bar (1.28 L/min nitrogen flow rate) and 0.37 L volume of FEP tubes an approximate residence time can be calculated to be 28 seconds.

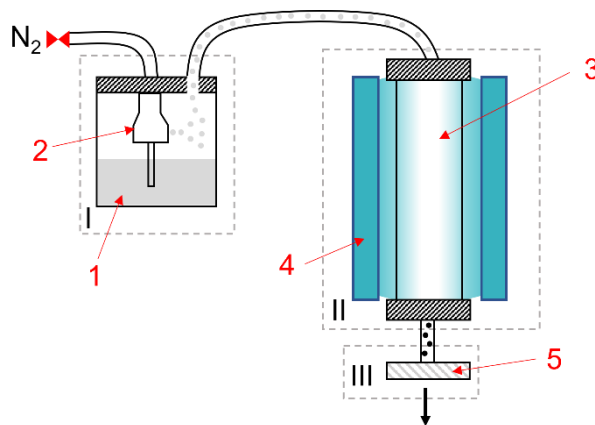


Figure 3. 2. Aerosol Photopolymerization setup: I – atomization unit, II – photoreaction unit, III – collection unit; 1) Spray solution, 2) Nozzle, 3) Reactor, 4) UV fluorescent devices, 5) particle collection (membrane filter housing).

3.2.3. Experiments

Preparation of spray solutions. The formulations of spray solutions are presented in **Table 3. 1.** The spray solution for the aerosol photopolymerization process was prepared by mixing the thiol and alkene monomers and then adding the solvent and photoinitiator in an amber flask wrapped with aluminum foil to prevent premature polymerization. In some cases, thiol and alkene monomers were not miscible, but with the addition of an appropriate solvent have formed a homogeneous solution. Solvent of choice was ethanol, however as Tetrathiol and TMPIC were not miscible with ethanol, the atomization was carried out in acetone (AcO) or acetonitrile (MeCN). The photoinitiator was added to all spray solution formulations and stirred for five minutes before the atomization; quantity of photoinitiator in all spray solutions corresponded to 1 wt% of quantity of two monomers combined. **Table 3. 1.** contains some of the formulations of the spray solutions prepared for aerosol photopolymerization (in addition, see Supporting information Appendix A).

Ellman's tests. The qualitative analysis of reactive -SH groups of the polymer nanoparticles were carried out using Ellman's reagent – DTNB. 4 mg of DTNB was dissolved in 5 mL of phosphate buffer saline (PBS) pH 7.4. 5 mg of nanoparticles were dispersed in 5 mL of PBS pH 7.4 and sonicated in ultrasonic bath (Sonorex Digital 10 P) at 80% amplitude for 10 minutes at room temperature. The dispersions of nanoparticles (100 μ L) from different samples (P1-P4, P9-P13, P15-P19, **Table 3. 1.**) were placed inside the Thermo Scientific™ 96-Well-Microtiter plates, 100 μ L of DTNB solution was introduced to the dispersion and a coloration change was observed. The samples P1, P5, P15 were purified in acetone (centrifugation, 2x20 mL AcO) dried, redispersed in PBS and tested again for presence of -SH groups after purification.

Table 3. 1. Formulations of spray solutions with monomers and their quantities and the chosen solvent. The amount of the solvent is the same (10 g) in all samples, the amount of photoinitiator in all spray solutions is 1wt.% ratio to combined monomers. Equal stoichiometry (1:1 ratio) of functional groups (-SH for thiol and -C=C for double bonds) was considered in each spray solution.

Spray Solution	Thiol	Thiol qty (mM)	Alkene	Alkene qty (mM)	Functional Group ratio	Solvent
P1	Trithiol	14.4	TMPTA	14.4	3-SH:3-C=C	EtOH
P2	Trithiol	13.9	NPG	20.9	2(3-SH):3(2-C=C)	EtOH
P3	Trithiol	13.5	DAA	20.3	2(3-SH):3(2-C=C)	EtOH
P4	Trithiol	14.2	TEG-DVE	21.3	2(3-SH):3(2-C=C)	EtOH
P5	Trithiol	15.4	TATT	15.4	3-SH:3-C=C	AcO
P6	TMPIC	12.1	TMPTA	12.1	3-SH:3-C=C	AcO
P7	TMPIC	11.8	NPG	17.8	2(3-SH):3(2-C=C)	AcO
P8	TMPIC	11.6	DAA	17.3	2(3-SH):3(2-C=C)	AcO
P9	TMPIC	12.1	TEG-DVE	18.1	2(3-SH):3(2-C=C)	AcO
P10	TMPIC	12.9	TATT	12.9	3-SH:3-C=C	MeCN
P11	Tetrathiol	11.3	TMPTA	15.1	3(4-SH):4(3-C=C)	MeCN
P12	Tetrathiol	10.9	NPG	21.9	4-SH:2(2-C=C)	MeCN
P13	Tetrathiol	10.6	DAA	21.3	4-SH:2(2-C=C)	MeCN
P14	Tetrathiol	11.2	TEG-DVE	22.3	4-SH:2(2-C=C)	MeCN
P15	Tetrathiol	12.2	TATT	16.2	3(4-SH):4(3-C=C)	MeCN

3.2.4. Analysis methods

Scanning Electron Microscopy (SEM). Nanoparticles were dispersed in acetone and 100 μ L of the dispersion was distributed on silicon wafers, dried and sputtered with platinum. The plate was then placed inside LEO1530 (Carl Zeiss AG, Oberkochen, Germany) microscope. The SEM images of nanoparticles were taken at three different magnifications 2000, 10000 and 25000.

Image analysis of SEM micrographs. SEM images of some samples were analyzed for size distribution studies using open-source ImageJ software. The diameter of nanoparticles was determined manually for each nanoparticle on the micrograph, and the count rate of nanoparticles was equalized for each sample. The histograms of the determined diameters were built using OriginLab[®] software.

3.3. Results and Discussion

3.3.1. Polymer nanoparticles from aerosol thiol-ene photopolymerization

Some acrylate and vinyl ether monomers have already been used to produce polymer nanoparticles via APP [22]. In this research thiol and alkene monomers are tested employing aerosol photopolymerization. A great variety of thiol and alkene monomers with different quantities of functional groups (-SH and -C=C-, respectively) were studied to determine the set of monomer combinations suitable for the synthesis of spherical, individual poly(thio-ether) nanoparticles. For each alkene monomer, homopolymerization was attempted before investigating the thiol-ene photopolymerization. Not all used alkene monomers formed polymers in a radically initiated aerosol photopolymerization process. Due to the short residence time inside the photoreactor, only fast propagating monomers can form homopolymer nanoparticles via APP. The extremely low reactivity of allyl and vinyl ether towards free radical polymerization is most probably a consequence of high stability of the propagating radicals. Nevertheless, cationic chain-growth reaction can be very fast and has shown great compatibility with APP using TEG-DVE as monomer [29]. Allyls and vinyl ethers cannot be homopolymerized employing free radical initiation because of degradative chain transfer leading to oligomers or low molecular weight products. Only with multifunctional monomers (as for TATT) and high initiator concentrations polymeric products had been obtained after long reaction times [161].

Acrylate monomers, on the other hand, react in a free radical chain-growth polymerization [162] fast enough to proceed under APP conditions. The products of these reactions can be analyzed via SEM (Supporting information III, Appendix 1).

The aerosol photopolymerization of spray solutions specified in **Table 3. 1**. leads to formation of polymer nanoparticles; SEM images of these nanoparticle samples are presented in **Figure 3. 3**. Polymer nanoparticles produced from monomers with a 1:1 stoichiometric ratio of functional groups are presented in this figure. Other functional group ratios (especially with a higher amount of thiol) showed agglomerated or highly agglomerated polymer material (Supporting information, Appendix A). Additionally, it has to be mentioned that sample preparation for SEM imaging might result in increased agglomeration of polymer nanoparticles.

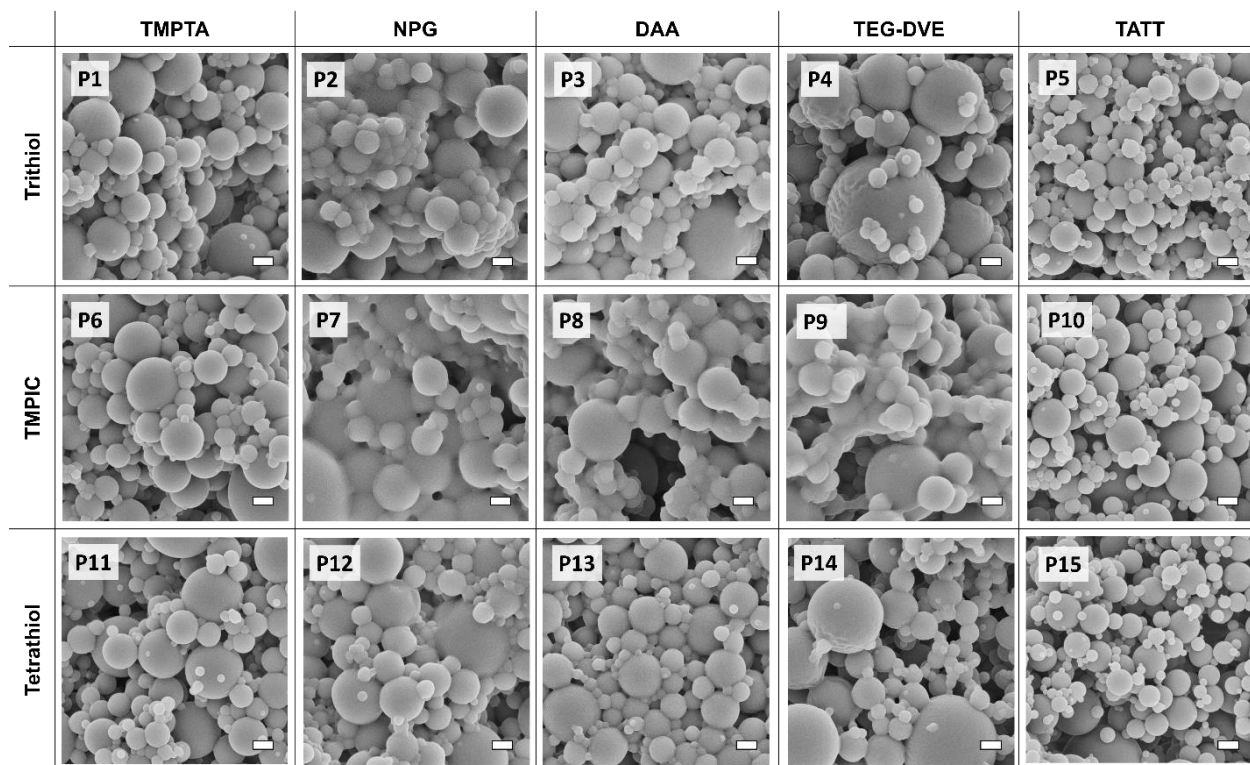


Figure 3. 3. SEM images of polymer nanoparticles produced via aerosol photopolymerization from various thiol-ene monomer combinations. For simplicity, nomenclature of thiol and alkene monomers is presented on the left-hand side and on the top, respectively. The scalebar corresponds to 1 μ m. The nomenclature agrees with the formulations listed in **Table 3. 1**.

The polymer nanoparticles produced from the combination of Trithiol with TMPTA (triacylate) (P1) appear less agglomerated than combinations of Trithiol with other alkene monomers (DAA, NPG, TEG-DVE) in ethanol. The combination of TMPIIC with TMPTA (P6) and Tetrathiol with TMPTA (P11) also produce individual polymer nanoparticles. Solid-state ^{13}C NMR spectra of TMPTA (M1) homopolymer and Trithiol-TMPTA (P1) heteropolymer nanoparticles (Supporting information I) reveal that in the P1 nanoparticles all TMPTA double bonds reacted, whereas in the TMPTA-homopolymerization reaction the conversion of the double bonds was lower. The results obtained from ^{13}C NMR were confirmed with Fourier-transform infrared (FT-IR) analysis (Supporting Information, Appendix A). In the case of P1, both homo- (acrylic chain) and heteropolymerization (thiol-ene step growth) can be competing reactions. Mixed step and chain-growth polymerization reaction has been observed [46, 163] for acrylic monomers in thiol-ene photopolymerization reaction systems. The so-called mixed mode polymerization is based on free radical polymerization reactions that show different development of molecular weight compared to chain and step polymerization individually, thus resulting in a rapid polymerization reaction with cross-linking (in case of multifunctional monomers) [164].

A similar phenomenon can be observed for a combination of NPG (diacylate) and thiols. Although NPG homopolymerization (M2, Supporting Information, Appendix A) reaction produces individual polymer nanoparticles, thiol-ene heteropolymerization with Trithiol (P2)

resulted in highly agglomerated polymer material. The behavior of other thiol monomers with NPG in P12 (Tetrathiol) results in a low degree of agglomeration and P7 (TMPIC) results in the formation of highly agglomerated material. These outcome also showcases the possibility of occurrence of mixed mode polymerization, but one can expect that the degree of cross-linking is lower than in the case of TMPTA because monomers with three or more functional groups are more prone to the formation of highly cross-linked polymers [156]. This can relate to the formation of more individual nanoparticles in P1 (Trithiol+TMPTA) formulation, compared to P2 (Trithiol+NPG). A combination of trifunctional thiol with trifunctional alkene (3FG-3FG) is expected to result in higher cross-linking within the polymer matrix, compared to combinations of trifunctional thiol with difunctional alkene (3FG-2FG), providing the stoichiometry of functional groups is kept equal.

Polymer nanoparticles can be produced from combinations of DAA (diallyl) with tri- and tetrafunctional thiols (P3, P8, P13) and TEG-DVE (divinyl ether) with the same set of thiols (P4, P9, P14). In the case of TMPIC (P8, P9), the nanoparticles appear to have a high degree of agglomeration compared to other thiols; when using another solvent (MeCN) in samples P17 and P18 (Supporting Information II), the nanoparticles still appear heavily agglomerated. In the case of combinations of DAA (P3, P8, P13) and TEG-DVE (P4, P9, P14), the mixed mode can be excluded, because almost no homopolymerization of alkene is expected to take place. Therefore, the products of P3, P4, P8, P9, P13, P14 formulations are products of thiol-ene polymerization reaction, exclusively. As in the case of NPG, DAA and TEG-DVE each possess only two functional groups, which may lead to a lower degree of cross-linking in thiol-ene reactions with tri- and tetrafunctional thiols, compared to reactions with the trifunctional monomer TMPTA.

With the set-up used, TATT (triallyl) cannot yield homopolymers via free-radical aerosol photopolymerization, however spherical and individual polymer nanoparticles can be produced via thiol-ene photopolymerization reactions (P5, P10, P15) with tri- and tetrafunctional thiols. And in case of these reactions, only step-growth thiol-ene polymerization has to be taken into account, and highly cross-linked poly(thio-ether) nanoparticles are expected to be produced considering that TATT comprises three ene functional groups.

Aerosol photopolymerization of alkenes with a difunctional thiol (Dithiol) was also studied and the results are presented in Supporting information III.

The results presented in this section underline the use of thiol-ene chemistry for aerosol photopolymerization and showcases a set of monomer combinations that results in spherical individual polymer nanoparticles. Trifunctional thiols with trifunctional alkene monomers in an equal stoichiometry of functional groups are the best tool in producing cross-linked and individual polymer nanoparticles.

3.3.2. *Ellman's test*

The presence of -SH groups within the polymer particles can be determined using FTIR; however, the -SH stretching mode shows a very weak absorption peak in trithiol. In Figure S2, the

signals of -SH groups are visible for P1 polymer nanoparticles, which were synthesized through a mixed mode polymerization mechanism. In the case of the pure thiol-ene polymerization (P5), no trace of -SH groups is observed. However, a more precise method is necessary due to the low sensitivity of ATR-FTIR towards detecting thiol groups.

Elman's test was carried out with polymer nanoparticles (from **Table 3. 1**) produced via aerosol thiol-ene photopolymerization to determine the presence of reactive -SH groups. Homopolymers of TMPTA and NPG (M1 and M2, respectively) do not show coloration, as expected, whereas all polymer nanoparticles produced from thiol-ene combinations showed various intensities of coloration in reactions with DTNB. The most intense coloration was observed for thiol-acrylate combinations (P1, P2, P6, P7, P11, P12). In mixed mode photopolymerization between thiols and acrylates, acrylate monomers react in both homopolymerization and heteropolymerization with the thiol. This can be evidence of higher consumption of -C=C during the mixed mode photopolymerization; consequently, more -SH could remain unreacted. In the products of pure thiol-ene polymerization reactions, less intense coloration was observed after the reaction with DTNB. Polymer nanoparticles from different monomer combinations disperse differently in PBS, and some materials tend to form aggregates. Quantitative analysis, therefore, cannot be carried out accurately. Nevertheless, these results confirm the abundance of reactive -SH groups within thiol-acrylate nanoparticles. The reactive -SH groups can be utilized for the post-polymerization functionalization via thiol-Michael 'click' reactions to conjugate the polymer nanoparticles with biomolecules for their future applications, for example, in biotechnology and biomedicine.

3.3.3. Size distribution studies

Polymer nanoparticles produced via aerosol photopolymerization are not monodisperse. *Akgün* et al. have studied the size distribution of the aerosol droplets and the polymer nanoparticles in an on-line measurement using Scanning Mobility Particle Sizer consisting of electrostatic classifier and differential mobility analyzer. They have confirmed that the diameter of the majority of the polymer nanoparticles was below 300 nm [22]. Several factors affect the particle size and dispersity, while this paper only investigates the narrowing of the size distribution via decreasing the viscosity, *i. e.* increasing the ratio of solvent to monomers. An additional effect which must be considered is the evaporation of the relatively volatile solvent during the flight of the droplets until polymerization is completed. Significant changes to the size distribution of the nanoparticles are observed when the solvent amount exceeds the amount of monomers 20 times (**Figure 3. 4.**). The size distribution narrows and shifts into the region of smaller nanoparticle size. These changes were confirmed from the analysis of SEM images by deducing histograms (**Figure 3. 4.**, right). All D-values were decreased from sample P1 to P1-S*20 (**Figure 3. 4.**, left): D50 from 398 to 247, D90 from 625 to 483, and D10 from 150 to 137. Low yield in highly diluted spray solutions is one of the drawbacks of using this method to narrow the size distribution of polymer nanoparticles. The 20 times increase in solvent (EtOH) amount leads to a three-fold decrease in yield. Throughout

this paper higher ratios of solvent to monomers were studied as well, decent mass yields (80 mg) can be achieved up to a 30:1 solvent:monomers ratio. The nanoparticles form aggregates in many solvents making use of other particle size analysis techniques unreliable. The Dynamic Light Scattering (DLS) was one of the methods that were tested to acquire particle size distribution. The more stable dispersions of nanoparticles can be obtained in dimethylsulfoxide (DMSO). Dispersions of nanoparticles in DMSO can also be used for syringe filtration in order to remove bigger nanoparticles and keep the size distribution in the range between 50 and 500 nm.

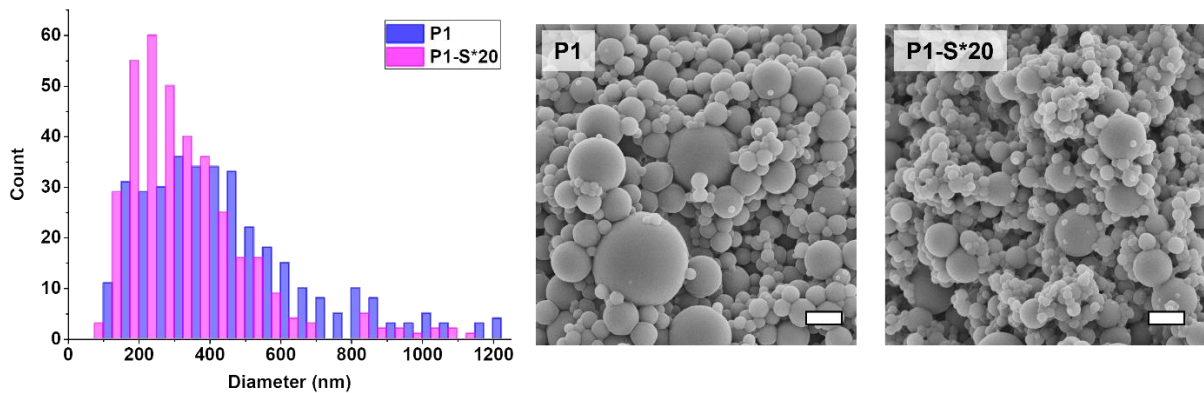


Figure 3. 4. Size distribution histogram (left) as a function of particle diameter and particle count (graphed using image analysis of SEM micrographs) and corresponding SEM images of the polymer nanoparticles produced from solutions P1 and P1-S*20 (right). Scalebar - 1 μ m.

3.4. Conclusion

This research demonstrates that polymer nanoparticles bearing active -SH groups can be produced from thiol and alkene monomers via aerosol photopolymerization. Combinations of trifunctional alkenes and trifunctional thiols, as well as trifunctional alkenes and tetrafunctional thiols, work best in an equal stoichiometry of functional groups to produce spherical individual cross-linked poly(thio-ether) nanoparticles. Several other monomer combinations, *e. g.* with difunctional alkene and trifunctional thiol (2FG-3FG), work as well, but the produced nanoparticles are not as individual as nanoparticles from 3FG-3FG combinations. The poly(Trithiol-TMPTA) nanoparticles contain no traces of unreacted ene groups, leading to the conclusion that all TMPTA has reacted under cross-linking during photopolymerization. Poly(Trithiol-TMPTA) nanoparticles were produced from mixed mode polymerization, where both homopolymerization of TMPTA and copolymerization of TMPTA and Trithiol took place. Poly(Trithiol-TATT) nanoparticles are a product of copolymerization of Trithiol and TATT, due to the inability of TATT to produce nanoparticles via free radical aerosol photopolymerization. The products of the “true” thiol-ene reaction (poly(Trithiol-TATT)) do not have any thiol

functionalities as seen on ATR-FTIR. These results also mark a good start into the study of mixed mode polymerization reaction in aerosol thiol-ene photopolymerization systems, due to the high purity of polymer material collected in a dry state. The size distribution of nanoparticles was narrowed by increasing the solvent amount in a spray solution, simultaneously lowering its viscosity. The produced nanoparticles have active -SH groups that were traced via Elman's test. The nanoparticles can further be adapted with biofunctionalization techniques for targeted drug delivery and other biomedical applications.

4. Synthesis of spherical nanoparticle hybrids via aerosol thiol-ene photopolymerization and their bioconjugation

N. Suvarli, M. Frentzel, I. Perner-Nochta, J. Hubbuch, M. Wörner*

Karlsruhe Institute of Technology (KIT), Institute of Process Engineering in Life Sciences, Section IV: Biomolecular Separation Engineering, Karlsruhe, Germany

*Corresponding author

Abstract

Hybrid nanomaterials possess the properties of both organic and inorganic components and find applications in various fields of research and technology. In this study, aerosol photopolymerization is used in combination with thiol-ene chemistry to produce silver poly(thio-ether) hybrid nanospheres. In aerosol photopolymerization, a spray solution of monomers is atomized, forming a droplet aerosol which then polymerizes to produce spherical polymer nanoparticles. To produce silver poly(thio-ether) hybrids, silver nanoparticles were introduced to the spray solution. Diverse methods of stabilization were used to produce stable dispersions of silver nanoparticles to prevent their agglomeration before the photopolymerization process. Successfully stabilized silver nanoparticle dispersions in the spray solution subsequently formed nanocomposites with non-agglomerated silver nanoparticles inside the polymer matrix. Nanocomposite particles were analyzed via scanning and transmission electron microscopy to study the degree of agglomeration of silver nanoparticles and their location inside the polymer spheres. The nanoparticle hybrids were then introduced into various biofunctionalization reactions. A two-step bioconjugation process was developed involving the hybrid nanoparticles: 1) conjugation of (biotin-)maleimide to thiol-groups on the polymer network of the hybrids, and 2) biotin-streptavidin binding. The biofunctionalization with gold nanoparticle-conjugates was carried out to confirm the reactivity of -SH groups on each conjugation step. Fluorescence-labeled biomolecules were conjugated to spherical nanoparticle hybrids (applying the two-step bioconjugation process) verified using Fluorescence Spectroscopy and Fluorescence Microscopy. Presented research offers an effective method of synthesis of smart systems that can further be used in biosensors and various other biomedical applications.

Keywords: nanoparticle hybrids, silver stabilization, thiol-ene polymerization, aerosol photopolymerization, thiol-maleimide bioconjugation, streptavidin-biotin binding

4.1. Introduction

Development of new sustainable eco-efficient [165, 166] methods for synthesis of nanomaterials has become a focus of many researchers in the last decades [167]. Synthesis of organic-inorganic hybrid nanoparticles can be carried out using various techniques [168, 169]. *In situ* free radical chain polymerization in bulk is one of the widely used industrial methods to produce nanocomposites [71, 170, 171]. Harmful matrices, capping agents, and toxic solvents in the synthesis of organic-inorganic nanocomposites are used very often [172]. Aerosol photopolymerization offers an environment-friendly, cost-effective, continuous flow-through method for the synthesis of nanoparticles [22, 24, 150]. In contrast to other polymerization methods, aerosol photopolymerization does not require heating, high-energy homogenization, surfactants, stabilizers, and co-stabilizers. Aerosol photopolymerization has already been used to synthesize zinc oxide-polymer nanoparticle hybrids [24], and was chosen in this study to produce silver-poly(thio-ether) nanoparticle hybrids because the photopolymerization reaction is supported by the instantaneous formation of radicals and presents a more effective and simple method over thermally initiated polymerization, thus, the synthesis can be carried out at room temperature in an integrated continuous process.

Promising studies have demonstrated extraordinary benefits of thiol-ene photopolymerization [173]. Rapid step-growth thiol-ene photopolymerization reactions are insensitive to oxygen and offer low shrinkage [174]. Thiol-ene photopolymerization is a promising alternative to acrylate-based polymerization reactions [175]. It offers linear and cross-linking polymerizations depending on the number of functional groups of thiols, alkenes, presence of crosslinker, etc. Various thiols can be used in combination with different alkene compounds, creating multifunctional structures of polymers. Thiol-ene reactions also offer a synthesis of biocompatible and biodegradable polymers [176, 177].

Polymer nanoparticle hybrids produced by aerosol photopolymerization possess accessible -SH groups, according to previous work [178]. These functional groups can be an excellent tool for thiol-ene “click” reactions [28, 50]. Cancer targeting molecules, biomarkers, antibodies, etc. can easily be conjugated onto the surface of nanoparticles via these available groups. Maleimides present a promising tool for bioconjugation especially with thiol-groups of nanoparticles through Michael-type addition [49]. A great variety of commercially available derivatives of maleimide (e.g., biotin-maleimide) can be applied for further functionalization. Conjugation of biotin-maleimide to the silver-polymer nanoparticle hybrids allows conjugation of streptavidin through high-affinity biotin-streptavidin binding [179].

Cancer nanotechnology is a fast-developing field mainly focused on the use of nanomaterials in diagnostics and treatment of cancer by addressing selectivity – one of the major issues in present cancer treatment techniques [180-183]. The tunable properties of nanomaterials are the key to their versatile applications in targeting cancer. Despite their small size (1-1000 nm), nanoparticles can carry a great quantity and variety of drug and antibody molecules; nanoparticles

can be functionalized to specifically target cancer cells, and are inert to resistance mechanisms of the organism [184].

Strong optical absorbance and scattering properties of noble metal nanoparticles make them a desirable tool for combination therapies [185-187]. A great amount of research has been carried out to establish applications of gold nanoparticles for *in vitro* assays, *in vitro* and *in vivo* imaging, cancer therapy, and drug delivery [74]. Localized surface plasmon resonance (LSPR) is an effect observed in metal nanoparticles, resulting in radiation scattering and absorption of light [188]. Localized heating that occurs due to LSPR carries on to apoptosis of surrounding cells and/or releases therapeutics. LSPR of gold nanoparticles majorly contributes to the use of photoimaging and photothermal therapy of cancer tumors [189]. LSPR wavelengths of gold and silver nanoparticles are in the range of the visible spectrum of light [188]. Although, silver and gold nanoparticles have similar plasmon resonance sensitivity, sharper and more intense resonance peaks of silver nanoparticles are advantageous in sensor applications [190]. Silver nanomaterials have already been applied in cancer research due to their bactericide antimicrobial features [185]. However, their cytotoxicity and genotoxicity due to the presence of both silver ions (Ag^+) and reactive oxygen species (ROS), generated by silver nanoparticles incorporated in human cells [81, 191], have restricted their wide application in cancer treatment. The optical properties of silver nanoparticles in cancer diagnostics have only been used in a limited number of studies [192, 193]. Optical properties of silver nanoparticles are better than those of gold nanoparticles [194], therefore the use of silver nanoparticles in cancer diagnostics might result in higher sensitivity compared to gold nanoparticles. Less research was found on the sensor applications of silver nanoparticles for cancer diagnostics and treatment, compared to gold nanoparticles.

In our recent paper [178], we investigated several thiol-ene monomer combinations that worked well in combination with aerosol photopolymerization to form spherical individual nanoparticles with reactive -SH groups. In the present study, we aim to establish a working combination to produce spherical individual polymer nanoparticles that contain individual silver nanospheres inside. The resulting particles should possess accessible -SH groups for conjugation of biomolecules, and silver nanoparticles provide *e.g.*, plasmon resonance properties for imaging techniques.

4.2. Experimental

4.2.1. Chemicals

Trimethylolpropane tris (3-mercaptopropionate) (Trithiol, Sigma-Aldrich, 95%, St. Louis, MO, USA) and trimethylpropane triacrylate (TMPTA, Sigma-Aldrich, contains 600 ppm monomethyl ether hydroquinone as inhibitor) were used as thiol and alkene monomers, respectively. 2-Methyl-4'-(methylthio)-2 morpholinopropiophenone (MT-2MP, Sigma-Aldrich, 98%, St. Louis, MO, USA) was used as a photoinitiator. Silver nanoparticles of different grades

were used in preparation of the spray solution: silver nanoparticles ink (AgINK, 115 nm (d_{90}), 70 nm (d_{50}), Merck KGaA, Darmstadt, Germany, 50 wt. % dispersion in tripropylene glycol mono methyl ether), dried silver nanoparticles (Ag25 nm, Nanocomposix, Econix PVP coated), dried silver nanoparticles (Ag50 nm, Nanocomposix, Econix PVP coated). Stabilization of silver nanoparticles was carried out using the following compounds: \pm α -Lipoic acid (α -LA, $\geq 98\%$, Sigma-Aldrich, St. Louis, MO, USA), 11-Mercapto-1-undecanol (MUL, 99%, Sigma-Aldrich, St. Louis, MO, USA). 5,5'-dithiobis-(2-nitrobenzoic acid) (DTNB, ReagentPlus[®], 99%, Merck KGaA, Darmstadt, Germany) was among the main components for Ellman's reaction for the determination of -SH groups. Gold nanoparticles (Au@Mal, maleimide functionalized, conjugation kit, CytoDiagnostics Inc., Sigma-Aldrich, St. Louis, MO, USA), Bio-ready Gold Nanospheres-Streptavidin (Au@Strep, Nanocomposix, San Diego, CA, USA), Atto 425-Streptavidin (425-St, $\lambda_{em} = 477$ nm, Merck KGaA, Darmstadt, Germany), Biotin-Maleimide (b-M, $\geq 95\%$ (TLC) powder, Merck KGaA, Darmstadt, Germany), iFluor-Maleimide-350 (i-FM, $\lambda_{em} = 441$ nm, AAT Bioquest Inc., Sunnyvale, CA, USA) were used for (bio)conjugation reactions. Phosphate buffered saline (PBS) pH 7.4 was used as a buffer for streptavidin conjugation (137 mM Sodium Chloride, 2.7 mM of Potassium Chloride, 10 mM of Di-sodium hydrogen phosphate, and 1.8 mM of Potassium di-hydrogen phosphate in distilled water). Dimethyl Sulfoxide (DMSO, anhydrous, $\geq 99.7\%$, Carl Roth GmbH, Karlsruhe, Germany) was used as a solvent.

4.2.2. Aerosol photopolymerization

The schematic representation of the aerosol photopolymerization setup is presented in **Figure 4.1**. The spray solution placed inside the aerosol generation unit (ATM 220, Topas GmbH, Dresden, Germany) is atomized under the stream of pressurized nitrogen, forming a droplet aerosol which, subsequently, passes to the photoreactor unit. In the photoreactor, droplets polymerize under the irradiation of UV-fluorescence lamps ($\lambda_{max} = 312$ nm T-15.C, Vilber Lourmat, incident irradiance $E = 15.4$ mW/cm² (measured via UV-Pad-E from Opsytec Dr. Gröbel GmbH)) to form polymer nanoparticles, which are collected on 0.1 μ m pore size Durapore[®] hydrophilic membrane filter. During the process, while the volatile solvent in the spray solution is partially evaporated, every 30 min after the start of the reaction, the solvent is added to compensate for the evaporated amount.

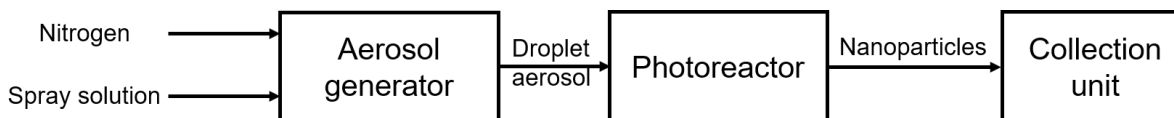


Figure 4.1. Schematic representation of the aerosol photopolymerization setup.

4.2.3. Experimental methods

Preparation of spray solutions. The spray solutions prepared for the aerosol photopolymerization contain thiol-ene monomers, organic volatile solvent, photoinitiator,

silver nanoparticles and if required, a silver nanoparticle stabilizer. The formulations of the spray solutions used within the scope of this paper are presented in **Table 4.1**. For the spray solution preparation, silver nanoparticles were first introduced into the solvent (with stabilizer) and stirred or sonicated (according to stabilizer of choice) until a colloidal stable dispersion was obtained. Then, the monomers (0.7108 g of Trithiol and 0.9559g of TMPTA) were introduced into the dispersion, followed by the addition of the photoinitiator (0.0017g) right before the photopolymerization process.

Spray solutions were treated differently depending on chosen stabilization techniques. In the case of α -LA, the silver nanoparticles were stirred with a 0.1 mM α -LA ethanol solution for 30 minutes. The same stabilization method was used with MUL. Stabilization via sonication was carried out with the sprays solution flask immersed in an ultrasonic bath (Sonorex Digital 10P, 80% amplitude, 3 minutes, 22°C) during each solvent addition step.

Table 4.1. Formulations of the spray solutions used to produce silver-poly(thio-ether) nanoparticle hybrids. Amounts of monomers and photoinitiator were kept the same in all presented spray solution formulations.

Spray solution	Silver NPs	Silver NPs quantity	Stabilization method	Stabilizer concentration	Solvent – Quantity (g)
NC-0	-	-	-	-	EtOH – 50
NC-1	AgINK	0.17 g	-	-	EtOH – 50
NC-2	AgINK	0.17 g	α -LA	0.1 g	EtOH – 50
NC-3	AgINK	0.017 g	MUL	0.01 g	EtOH – 50
NC-4	AgINK	0.17 g	Sonication	-	EtOH – 50
NC-5	Ag25nm	0.05 g	-	-	EtOH – 50
NC-6	Ag25nm	0.1 g	α -LA	0.08 g	EtOH – 25
NC-7	Ag50nm	0.01 g	-	-	EtOH – 50
NC-8	AgINK	0.17 g	α -LA	0.13 g	n-PrOH – 50

Biofunctionalization. The nanoparticles obtained via aerosol photopolymerization were tested for the presence of reactive -SH groups using Ellman’s reaction [195]. The solution of DTNB in phosphate-buffered saline (PBS) was prepared and added to the dispersion of nanoparticles. The instant reaction that showed the appearance of yellow colour confirms the presence of unreacted -SH groups. Poly(TMPTA) nanoparticles (without -SH groups) were used as a blank experiment.

Maleimide conjugated gold nanoparticles (Au@M) that can be visualized via electron microscopy were used to investigate the availability of binding sites on the surface of the polymer nanoparticle layer (**Figure 4. 2**, A-1.). To avoid misinterpretation of electron microscopy images, the plain polymer nanoparticles without AgNPs were used (formula NC-0 **Table 4.1**). 1 mg of Au@M was dissolved in 1 mL of reagent buffer (provided with the conjugation kit) and added to

5 mg in 1 mL of dimethyl sulfoxide (DMSO, anhydrous). The reaction was carried out for 12 hours, followed by purification via centrifugation. The particles were quenched with 3x5 mL of EtOH.

The availability of binding sites was also measured for the reaction with streptavidin, by consecutive addition of biotin-maleimide (b-M) and streptavidin conjugated to gold nanoparticles (Au@Strep) (**Figure 4. 2, A-2.**). 1 mg of b-M was dissolved in 1 mL of DMSO and added dropwise to the dispersion of 5 mg of NC-0 NPs in 1 mL of DMSO. The reaction was carried out for 12 hours at room temperature. The particles were purified with 3x5 mL of EtOH and left to dry. The dry b-M-NC-0 nanoparticles were then dispersed in 1 mL of 3% DMSO in phosphate-buffered saline (PBS) (pH 7.4) and introduced into the reaction with 200 μ L of Au@Strep dispersion. The reaction was left stirring for 12 hours and then purified via centrifugation with 3x5 mL of PBS (pH 7.4).

The reaction of maleimide-fluorophore (i-FM) with nanoparticles (**Figure 4. 2, B-1.**) was also carried out in DMSO. At first, 1 mg of i-FM was dissolved in 1 mL of DMSO. Then, 10 mg of NC-7 nanoparticles were dispersed in 4 mL of DMSO and stirred. The solution of i-FM was added to the dispersion of nanoparticles dropwise under vigorous stirring. The mixture was left to react overnight. Afterwards, the reaction mixture was purified by centrifugation with 2x10 mL of DMSO and 2x10 mL of EtOH. Each supernatant was tested via fluorescence spectroscopy for the presence of unreacted fluorescein-maleimide.

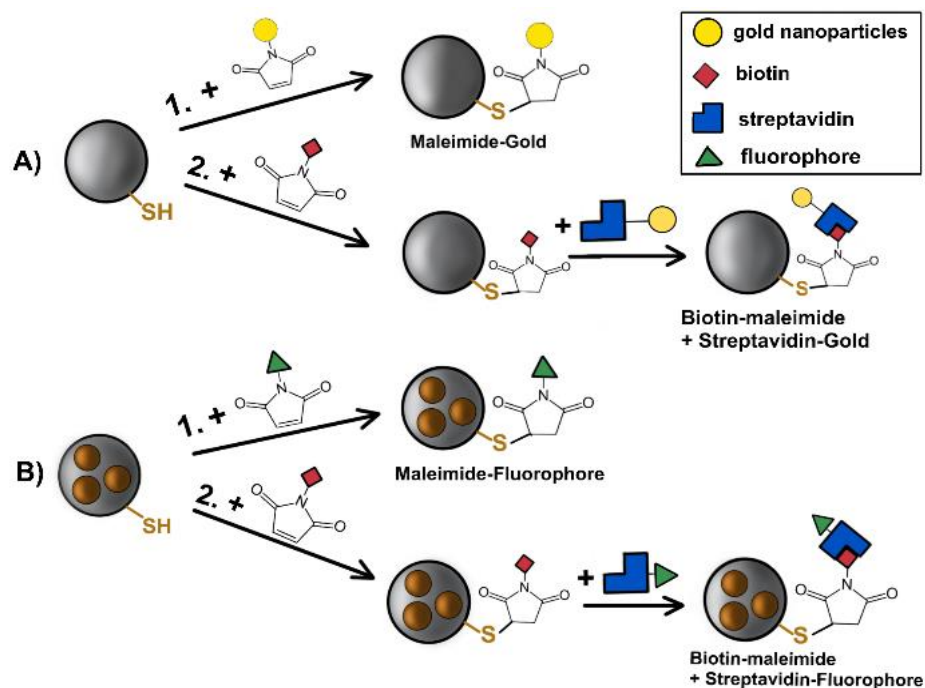


Figure 4. 2. Diagram of bioconjugation of gold nanoparticles onto the surface of polymer nanoparticles (A) and bioconjugation of fluorescence-tagged molecules to the hybrid nanoparticles (B). Legend is in the top right corner.

The reaction of nanoparticles with biotin-maleimide was carried out in the same way as the abovementioned reaction with NC-0. The resulted (b-M)-NC-7 nanoparticles were used in further reactions with fluorescein-streptavidin (**Figure 4. 2, B-2.**).

The reaction of (b-M)-NC-7 nanoparticles with 425-St was carried out in PBS (pH 7.4). 1 mg of 425-St was dissolved in 1 mL of PBS. 10 mg of nanoparticles were dispersed in PBS stirred for 10 min and sonicated in an ultrasonic bath (Sonorex Digital 10P, 100% amplitude, 5 minutes, 22°C). The 425-St was added dropwise to the nanoparticle dispersion under vigorous stirring and stirred overnight. The reaction mixture was purified by centrifugation with 2x20 mL of PBS and then 2x20 mL of EtOH-PBS mixture.

4.2.4. Analytical methods

Scanning Electron Microscopy (SEM) was used to observe the size, shape, degree of aggregation, and encapsulation of AgNPs inside the polymer matrix of Ag@poly(Trithiol-TMPTA) nanoparticle hybrids produced via aerosol thiol-ene photopolymerization. The samples for the analysis were prepared as follows: the dry nanoparticle product was dispersed in acetone and stirred for 30 minutes, 100 μ L of the dispersion was distributed on silicon wafers, dried, and sputtered with platinum. A LEO1530 (Carl Zeiss Microscopy GmbH, Jena, Germany) SEM was used in all experiments and images were taken at magnifications of 2000, 10000 and 25000. The images were recorded at working distance 5.5–6 mm, the acceleration voltage of the microscope was 5 keV.

Transmission Electron Microscopy (TEM) was used to observe the degree of aggregation and location of silver nanoparticles within the polymer matrix in the obtained Ag@poly(Trithiol-TMPTA) nanoparticles and conjugation of bioconjugated gold nanoparticles onto the surface of poly(Trithiol-TMPTA) nanoparticles. The samples for the analysis were prepared as follows: an ultrathin 3nm carbon film on Lacey carbon film 300 copper mesh TEM grid was placed on top of the membrane filter inside the filter housing during the polymerization reaction for five minutes, collecting the nanoparticles. The TEM grids were analysed with a CM 200 TEM (Phillips, Amsterdam, Netherlands) microscope (operated on an acceleration voltage of 200 keV). The images were taken by zooming into individual nanoparticles or nanoparticle clusters.

UV-Vis spectrophotometry. The quantitative analysis in Ellman's test was carried out in 96 well UV-Star® microplates (Greiner Bio-One) using a Tecan Infinite® UV-VIS Spectrophotometer. Samples were prepared as follows: 5 mg of nanoparticles were dispersed in 1ml of PBS pH 7.4; 100 μ L of this dispersion was placed inside a well and 100 μ L of DTNB dissolved in PBS pH 7.4 was added to the same well. The absorption measurements were carried out at 412 nm wavelength at 22°C.

Fluorescence Spectroscopy (FS). Fluorescent properties of fluorescein-maleimide-labelled nanocomposites were analysed using an OceanOptics Maya2000 Pro (Ocean Insight) fibre optic spectrophotometer with a quasi-monochromatic LED, $\lambda_{\text{max}} = 365 \text{ nm}$ (HAMAMATSU, LC1) and a long-pass filter (cut on 400 nm). Samples were prepared by placing 2.5 ml of the appropriate solution/dispersion into 10 mm Hellma™ Suprasil™ cuvettes.

Fluorescence Microscopy (FM). Fluorescein-maleimide and Fluorescein-Streptavidin labelled nanocomposites were visualized using Olympus IX81F-ZDC2 Confocal Laser Scanning Microscope (Olympus) at 405 nm and 488 nm, respectively. A 525/50 Filter was used during the analysis. Sample preparation for fluorescence microscopy included dispersion of labelled nanocomposites in appropriate solvents (EtOH or PBS), placing 50 μL of this dispersion onto the 76x26 mm (thickness 1mm) microscope slides covered with 18x18mm cover glass.

4.3. Results and discussion

4.3.1. *Silver@poly(thio-ether) nanoparticle hybrids*

Uncoated silver nanoparticles (AgNPs) are prone to aggregate in dispersed media in presence of alkenes and other compounds [196], depending on pH, ionic strength and electrolyte composition of the dispersion [197]. Therefore, stabilization techniques are required to prevent their aggregation. Among several stabilization mechanisms available steric and electrostatic stabilization methods have shown to be more effective in preventing the aggregation of silver nanoparticles [198]. In the present study, stabilization with $\pm\alpha$ -lipoic acid [199] and steric stabilization with 11-mercapto-1-undecanol [200] were examined.

Various grades of AgNPs were considered in order to establish a convenient method of synthesis. Ink dispersion of silver nanoparticles in tripropylene glycol monomethyl ether (AgINK) was one of the most available and cost-effective variants. Polyvinylpyrrolidone (PVP) coated dried silver nanospheres (Ag25nm and Ag50nm) although less cost-effective, provided stabilized silver nanoparticles less prone to aggregation. 70-90% of the weight of Ag25nm and Ag50nm was PVP and only 10-30% was silver. Ag25nm and Ag50nm also possessed narrow particle size distributions, whereas AgINK revealed a broad size distribution and various shapes of nanoparticles (small triangles, ovals, squares). Therefore, the stabilization of AgINK was the primary goal.

The first step in every experiment was to stabilize the dispersion of monomers and AgINK. Several experiments showed aggregation of nanoparticles into visible flakes during the first 30 minutes of the atomization process. The attempts to stabilize the nanoparticles in dispersion included use of different stabilizers, dialysis with other solvents, as well as intermittent sonication. Nanoparticle hybrids obtained from NC-1 (no silver stabilization) formulation have shown

aggregation of silver nanoparticles employing TEM (see *Figure 4. 3.*). In addition, silver nanoparticles appeared on the SEM (and the TEM) images on the surface of nanoparticles – they are not completely encapsulated inside the polymer matrix, which might be an issue in biomedical applications. The formation of flakes (big aggregates of silver nanoparticles) in the spray solution

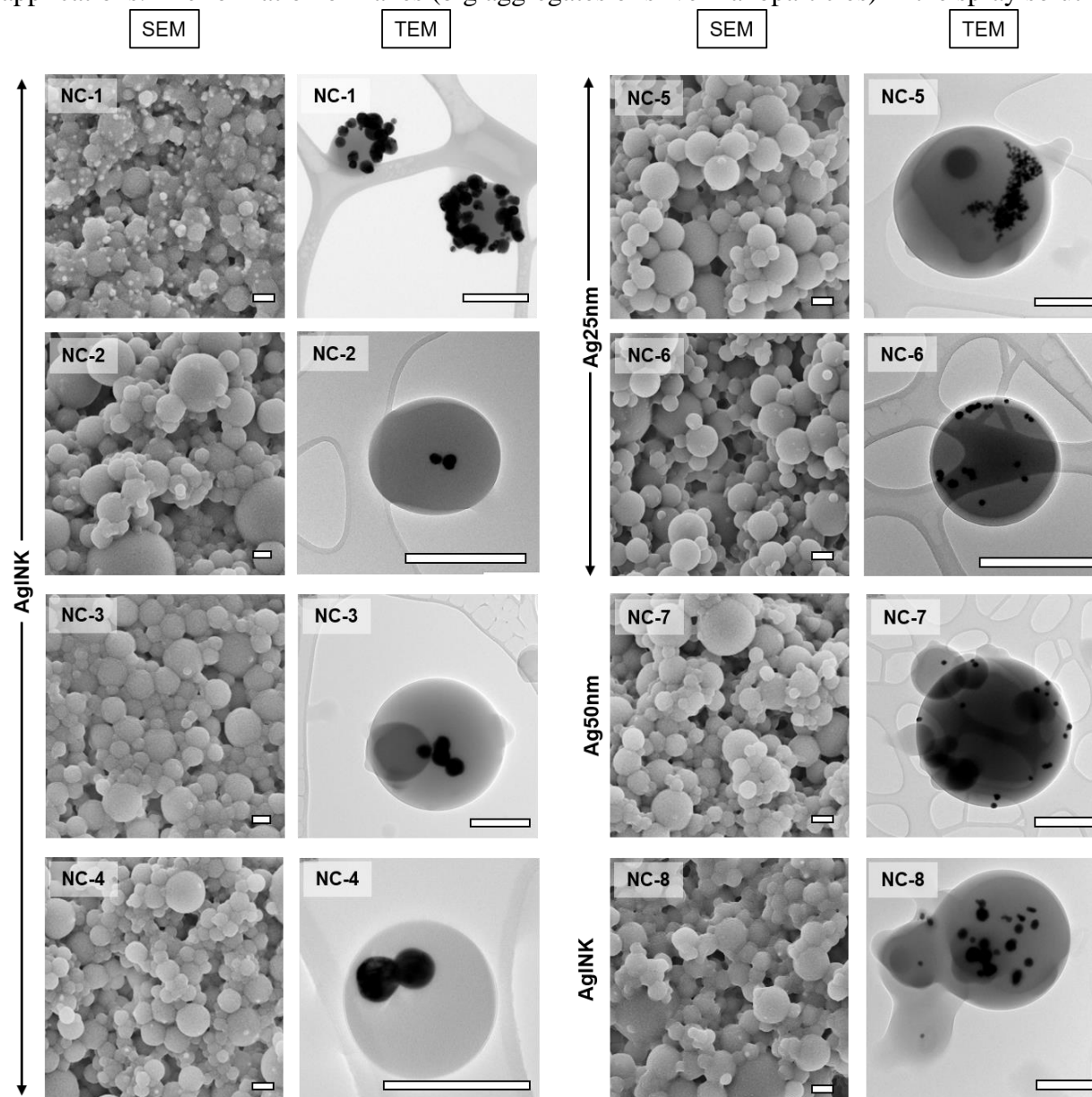


Figure 4. 3. SEM and TEM images of the Ag@poly(Trithiol-TMPTA) nanoparticles produced via Aerosol Photopolymerization. The nomenclature corresponds to spray solution formulations presented in Table I. Black particles on TEM represent silver nanoparticles, the grey spheres represent polymer layer. The small radiant white spots on SEM represent the silver nanoparticles, whereas bigger grey speres are polymer matrix. The scalebars correspond to 0.5 μ m. Vertical labels on the left correspond to the type of silver nanoparticles used in the reaction and agrees with the data in Table 4. 1.

during the photopolymerization process can be associated with the observation of silver nanoparticle aggregates on the surface as well as within the polymer (image not presented).

The aggregation behavior of silver nanoparticles is well studied [196, 198]. According to research by Guzman-Soto *et al.* [201] α -LA can improve the oxidative stability of silver nanoparticles. AgINK stirred in combination with EtOH and α -LA for 30 min prior to the atomization process showed better stability of the spray solution throughout the reaction. The nanohybrids obtained from this photopolymerization process showed a lower tendency to aggregation of AgNPs (**Figure 4. 3**, NC-2). The addition of α -LA to the spray solution showed minimal change in the appearance of polymer nanoparticles on the SEM, although it was discovered during this research that there is a certain concentration of α -LA beyond which the polymer nanoparticles showed to start the agglomeration. Therefore, the concentration of α -LA was kept in a range of 10-15 mL of 10 mM solution (in EtOH). Stabilization with α -LA resulted in superb stabilization of AgINK and full encapsulation inside polymer nanoparticles, but very small quantities of silver nanoparticles were observed inside polymer nanoparticles on TEM images.

Other methods of silver nanoparticles stabilization were considered as well. 11-Mercapto-1-undecanol (MUL) was used as a steric stabilizer for silver nanoparticles in ink [202]. MUL showed substantial improvement of the dispersion of silver nanoparticles within the polymer matrix. In comparison to α -LA, silver nanoparticles with MUL show a lower tendency for aggregation. This can be explained by the formation of a MUL layer around the silver nanoparticles [202]. TEM images reveal that the silver nanoparticles are both individual and fully encapsulated inside the polymer matrix (**Figure 4. 3**, NC-3). In addition, silver nanoparticles were not present on the surface of polymer nanoparticles in SEM images.

Stabilization via sonication of silver nanoparticle dispersions was attempted to break down the aggregates of silver formed during the aerosol generation process. Ultrasonic agitation of the spray solution resulted in the temporary breaking of aggregates of silver nanoparticles but had to be repeated every 30 minutes as aggregates redeveloped. SEM and TEM images (**Figure 4. 3**, NC-4) of nanocomposites from sonicated spray solutions show reduced aggregation of silver nanoparticles compared to non-sonicated spray solutions (NC-1).

The influence of the solvent on the formation of polymer nanoparticles and aggregation of silver nanoparticles was studied by replacing ethanol with 1-propanol. SEM images of the hybrid nanoparticles particles (**Figure 4. 3**, NC-8) obtained from the spray solution with 1-propanol showed increased agglomeration of the polymer nanoparticles, whereas the silver nanoparticles exhibited lowered aggregation and full encapsulation within the polymer matrix. Some silver nanoparticles still appeared outside the polymer nanoparticles. The TEM image of lower magnification (with several polymer nanoparticle hybrids is presented in **Figure S4.1**). Only one image of NC-8 polymer nanoparticle hybrids is shown as an example of how the hybrids are observed on a TEM image from a lower magnification, proving that the majority of polymer hybrid had an average amount of silver nanoparticles inside (3–4 AgNPs per hybrid). However, some smaller polymer particles appear to have no AgNPs.

PVP-coated silver nanoparticles are of higher quality than AgINK nanodispersion; Ag25 and Ag50 NPs did not require predispersion due to the PVP coating that prevented aggregation of silver nanoparticles in the spray solution. Nevertheless, the PVP coating makes up for 70-90% of Ag25nm and Ag50nm nanoparticles, which might be a downside for potential applications. Ag25nm and Ag50nm behaved differently when incorporated in the polymer matrix. Samples with Ag25nm (**Figure 4. 3**, NC-5) showed high amounts of aggregates of silver nanoparticles, but a lower aggregation of silver NPs was observed when α -LA was added (**Figure 4. 3**, NC-6), whereas Ag50nm (**Figure 4. 3**, NC-7) samples revealed desired individual and well-distributed silver NPs within the polymer matrix.

The size distributions of silver nanoparticles, gold nanoparticles and polymer nanoparticle hybrids are presented in Supporting information (**Figure S4.2**). In **Figure S4.2. A**, a histogram of NC-7 polymer nanoparticle hybrids is presented, where d_{50} of the particles is 325 nm. The size of the nanoparticle hybrids can always be narrowed by varying the parameters of the aerosol photopolymerization, e.g., solvent amount. As presented in our previous work [178], increasing solvent amount of the spray solution the size of polymer nanoparticles can be narrowed to fit appropriate applications.

Figure S4.2.C shows the size distributions of AgINK, Ag50 nm, and Ag25 nm nanoparticles, to show the advantages of using Ag50 nm for further applications due to the narrower size distribution, compared to AgINK, where the size distribution is very broad. However, more experiments were carried out with cost-effective AgINK nanoparticles compared to more expensive and purer Ag50 nm.

Encapsulation of silver nanoparticles inside the polymer matrix is a possible strategy of stabilization, eliminating their cytotoxicity in future applications [84].

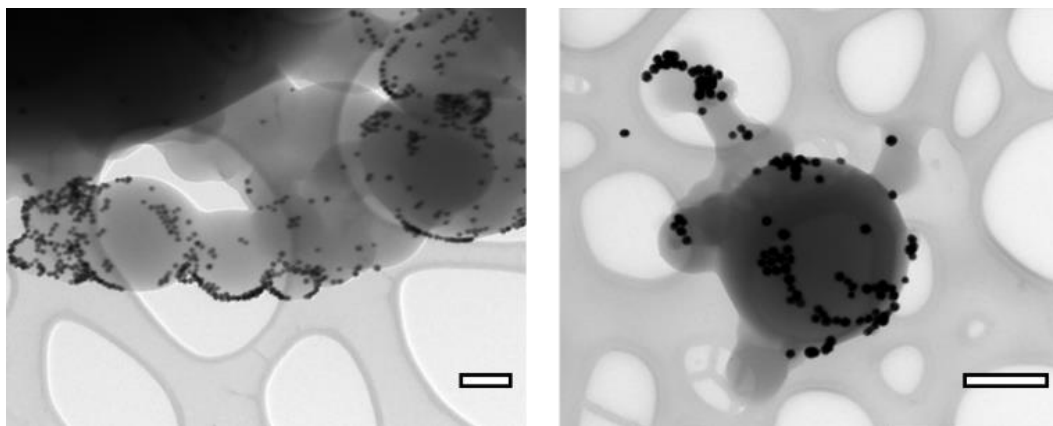


Figure 4. 4. Maleimide-gold NPs conjugated to poly(Trithiol-TMPTA) nanoparticles (left) and Streptavidin-gold NPs conjugated to bM-poly(Trithiol-TMPTA) nanoparticles (right) as an evidence of presence of reactive $-SH$ groups on the surface of these nanoparticles (for Au-Mal@poly(Trithiol-TMPTA)) and effective biotin-Streptavidin bonding (for Au-Strep@bM-poly(Trithiol-TMPTA)). The scalebars correspond to $0.5\mu\text{m}$.

4.3.2. Nanoparticle binding sites

To visualize the presence of the accessible binding sites on the surface of polymer nanoparticles employing TEM, a one-step conjugation to gold NPs-maleimide (Au@Mal) and a two-step conjugation to biotin-maleimide and gold NPs-streptavidin (Au@Strep) were carried out. The conjugation to Au@Mal resulted in the formation of polymer nanoparticles with many gold nanoparticles located on the surface of the polymer (**Figure 4. 4**, left). This evinces the presence of reactive -SH groups. The two-step conjugation (1. biotin-maleimide, 2. streptavidin-gold) leads to the conclusion that a sufficient number of binding sites on the polymer nanospheres is available (**Figure 4. 4**, right). From the presented results, the number of binding sites in one-step conjugation seems higher than in a two-step conjugation process. This might be a result of higher steric accessibility of Au@Mal to the -SH groups, compared to the bulkier streptavidin in Au@Strep. Sizes of Au@Mal and Au@Strep nanoparticles were evaluated via image analysis of TEM micrographs and the size distributions of these nanoparticles are presented in **Figure S4.2 B**.

4.3.3. Bioconjugation of silver@poly(thio-ether) nanoparticle hybrids

The presence of reactive -SH was also tested via Ellman's reaction. Solution of DTNB mixed with the dispersion of nanoparticles results in distinctive yellow coloration. To ensure that the coloration is not due to unreacted thiol monomers within the polymer matrix, a purification procedure was carried out in acetone (centrifugation, 10000 g, 3x20 mL). Purified and non-purified nanoparticles show different results with DTNB. In **Table 4. 2.** absorption of DTNB and nanoparticles (reacted with DTNB) at 412 nm are shown. Absorption of 0,7 mM DTNB (the reagent solution) is presented for comparison. The concentration of -SH groups is calculated using the Beer-Lambert law, taking $14500 \text{ M}^{-1} \text{ cm}^{-1}$ as the extinction coefficient for DTNB in buffer solutions of pH = 7.4. The stray light correction and absorption contrast were carried out with poly(TMPTA) nanoparticles. Purification of the nanoparticles results in an about ten-fold decrease of determined -SH groups within the polymer matrix of the nanoparticles. This decrease can be due to oxidation of -SH groups during purification procedure and/or removal of unreacted thiol monomers from the nanoparticles during purification.

Silver-polymer nanocomposites were conjugated with fluorescein labelled maleimide (i-FM), and with biotin-maleimide (b-M) and fluorescein labelled streptavidin (425-St), sequentially. Functionalization with maleimide-fluorophore was considered to confirm the presence of -SH groups on the nanoparticles, whereas functionalization with streptavidin-fluorophore confirms the possibility of a multi-step conjugation. Functionalized maleimide reacts with thiol groups of nanoparticles via thiol-Michael addition in a one-step (bio)conjugation. The basis of the first step of the two-step bioconjugation is also thiol-ene "click" chemistry (biotinylation), whereas the second step is biotin-streptavidin binding (**Figure 4. 1.**). The successful formation of

bioconjugated particles was visualized by Fluorescence Spectrometry (FS) and Fluorescence Microscopy (FM).

Table 4. 2. Absorption and approximate concentration of free -SH groups in purified and non-purified nanoparticles

Sample	Absorption	Concentration of -SH (M/mg)
DTNB (0.7 mM)	0.2056	-
Purified NPs (1mg/ml)	0.2793	0.009×10^{-3}
Non-purified NPs (1mg/ml)	0.8896	0.087×10^{-3}

Purified fluorescence-labelled nanoparticle hybrids (NC-7-i-FM) show intense fluorescence with a maximum at ~430 nm via FS (**Figure 4. 5**, left). The fluorescence spectrum of pure i-FM in DMSO shows a narrow peak at 434 nm. This peak can also be well observed for supernatants of the first four purification steps. The apparent stray light peak of NC-7-i-FM is due to the presence of nanoparticles in purified dispersion and can be observed in **Figure 4. 5**. ($\lambda_{\max} \approx 385$ nm), in contrast to the supernatant spectrum. FM images of these nanoparticles at 405 nm excitation wavelength also showed the presence of nanoparticles tagged with fluorescence label (**Figure 4. 5**, right). No fluorescence was observed for non-conjugated nanoparticle hybrids (NC-7, not presented).

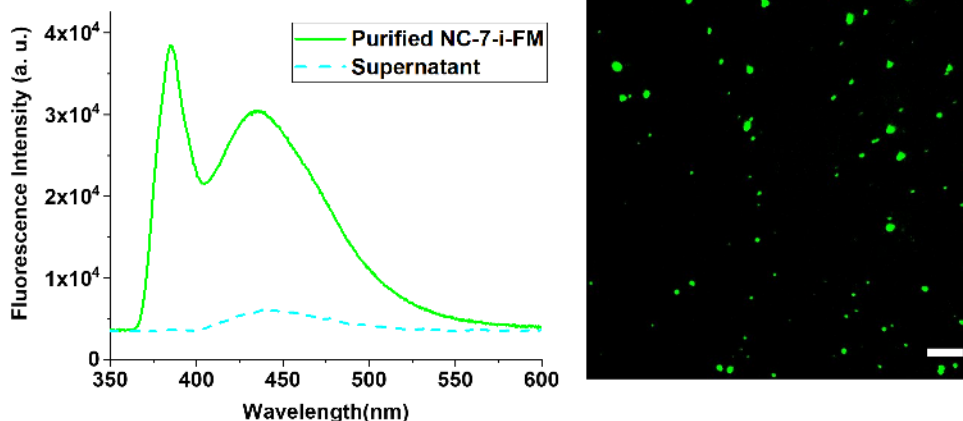


Figure 4. 5. Fluorescence Spectra (left) and Fluorescence Microscopy image (right) of *i*-Fluor-Maleimide conjugated NC-7 nanoparticles (NC-7-i-FM). The solid green line represents the spectrum of purified NC-7-i-FM NPs dispersed in ethanol (1mg/5mL) and the dashed blue line represents the spectrum of the last supernatant of these nanoparticles after the purification. Fluorescence microscopy image ($\lambda_{em}=405$ nm, scalebar 10 μ m) confirms that the NC-7-i-FM nanoparticles are the cause of fluorescence and sporadic agglomerates of the nanoparticles can be observed.

The degree of conjugation of b-M to the nanoparticles is unknown, but the results of the subsequent reaction with 425-St evince presence of fluorescence-labelled material (see **Figure 4. 6**). The nanoparticles at 405 nm excitation wavelength are not as well dispersed as for NC-7-i-

FM. In the reaction of NC-7-b-M with 425-St a PBS solution was used instead of DMSO to control the pH and ionic strength of the experiment, following the recommendations of the supplier of 425-St. The NC-series nanoparticle composites dispersed in polar solvents such as PBS form flakes, in contrast to a stable dispersion of these nanocomposites in DMSO. Therefore, the microscopy analysis did not show well-dispersed nanoparticles. Fluorescence spectra show an apparent stray light peak of NPs at ~ 385 nm and a fluorescence peak at ~ 475 nm in the purified dispersion of (NC-7-b-M-St) streptavidin-conjugated nanoparticles, which confirms successful two-step bioconjugation.

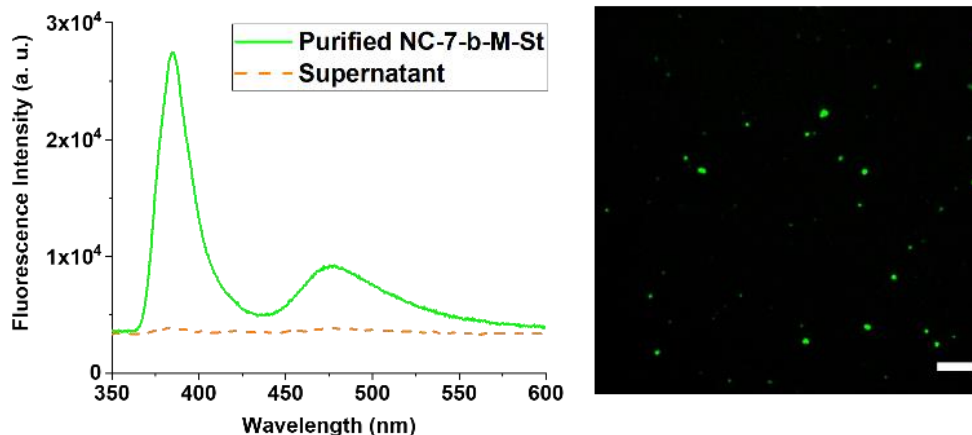


Figure 4. 6. Fluorescence Spectra (left) and Fluorescence Microscopy image (right) of biotin-maleimide and Atto-425-Streptavidin conjugated NC-7 (NC-7-b-M-St) nanoparticles. The solid green line represents the spectrum of purified NC-7-b-M-St NPs dispersed in 3% DMSO in 100mM phosphate buffer (pH 7) (1mg/5mL) and the dashed red line represents the spectrum of the last supernatant of these nanoparticles after the purification. Fluorescence microscopy image ($\lambda_{em}=450$ nm, scalebar $10\mu\text{m}$) confirms that the NC-7-b-M-St nanoparticles are the cause of fluorescence and sporadic agglomerates of the nanoparticles can be observed.

The above-presented fluorescence spectroscopy and microscopy results evince the availability and accessibility of functional -SH groups on the surfaces of Ag@poly(Trithiol-TMPTA) nanoparticle hybrids and their subsequent biofunctionalization. We anticipate that the cytotoxicity of silver nanoparticles is reduced due to the availability of -SH groups within the polymer matrix. They have a high adsorption capacity of Ag^+ , subsequently stabilizing the AgNPs [203] and suppressing their cytotoxicity. The reactive SH-groups are an otherwise effective tool for the functionalization of complex biomolecules e.g., to target cancer cells specifically. The size of the produced nanocomposites can be toggled [178] to match the specific applications.

4.4. Conclusion

Hybrid nanomaterials are systems that combine unique physical and chemical properties of their single components and thus can be used for various applications. It is necessary to look for convenient, sustainable methods of synthesis, control physical properties and investigate the range of new possible applications of the hybrid nanomaterials.

Aerosol thiol-ene photopolymerization provides an easy, non-toxic, eco-efficient method for the synthesis of spherical polymer matrix nanocomposites with silver nanoparticles inside. As with many metal nanoparticles, stabilization of silver nanoparticles was required to avoid their aggregation. All stabilization strategies studied in this paper proved to be effective in forming individual silver nanoparticles well dispersed within the polymer matrix. The application of α -Lipoic acid provided slightly better results, compared to 11-mercapto-1-undecanol and stepwise sonication of cost-effective AgINK. Polyvinylpyrrolidone-coated silver nanoparticles (Ag25nm) should be stabilized with α -LA for the synthesis of nanocomposites with well-dispersed silver nanoparticles. Ag50nm did not require any additional stabilizer. Ag50nm showed exceptional compatibility with aerosol thiol-ene photopolymerization for the synthesis of hybrid nanoparticles.

The obtained nanocomposites possess -SH groups on their surface and can, thus, be used in bioconjugation. The reactivity of binding sites was successfully confirmed by using gold-tagged and fluorescence-labelled biomolecules.

Nanoparticle hybrids produced in this study can find applications in cancer diagnostics and treatment, as well as many other areas of biomedicine and biosensors.

5. Immobilization of β -galactosidase by encapsulation of enzyme-conjugated polymer nanoparticles inside hydrogel microparticles

N. Suvarli, L. Wenger, C. Serra, I. Perner-Nochta, J. Hubbuch, M. Wörner*

Karlsruhe Institute of Technology (KIT), Institute of Process Engineering in Life Sciences,
Section IV: Biomolecular Separation Engineering, Karlsruhe, Germany

*Corresponding author

Abstract

Increasing the shelf life of enzymes and making them reusable is a prominent topic in biotechnology. The encapsulation inside hydrogel microparticles (HMPs) can enhance the enzyme's stability by preserving the native conformation and facilitating continuous biocatalytic processes and enzyme recovery. In this study, we present a method to immobilize β -galactosidase by, first, conjugating the enzyme onto the surface of polymer nanoparticles and then encapsulating these enzyme-conjugated nanoparticles (ENPs) inside HMPs using microfluidic device paired with UV-LEDs. Polymer nanoparticles act as anchors for enzyme molecules, potentially preventing their leaching through the hydrogel network especially during swelling. The affinity binding (through streptavidin-biotin interaction) was used as an immobilization process of enzyme on the surface of polymer nanoparticles. The hydrogel microparticles of roughly 400 μm in size (swollen state) containing unbound enzyme and ENPs were produced. The effects of encapsulation and storage in different conditions were evaluated. It was discovered that the encapsulation in acrylamide (AcAm) microparticles caused an almost complete loss of enzymatic activity. Encapsulation in poly(ethylene glycol)-diacrylate microparticles, on the other hand, showed a residual activity of 15-25 %, presumably due to a protective effect of PEG during polymerization. One of the major factors that affected the enzyme activity was presence of photoinitiator exposed to UV-irradiation. Storage studies were carried out at room temperature, in the fridge and in the freezer throughout 1, 7 and 28 days. The polymer nanoparticles showcased excellent immobilization properties and preserved the activity of the conjugated enzyme at room temperature (115 % residual activity after 28 days), while a slight decrease was observed for the unbound enzyme (94 % after 28 days). Similar trends were observed for encapsulated ENPs and unbound enzyme. Nevertheless, storage at $-26\text{ }^{\circ}\text{C}$ resulted in an almost complete loss of enzymatic activity for all samples.

Keywords: hydrogels, polymer, nanoparticles, immobilization, enzyme, microfluidics, bioconjugation

5.1. Introduction

Catalytic properties of enzymes are applied in many fields of modern science and industry: chemical synthesis [204], pharmaceuticals [205], food [206], feed [207], detergent [208], textile [209] industries, and many more [210, 211]. β -D-Galactosidase (or lactase) is an enzyme present in the human intestine that catalyzes the hydrolysis of lactose and breaks it down into glucose and galactose [212]. However, a large part of the global adult population lacks adequate levels of β -galactosidase for the digestion of milk-based products. β -Galactosidase extracted from microbial sources is one of the most relevant enzymes in the food industry and is used in the production of dairy products like ice cream and cheese or for whey hydrolysis [213].

The widespread applications of enzymes call for the prolongation of their shelf life, reusability, and structural stability [214], and the use of enzymes on an industrial scale requires optimizations of their properties. The immobilization is a physical or chemical confinement of the enzyme in an environment that can allow its reuse [98]. In addition, immobilization facilitates the removal of the enzyme from the product, thereby avoiding product contamination. The choice of the immobilization method should always consider the effect on the structure of the enzyme and its native biological function [103]. The immobilization of enzymes can be achieved via adsorption, affinity binding, covalent attachment, chemical aggregation, entrapment, or encapsulation [103]. Affinity binding is an immobilization technique based on physical interactions with an excellent selectivity and minimal changes of the enzyme's conformation [101]. This type of binding provides high retention of the enzyme activity [215]. Hydrogels and hydrogel beads [216-218] have already demonstrated their suitability for the immobilization of enzymes. Nanoparticles are also widely used to immobilize enzymes [13, 219].

Immobilization of β -D-galactosidase via adsorption is a simple method that supposedly involves ionic interactions, thereby making the effectivity of the immobilization and the enzyme activity yield susceptible to small changes in the nature of the enzyme or the buffer [220]. Entrapment immobilization of β -D-galactosidase tends to improve pH and temperature stability, but the supports used for this immobilization technique cannot be reused when the enzyme activity is lost [221]. Many commercially available supports have been introduced over the years for covalent binding immobilization. On one hand, this method is one of the most studied immobilization techniques for β -D-galactosidase; on the other hand, it usually requires an additional treatment of the support with a reactive compound [213].

Nanomaterials are suitable carriers for enzyme immobilization due to their chemical stability, high loading density (due to their large surface area), low minimal mass transfer resistance, etc. [13, 222]. Immobilization on magnetic nanoparticles may improve the activity of the enzyme and its tolerance to pH, temperature and substrate concentration [223]. Nanoparticles

based on gold [224] and titanium oxide [225] among other systems have shown substantial improvement in catalytic properties in the process of bioenzymatic nanoimmobilization. Polymer nanomaterials, such as chitosan nanoparticles [226] and poly(methyl methacrylate) [227] nanoparticles have many benefits as support materials for enzyme immobilization: easy synthesis methods (usually one single reaction) and high colloidal stability in suspension.

Aerosol photopolymerization is an easy, eco-efficient and continuous method for the synthesis of polymer nanoparticles that does not require the use of hazardous organic solvents, surfactants, or heating [22]. In other methods, e.g. emulsion polymerization, additional separation procedures are required to obtain pure nanoparticles for conjugation of the enzyme. The combination of aerosol photopolymerization with thiol-ene monomers ensures the synthesis of spherical cross-linked polymer nanoparticles with reactive -SH groups [178] that are not present on other types of nanoparticles, such as silicon or gold nanoparticles. A two-step bioconjugation process that can bind various biomolecules onto -SH-groups of polymer nanoparticles via thiol-ene “click” reactions was previously introduced [228].

Immobilizing enzymes via entrapment in hydrogel microparticles is another method to preserve enzymatic activity for long periods of time. Poly(ethylene glycol) (PEG)-based hydrogels have found many biotechnological applications due to their high water content, hydrophilicity, and biocompatibility [229]. Enzymes encapsulated inside hydrogel microparticles made from interpenetrating polymer networks of PEG and poly(acrylamide) have not shown a significant loss of activity [218]. Some other hydrogels have even shown enhancement of the activity of encapsulated enzyme compared to the unbound enzyme [128].

Microfluidic devices are state-of-the-art systems that (in combination with curing) can be used to produce polymer particles from monodisperse emulsions [230]. Among other benefits, avoiding the use of surfactants and easy control of the particle size are fundamental advantages for the application of the device in this study. Particles of different shapes, sizes and compositions can be produced by changing the design and parameters of the microfluidic system [122]. Previous research has already succeeded in encapsulating gold and silver nanoparticles inside polymer microparticles using microfluidic devices [126]. *Dang et al.* have successfully encapsulated polystyrene-based microbeads inside monodisperse hydrogel microparticles using a flow-focusing microfluidic device paired with a UV-irradiation source [231].

In this study, the activity of β -galactosidase immobilized by bioconjugation on the surface of polymer nanoparticles and encapsulated inside hydrogel microparticles was investigated. The combination of immobilization methods (conjugated on nanoparticles and encapsulated in hydrogel) aims at identifying synergistic effects. Nanoimmobilization preserves the enzyme's activity for a long time; encapsulation in hydrogel microparticles preserves the enzyme's native conformation and offers reusability.

Polymer nanoparticles were synthesized via aerosol thiol-ene photopolymerization. The accessible -SH groups on the surface of these polymer nanoparticles offer an effective way of bioconjugation through a thiol-ene “click” reaction with maleimide-biotin and subsequent addition of streptavidin derivatives [178, 228]. An affinity binding immobilization technique was applied

with biotin-conjugated nanoparticles and a commercially available streptavidin- β -galactosidase. The conjugated nanoparticles were then introduced into a hydrogel precursor solution. This suspension was used as a dispersed phase in microfluidic emulsion photopolymerization to produce hydrogel microparticles with enzyme-conjugated nanoparticles inside. The impact of the encapsulation in different hydrogels on enzymatic activity was studied and the impact of hydrogel components in enzymatic inactivation was evaluated. Storage studies at different temperatures were performed to investigate the long-term stability of the produced microparticles compared to free unbound enzyme and enzyme-conjugated polymer nanoparticles.

5.2. Materials and Methods

5.2.1. Chemicals

Trimethylolpropane tris (3-mercaptopropionate) (**Trithiol**, Sigma-Aldrich, 95 %) and trimethylpropane triacrylate (**TMPTA**, Sigma-Aldrich, contains 600 ppm monomethyl ether hydroquinone as inhibitor) were used as thiol and alkene monomers in aerosol photopolymerization. 2-Methyl-4'-(methylthio)-2 morpholinopropiophenone (**MT-2MP**, Sigma-Aldrich, 98 %) was used as a photoinitiator in the aerosol photopolymerization process. Biotin-Maleimide (**b-M**, ≥ 95 % (TLC) powder, Merck KGaA) and streptavidin- β -galactosidase (**E**, 150 units/mg, ThermoFisher Scientific) were used for bioconjugation reactions. β -Galactosidase from *Aspergillus oryzae* (**β -gal**, ≥ 8 units/mg solid, Sigma-Aldrich), 2-nitrophenol (**ONP**, Sigma-Aldrich) and 2-nitrophenyl β -D-galactopyranoside (**ONPG**, ≥ 98 %, enzymatic, Sigma-Aldrich) were used for enzyme activity assays. Poly(ethylene glycol)-diacrylate (**PEG-DA**, average Mn 575, Sigma-Aldrich), acrylamide (**AcAm**, ≥ 99 %, Sigma-Aldrich), N, N'-methylene bis(acrylamide) (**BisAc**, 99 %, Sigma-Aldrich) and lithium-phenyl-2,4,6-trimethylbenzoylphosphinate (**LAP**, ≥ 95 %, Sigma-Aldrich) were used in the dispersed phase of the microfluidic device to produce hydrogel microparticles. Silicone oil (viscosity 500 cst at 25 °C, Sigma-Aldrich) was used as a continuous phase. Poly(ethylene glycol) Mn 600 (**PEG**, for synthesis, Merck) was used as a non-reactive alternative of PEG-DA for exposure studies. Phosphate buffer (100 mM, pH 7) was prepared using 38 mM Na₂HPO₄ and 68 mM NaH₂PO₄.

5.2.2. Experimental methods

Synthesis of polymer nanoparticles

Polymer nanoparticles (50-1000 nm) were synthesized via aerosol thiol-ene photopolymerization. Trithiol and TMPTA monomers were utilized in 1:1 stoichiometry of functional groups (3*SH:3*C=C) in order to achieve spherical and individual nanoparticles. 1.15

g of Trithiol and 0.85 g of TMPTA were combined in a spray solution flask, 40 g of ethanol (EtOH) was added to the flask and stirred, followed by 0.02 g of MT-2MP photoinitiator. The spray solution flask was then placed inside the aerosol generator (TOPAS®, ATM220) which was connected to the photoreactor consisting of two UV-fluorescent devices (T-15.C, Vilber Lourmat, $\lambda_{\text{max}} = 312 \text{ nm}$) facing each other and a tube reactor located in between the UV-light sources. The mean residence time of the aerosol inside the reactor was 28 s. One 2-hour reaction resulted in almost 100 mg of polymer nanoparticle powder collected on 0.1 μm pore size Durapore® hydrophobic membrane filters.

Bioconjugation of polymer nanoparticles

The polymer nanoparticles produced via aerosol thiol-ene photopolymerization were tested for the presence of reactive -SH groups with Ellman's reaction. After the test confirmed the presence of -SH groups, the polymer nanoparticles were introduced into a two-step bioconjugation reaction: first, conjugation of biotin-maleimide (biotinylation) via thiol-Michael addition reaction, and second, conjugation of streptavidin- β -galactosidase to biotin (**Figure 5.1**).

For the bioconjugation with biotin-maleimide (b-M), 10 mg of dry polymer nanoparticles were dispersed in 9 mL of buffer (3 vol.% of dimethylsulfoxide (DMSO) in 100 mM phosphate buffer, pH 7.0, from here on, referred to as a buffer). 5 mg of b-M was diluted in 1 mL of buffer and added dropwise to the dispersion of nanoparticles under vigorous stirring. The reaction was carried out for 20 hours. The produced dispersion was centrifuged at 15000 g for 10 min and the

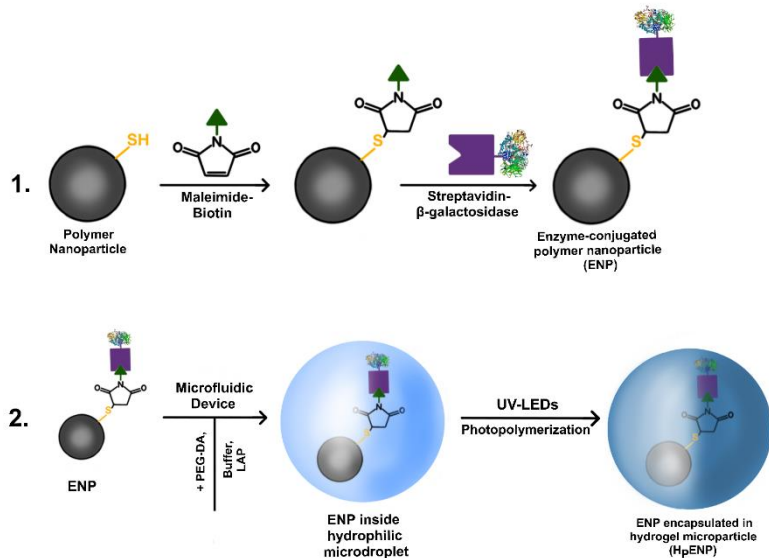


Figure 5. 1. A diagram of 1. immobilization of enzyme via two-step bioconjugation process, 2. encapsulation of enzyme-conjugated nanoparticles inside hydrogel microparticles using microfluidic device and UV-LEDs.

residual particles were purified with 3x10 mL of buffer to remove the unreacted biotin-maleimide. The purified nanoparticles were redispersed in buffer resulting in 10 mL of a 1 mg/mL dispersion for the next bioconjugation step.

The second step of the bioconjugation was carried out with 50 units of streptavidin- β -galactosidase diluted in 1 mL of buffer. The solution was added dropwise to the dispersion of b-M-conjugated polymer nanoparticles under mild stirring. The reaction was carried out for 28 h. The resulting ENPs mixture was purified via centrifugation at 10000 g for 10 minutes with 3x10 mL of buffer. The enzymatic activity of the supernatants of each purification step and the purified nanoparticles were tested via enzymatic activity assays using ONPG as substrate.

To assess the necessity of the two-step bioconjugation and to exclude the possibility of unspecific binding of the enzyme to the nanoparticles, a control experiment was performed with β -galactosidase instead of streptavidin- β -galactosidase (E). The nanoparticles (10 mg) were dispersed in 4.5 mL of buffer and 0.5 mL of enzyme solution (15 units/mL) was added to the dispersion. The mixture was incubated for 28 h under the same conditions as the second step of the two-step conjugation. The purification of E_{control}NPs was also carried out following the purification protocol of ENPs.

Synthesis of hydrogel microparticles via microfluidic device

An axisymmetric needle/tubing microfluidic device [230] with a set of UV-LED spots, as pictured in **Figure 5. 2**, was employed to produce microdroplets and polymerize them resulting in hydrogel microparticles. Dispersed phase (1) was introduced through a micro-scale diameter capillary (7), and the continuous (2) phase was introduced perpendicularly. The microfluidic device consisted of a set of polytetrafluorethylene (PTFE) tubes (0.75 mm inner diameter (ID), Upchurch Scientific) (3), and perfluoralkoxy-alkane (PFA) tubes (1.59 mm ID, Upchurch Scientific), a PEEK connection unit (0.020 inch ID, Upchurch Scientific) (4), a PEEK T-junction (0.040 inch ID, Upchurch Scientific) (5), a flexible fused silica capillary (150 μ m ID, 363 μ m outer diameter (OD), TSP standard polyimide coating, Molex®) (7) and a capillary sleeve (for 340-380 μ m capillaries, Upchurch Scientific) (6). Microdroplets were formed on the tip of the capillary and irradiated with an intensity of 17.5 mW/cm² by a set of four UV-LEDs (single color

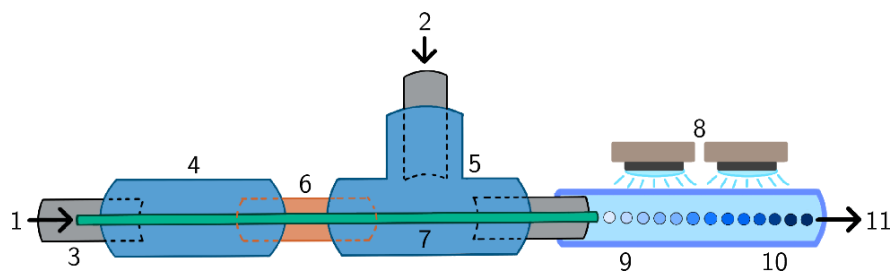


Figure 5. 2. Schematic representation of the microfluidic device. 1) Dispersed phase inlet, 2) continuous phase inlet, 3) PTFE tube, 4) connection unit, 5) T-junction, 6) capillary sleeve, 7) capillary, 8) UV LEDs, 9) microdroplets, 10) microparticles, 11) outlet.

365 nm LZ4 emitter, If,max = 1000 mA, LED Engin) connected in series (8). The irradiation initiated the photopolymerization reaction of the microdroplets (9) resulting in polymer microparticles (10). The dispersed phase was loaded into a 5 mL syringe which was placed inside a Nemesys 290N syringe pump (Cetoni GmbH). The silicone oil was loaded into a 20 mL syringe which was placed inside the syringe pump, as well. The flow rate of the hydrogel precursor solution was 0.05 mL/min, and the flow rate of the silicone oil was 1 mL/min. Under these settings, the microdroplets/microparticles were exposed to UV light for roughly 5 s.

Encapsulation of enzyme and enzyme-conjugated nanoparticles inside

hydrogel microparticles

To ensure the production of comparable samples of free unbound enzyme (E) and enzyme-conjugated nanoparticles (ENPs), the activities of the purified ENPs suspension and the E stock solution were determined. Based on the results, the concentrations of ENPs and E for the production of hydrogel microparticles were chosen to result in an equivalent final activity. The final concentration of 1 mg/mL ENPs corresponded to a free unbound enzyme concentration of 3.11 units/mL.

For ENPs encapsulated in PEG-DA hydrogel microparticles (H_PENPs) and AcAm hydrogel microparticles (H_AENPs) the concentrations of enzyme were chosen to be the same as for the unbound enzyme encapsulated inside PEG-DA hydrogel microparticles (H_PE) and AcAm hydrogel microparticles (H_AE).

For H_PENPs, 0.446 mL of dispersion of 5 mg/mL of enzyme-conjugated polymer nanoparticles in buffer was mixed with 2 g of PEG-DA, 2.5 g of buffer and 5 mg of photoinitiator (LAP). The final concentration of ENPs inside the hydrogel microparticles was roughly 1 mg/mL. Encapsulation of unbound enzyme into PEG-DA hydrogel microparticles (H_PE) was carried out with the same quantities of PEG-DA, buffer and LAP and 0.446 mL of buffer containing enzyme. The final concentration of E inside the hydrogel microparticles was roughly 3.11 units/mL.

For H_AENPs, 0.446 mL of dispersion of 5 mg/mL of enzyme-conjugated polymer nanoparticles in buffer was mixed with 2 g of AcAm, 0.2 g of BisAc, 2.5 g of buffer and 5 mg of LAP. Encapsulation of unbound enzyme into AcAm hydrogel microparticles (H_AE) was carried out with the same quantities of AcAm, BisAc, buffer and LAP and 0.446 mL of buffer containing enzyme. The resulting final concentrations of ENPs and E inside the AcAm microparticles were identical to the PEG-DA microparticles.

To purify the HMPs, the microparticle dispersion (in silicone oil) was centrifuged at 5000 rpm for 5 min and the silicone oil was physically removed. The residual oil was washed out with 20 mL of xylene three times. The remaining xylene was evaporated on air (for a short time to avoid drying of the hydrogel) and the HMPs were washed three times in buffer. The microparticles were then redispersed in buffer at a ratio of 1:1 by volume. It is important to

note that the microparticles were already slightly swollen (from washing cycles) when they were redispersed in buffer.

5.2.3. Analysis methods

Light microscopy

An inverted light and fluorescence microscope (Zeiss Axio Observer Z1, Carl Zeiss Microscopy GmbH) with EC Epiplan-Neofluar 2.5X M27 objective was used for imaging of the synthesized hydrogel microparticles in order to define their size and observe the success of encapsulation of ENPs inside the hydrogel microparticles. The swollen microparticles (purified with xylene and dispersed in buffer) were placed on microscope slides and the images were taken using the software ZEN blue (Version 3.3, Carl Zeiss Microscopy GmbH).

Scanning electron microscopy

The polymer nanoparticles synthesized via aerosol photopolymerization were analyzed with a LEO1530 scanning electron microscope (Carl Zeiss Microscopy GmbH). The dry nanoparticles were dispersed in acetone and distributed on silicon wafers which were sputtered with platinum. The images were taken at a working distance of 5.8 mm and an acceleration voltage of 5 kV.

Enzyme activity studies

The comparison studies were carried out with the following samples containing both free and immobilized enzyme:

- free unbound enzyme – streptavidin- β -galactosidase (**E**)
- free enzyme-conjugated polymer nanoparticles (**ENPs**)
- enzyme-conjugated polymer nanoparticles encapsulated in PEG-based hydrogel microparticles (**HPENPs**)
- enzyme-conjugated polymer nanoparticles encapsulated in AcAm-based hydrogel microparticles (**HAENPs**)
- unbound enzyme encapsulated in PEG-based hydrogel microparticles (**HPe**)
- unbound enzyme encapsulated in AcAm-based hydrogel microparticles (**HAe**)

Ten sets of microplates (96 well UV-Star®, Greiner Bio-One GmbH) were prepared with equal volumes of these samples (in triplicates with 40 μ L of buffer solution/dispersion per well). Samples with either buffer, AcAm-based or PEG-based microparticles (without

enzyme or ENPs, 1:1 volume concentration in buffer) were prepared in the same set of plates as the enzyme-containing samples to allow the generation of ONP calibration curves. All plates were sealed with adhesive aluminum foil (Axygen[®] PCR-AS-200) for storage. One plate was analyzed immediately after the preparation of the microparticles to establish a reference allowing the determination of relative activities. The remaining samples were stored at three different temperatures (-26 °C, 8 °C and 22 °C) for three different durations (1, 7 and 28 days) to analyze the change in enzymatic activity during storage. After the designated storage time, 100 μ L of different concentrations of ONP (0, 1, 2.5, 5, 7.5 and 10 mM) were added to the calibration samples and their absorbance at 460 nm was measured using a Tecan[®] Infinite M200 plate reader. The measurements of the required calibration data were followed by the analysis of the enzymatic activity. To determine the enzymatic activity, 100 μ L of 20 mM ONPG as a substrate were added to the enzyme-containing samples, and the absorbance at 460 nm was recorded at 25 °C for 60 min.

The results of the activity assays were evaluated using MATLAB R2020a (The MathWorks, Inc.). ONP calibration curves were generated from the absorbance data of the samples with known ONP concentration, as exemplarily shown in **Figure 5. 3. A**. Based on these curves, the ONP concentrations of the activity assays could be calculated. Examples of the absorbance data of three different samples (in triplicates) are shown in **Figure 5. 3. B** and the calculated ONP concentrations in **Figure 5. 3. C**. The resulting graphs of ONP concentration over time often showed an initially reduced slope, before reaching a slope maximum after a delay of several minutes. The maximum slope of a curve corresponds to the maximum enzymatic activity (a_{max}) and was determined for each sample individually by fitting the curve with a linear fit in a 12 min

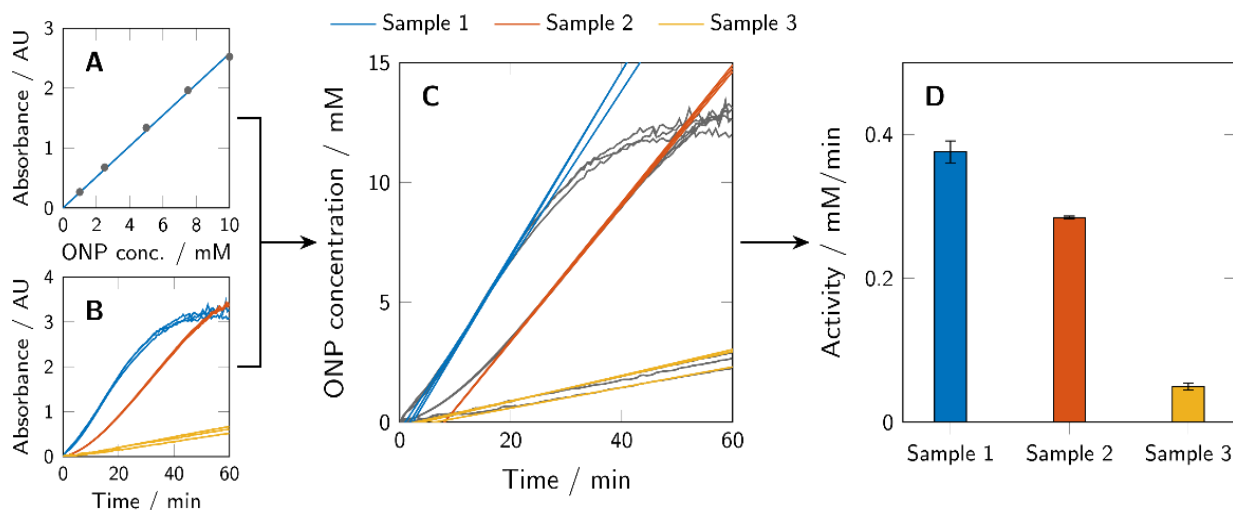


Figure 5. 3. Graphic representation of the activity assay evaluation method. ONP calibration curves were calculated from known ONP samples (A) to transform the obtained absorbance data of the activity assays (B) to ONP concentration profiles over time (C). The maximum activity of a sample (a_{max}) corresponds to the maximum slope of the respective curve and was determined using a 12 min rolling-window analysis. The obtained values of the maximum activity were presented using bar plots (D). Depicted here are generic samples.

rolling-window analysis. The determined fits of maximum activity are indicated in Figure 2 C, as well. The determined maximum activity can be depicted in common bar plots (*Figure 5. 3. D*).

Exposure studies

Exposure studies were carried out to determine the effect of acrylamide, PEG, the photoinitiator LAP and UV light (and combinations of several factors and components) on the activity of β -galactosidase. PEG was chosen to mimic the effect of PEG-DA without the ability to polymerize. A series of samples with the same amount of β -gal and different combinations of PEG, AcAm and LAP was prepared. The applied concentrations of the components were chosen to be representative of the microparticle production process (0.2 g/mL of PEG, 1 M of AcAm, 0.01wt. % of LAP relative to PEG or AcAm concentration). One set of samples was additionally exposed to UV light for roughly 5 s as in the microparticle production process, a second set was not exposed to UV as a control. Activity studies with all samples were carried out following the same protocol as stated in the previous section.

5.3. Results and Discussion

5.3.1. Conjugation of enzymes on the surface of polymer nanoparticles

The SEM image (*Figure 5. 4. A*) provides information on the shape (spherical, no heavy agglomeration) and size (30-1000 nm) of the polymer nanoparticles synthesized from TMPTA and Trithiol via aerosol thiol-ene photopolymerization. These polymer nanoparticles possess reactive -SH groups (confirmed via Ellman's test [232]) which offer an effective way of bioconjugation with maleimide [173].

Depending on the method of immobilization, different enzyme-conjugates can be designed to couple with the support [233]. Immobilization via affinity binding is based on physical interactions. In this paper, application of affinity binding with a streptavidin- β -galactosidase conjugate and polymer nanoparticles conjugated with biotin-maleimide was adopted, because the streptavidin-biotin binding is one of the strongest known non-covalent interactions [215]. Conjugation of maleimide to polymer nanoparticles synthesized employing aerosol thiol-ene photopolymerization has already been proven effective in previous studies [234]. In this study, we use a two-step bioconjugation procedure to attach streptavidin- β -galactosidase to the surface of polymer nanoparticles using a thiol-ene "click" reaction (first step, biotinylation) and biotin-streptavidin binding (second step). The nanoparticles conjugated with streptavidin- β -galactosidase showed activity corresponding to 3.11 units/mg of nanoparticles. This implies that approximately 31.1 units conjugated on

the surface of the nanoparticles out of 50 units of enzyme introduced into the reaction with 10 mg of nanoparticles (0). The removal of the unreacted enzyme proved to be complete

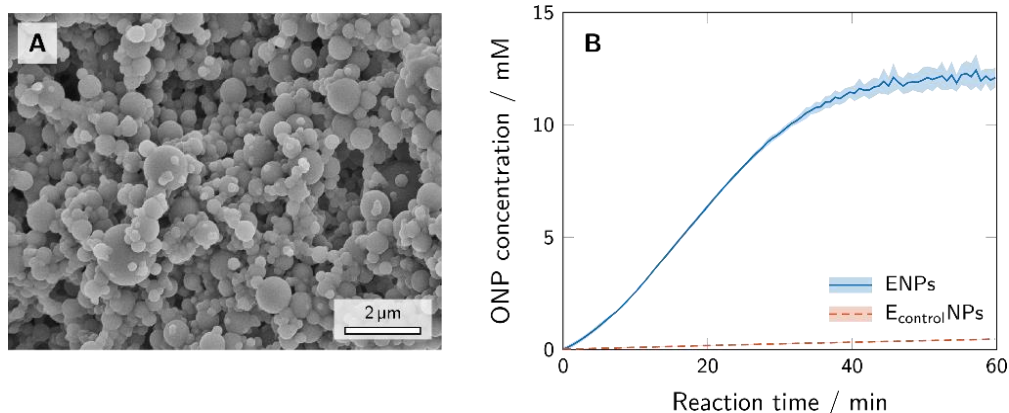


Figure 5. 4. SEM image of the polymer nanoparticles after the synthesis via aerosol photopolymerization (A) and the activity assays of the enzyme-conjugated polymer nanoparticles and polymer nanoparticles with unspecifically adhered enzyme, i. e. control experiment (B).

after washing cycles. The supernatants of the washed enzyme-conjugated nanoparticles were tested for presence of enzyme with ONPG, and the washing cycles continued until the amount of enzyme in the supernatant was negligible.

A control experiment mimicking the conjugation reaction with unmodified β -galactosidase instead of streptavidin- β -galactosidase was carried out to confirm that the binding occurs mostly due to specific biotin-streptavidin interaction and not due to unspecific adhesion. The products of the biotin-streptavidin reaction (ENPs) and the control experiment (E_{control}NPs) were assayed for their enzymatic activity. The results of these experiments are shown in **Figure 5. 4. B**. The activity assay with the ENPs sample showed a sharp increase in ONP concentration and a sigmoidal curve progression ($a_{max} = 38.3 \pm 0.4 \cdot 10^{-2} \frac{mM}{min}$), while the E_{control}NPs sample only showed a very low and linear increase in ONP ($a_{max} = 8.7 \pm 0.3 \cdot 10^{-3} \frac{mM}{min}$). These results reveal that only a negligible amount of enzyme is unspecifically adhered on the surface of the polymer nanoparticles, compared to a high enzyme conjugation yield via affinity binding. This evinced that a controlled two-step conjugation is an effective tool to specifically conjugate streptavidin- β -galactosidase on the surface of nanoparticles and hardly any unspecific binding of β -galactosidase takes place.

5.3.2. Encapsulation of enzyme-conjugated nanoparticles inside the hydrogel microparticles

The produced ENPs were encapsulated inside hydrogel microparticles using a microfluidic device. A 1 mg/mL dispersion of ENPs in hydrogel precursor solution (dispersed phase) was prepared and injected into a stream of silicone oil (continuous phase) through a capillary in a microfluidic device (**Figure 5. 2.**). The immiscibility of the dispersed and continuous phase leads

to the formation of microdroplets of uniform size which polymerize under UV irradiation and form hydrogel microparticles.

One of the key elements of this process was to make the hydrogel precursor dispersions stable so that the polymer nanoparticles do not form aggregates and sediment in the syringe or clog the PEEK capillary. The formulation of the hydrogel precursor dispersion was therefore adjusted (addition of 3 vol% of DMSO), and the dispersion showed stability for over 4 h.

Microscopic analysis of hydrogel microparticles

Light microscopy images (**Figure 5. 5.**) of PEG-based hydrogel microparticles with enzyme-conjugated nanoparticles (H_pENPs, A and B) reveal a successful encapsulation of the nanoparticles in contrast to hydrogel microparticles with unbound enzyme (H_pE, **Figure 5. 5. C** and D). In addition, the nanoparticles inside the H_pENPs are well distributed and no large aggregates of nanoparticles are observed. The hydrogel microparticles in the figures are swollen (2 days of swelling in buffer). The sizes of swollen H_pENPs and H_pE show no significant difference ($403 \pm 17 \mu\text{m}$ and $424 \pm 23 \mu\text{m}$, respectively). According to previous studies, viscosities of the dispersed and continuous phases affect the size of the microparticles produced in the microfluidic process [126], and increasing the viscosity of the dispersed phase will lead to bigger microparticles. The addition of nanoparticles to the hydrogel precursor solution could potentially cause a change in viscosity leading to a shift in microparticle size. The lack of a

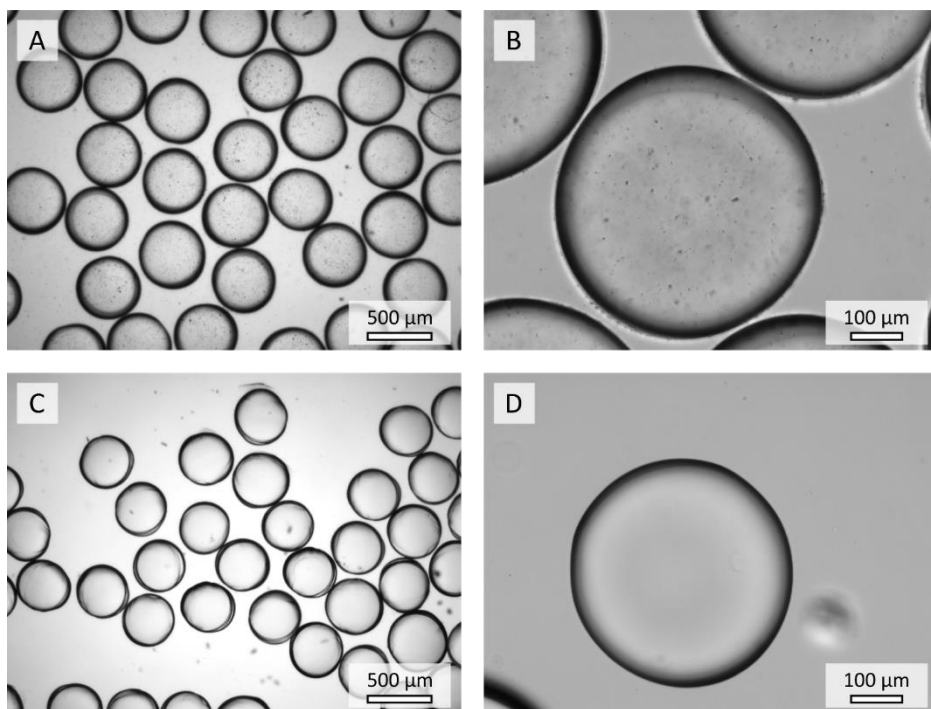


Figure 5. 5. Microscopic images of the hydrogel microparticles containing ENPs (A and B) and unbound enzyme (C and D).

significant observable size difference between H_PENPs and H_PE indicates that no drastic change in viscosity occurred upon the addition of the nanoparticles. Due to the negligible difference in microparticle size in our studies, its effect on enzyme activity was disregarded in the scope of this paper. However, the AcAm-based hydrogel microparticles were bigger (approximately 100 μm difference) than the PEG-based hydrogel microparticles.

Effect of the encapsulation process on the enzymatic activity

Two types of hydrogel microparticles were prepared: from acrylamide (with bisAc as cross-linker) and poly(ethylene glycol) diacrylate. ENPs and unbound enzyme were encapsulated into these hydrogel microparticles (sample names H_AENPs, H_AE, H_PENPs, H_PE). The activity assays of these microparticles before storage compared to non-encapsulated enzyme and ENPs are presented in **Figure 5. 6. A**. Enzyme and ENPs encapsulated into acrylamide microparticles (H_AMPs) showed hardly any activity ($a_{max} < 0.5 \cdot 10^{-2} \frac{mM}{min}$), while the H_PMPs revealed high enzymatic activity with both ENPs ($a_{max} = 4.6 \pm 0.7 \cdot 10^{-2} \frac{mM}{min}$) and unbound enzyme ($a_{max} = 7.1 \pm 0.3 \cdot 10^{-2} \frac{mM}{min}$). Compared to the samples of free unbound enzyme and ENPs, the activities of encapsulated samples exhibit a decrease of roughly 75-85 %. A certain reduction in activity is expected due to the mass transfer limitation caused by the HMPs, slowing down the supply of the enzyme with substrate and the removal of product. To counteract this phenomenon, it is desirable to produce smaller particles due to their more favorable surface-area-to-volume ratio. This could be achieved by modifying the flow rates or the capillary size in the microfluidic production process or by using a continuous phase with lower viscosity. Due to the almost identical size of the microparticles produced, the particle size does not explain the observed difference in activity between H_PMPs and H_AMPs. Other factors might be the density of the hydrogel polymer networks and the inactivation of the enzyme through interactions with components of the hydrogel precursor solutions, as examined in the following section.

The observed relative activity of H_PE was higher than the activity of H_PENPs (**Figure 5. 6. A**), although the enzyme concentration was adjusted to result in the same activity for both microparticle samples. Leaching of the unbound enzyme may be a potential explanation for the observation of higher activity in H_PE. Due to its small size, the unbound enzyme may be able to diffuse out of the hydrogel microparticles and exert higher activity in solution due to the reduced mass transfer limitations [235]. Although highly probable explanation to the observed activity change, the study of leaching was not in the scope of this paper.

The ENPs would retain inside the hydrogel network due to their large size. Encapsulated inside the hydrogel microparticles, ENPs might also be covalently bound to the hydrogel network. The conjugation of enzyme of the surface of the nanoparticles does not exclude the possibility of a small concentration of remaining -SH groups on the surface and these -SH groups can, therefore, participate in thiol-ene reactions with PEG-DA during the encapsulation process.

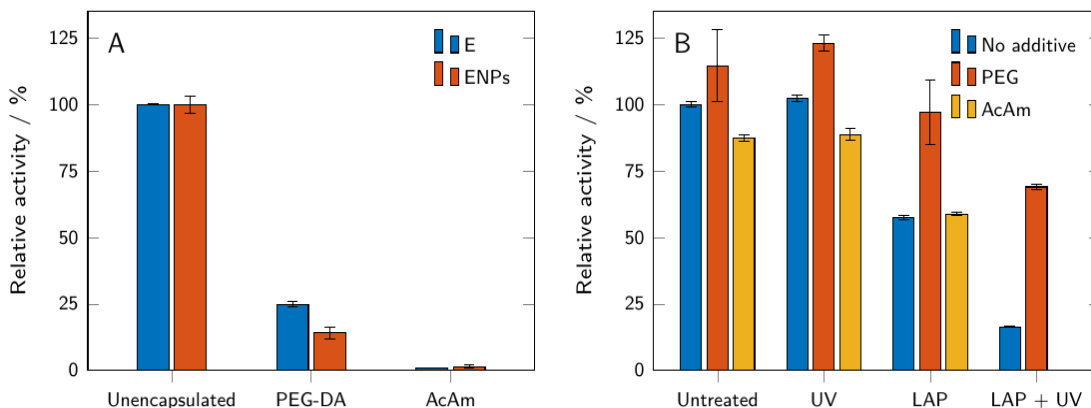


Figure 5. 6. (A) Relative activity of enzymes and ENPs in buffer, compared to PEG-DA and acrylamide-based microparticles containing enzyme and ENPs. The relative activities refer to the respective free (not encapsulated) samples. (B) Relative activity of free enzyme with and without additives after exposure to the photoinitiator LAP and UV light. The relative activities refer to the untreated sample without additive. All results are shown as mean values \pm standard deviation ($n = 3$).

Effect of the hydrogel precursor solutions on the enzymatic activity

To examine a possible link between components of the hydrogel precursor solutions and a reduction in enzymatic activity, unmodified β -galactosidase was dissolved in either buffer, a PEG 600 solution, or an AcAm solution. PEG 600 was chosen as a non-polymerizable mimicry of PEG-DA 575. The mixtures were either exposed to UV light, to the photoinitiator LAP, or both simultaneously. Untreated samples served as a control. After exposure, all samples were tested for their enzymatic activity. The results are shown in **Figure 5. 6. B**. The untreated samples show that the addition of PEG was accompanied by a small increase in activity (+15 %), while the addition of acrylamide caused a small decrease (-13 %). Exposing the samples to UV light did not change the observed activity compared to the untreated sample. The addition of the photoinitiator LAP caused a decrease of activity in all samples, but this decrease was far less pronounced for the PEG sample (-15 %) than for the AcAm sample (-33 %) or the sample without additive (-43 %). Exposure to both UV and LAP caused the strongest reduction in activity (-84 % for the sample without additive, -40 % for the PEG sample). Due to polymerization, the AcAm sample could not be assayed after exposure to LAP and UV. The results show that the addition of the photoinitiator LAP had a detrimental effect on the residual enzymatic activity of the samples, especially when accompanied by UV exposure. This indicates that free radicals generated during the

polymerization process are a major cause of activity loss in the produced HMPs. Reduction of the activity in presence of only LAP is observed because the initiator radicals can also be generated under daylight. The inactivation of enzymes by free radicals has been reported before [236]. The unchanged activity of the samples exposed to only UV shows that the inactivation is not caused by irradiation and/or heat generated from the UV-LEDs.

The presence of PEG in the sample seems to preserve and enhance the activity of β -galactosidase; the reduction in activity after exposure to LAP and UV is considerably reduced compared to the samples with AcAm or without any additive. Indeed, PEG has been reported to have a stabilizing effect on proteins under certain conditions [237]. This may explain the significantly higher activity of H_PMPS compared to the activity of H_AMPS and the reduction in enzymatic activity upon encapsulation which was higher for H_PENPs than for H_PE (depicted in **Figure 5. 6. A**). As the stabilizing effect of PEG depends both on its chain length and on protein size, the conjugation of the enzyme to nanoparticles might affect the PEG-enzyme interactions, resulting in a lower “protection” from free radicals.

5.3.3. Storage studies

Storage studies were carried out to evaluate the suitability of HMPs and ENPs for reusability and storage. Samples were stored in sealed microplates at different temperatures (22, 8 and -26 °C) for 1, 7 and 28 days and the residual activity was determined at different time points. **Figure 5. 7.** shows the results for free unbound enzyme and ENPs (A-C) compared to unbound enzyme and ENPs encapsulated in PEG-based HMPs (D-F). The results of AcAm-based HMPs are not shown due to their low residual activity even before storage.

Storage at room temperature

At 22 °C, free unbound enzyme showed a slight downward trend of activity over storage time with a residual activity of 94 % after 28 days (**Figure 5. 7. A**). Free ENPs showed the opposite trend, even increasing their activity to 115 % after 28 days. This indicates that the immobilization of enzyme on the surface of polymer nanoparticles may be beneficial regarding the retention of enzymatic activity over time at room temperature. However, the only minimal decrease in activity of the free unbound enzyme shows relatively high stability of streptavidin- β -galactosidase at room temperature.

The same trends (decreasing activity over time for E, increasing activity for ENPs) were observed for samples of unbound enzyme and ENPs encapsulated inside the hydrogel microparticles (**Figure 5. 7. D**). Although the encapsulation of unbound enzyme and ENPs inside the hydrogels leads to a significant decrease in activity, the microparticles still provide reusability which must be considered when assessing the overall effect of the encapsulation process. The loss in activity of the H_PE over time cannot be explained without additional extensive research on this topic. Leaching of the enzyme during swelling may counteract the loss of the activity to a certain

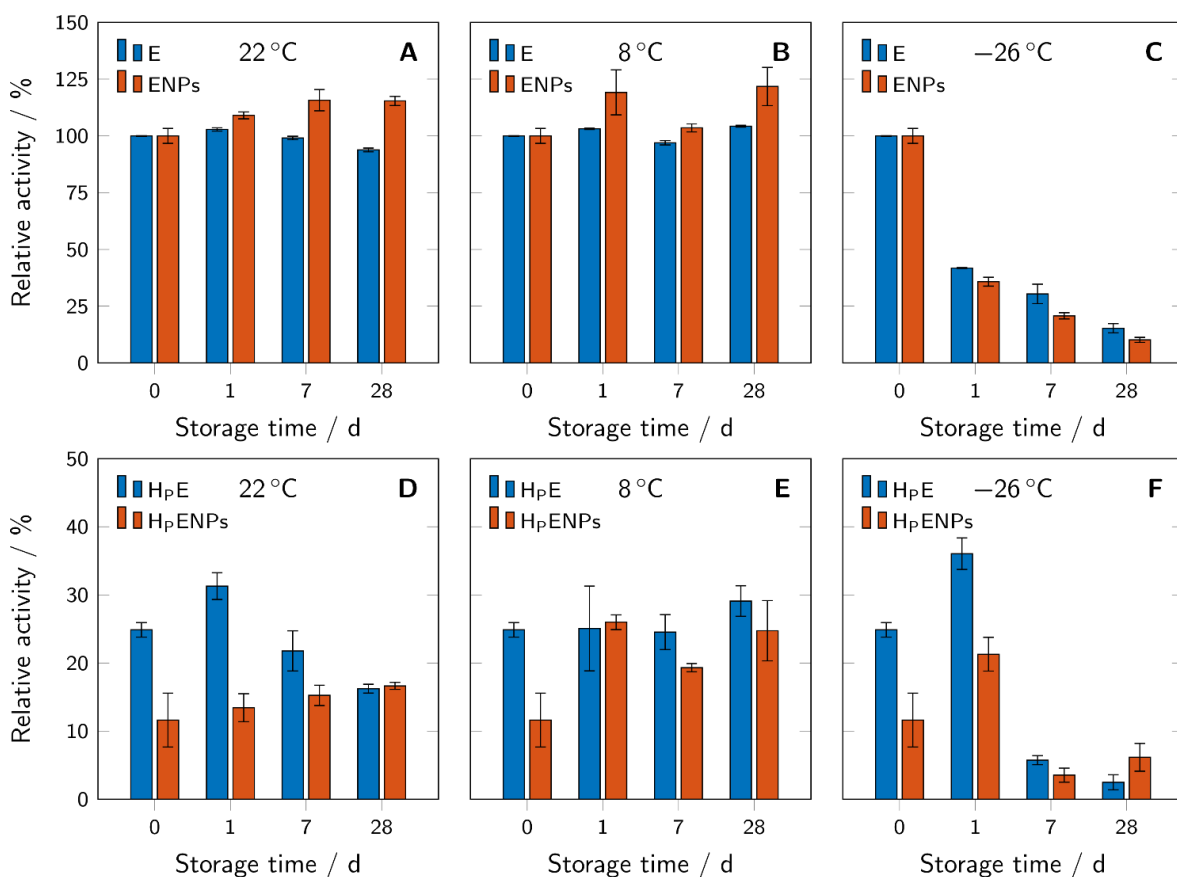


Figure 5.7. Relative activities of free ENPs and free unbound enzyme (A-C), compared to hydrogel microparticles containing ENPs (HpENPs) and free enzyme (HpE) (D-F). The samples were stored at different temperatures and for different durations. The relative activities refer to the respective unencapsulated samples before storage and are shown as mean values \pm standard deviation ($n = 3$).

degree because the leached unbound enzyme is not subjected to mass transfer limitations and can exert a higher activity. This may explain the spike in activity on day 1.

No concrete statements can be made about the cause of the observed increase of enzyme activity in ENPs over time. Improved enzymatic activity in an immobilized form (compared to the unbound form) has already been observed with some other enzymes. Lipase immobilized via adsorption and in presence of detergents showed increased activity compared to the native enzyme. This phenomenon was attributed to the different (open and closed) conformations of lipase in immobilized and native forms [238]. In the case of β -galactosidase, a conformational change due to immobilization, if any, would have appeared before storage (at storage time 0, Figures 4.7 A-C). The activity increase in nanoimmobilized β -galactosidase might be due to conformational changes induced by buffer-nanoparticle interactions in ENPs dispersions over time.

Storage in the fridge

Unlike at 22 °C, the free unbound enzyme samples showed no decrease in activity at 8 °C (**Figure 5. 7. B**). The free ENPs showed the same increasing trend as at 22 °C.

The behavior of unbound enzyme in HpE is also relatively unchanged throughout 28 days, whereas the activity of HpENPs shows a more than two-fold increase after one day (**Figure 5. 7. E**). The difference between the results of storage of HpE at room temperature and at 8 °C can be due to the lower degree of swelling of hydrogels, studied previously by *Urushizaki et al.* [239] on poly(vinyl alcohol) based hydrogels at lower temperatures (5 °C). If swelling is dependent on temperature in PEG-based hydrogels, further studies can be carried out to investigate the release of enzyme from the hydrogel at various temperatures.

Storage in the freezer

Samples stored at -26 °C showed a significant decrease in enzymatic activity over time (**Figure 5. 7. C and F**), making this storage condition unsuitable for the analyzed samples. The activity of the free unbound enzyme and free enzyme-conjugated nanoparticles (**Figure 5. 7. C**) is reduced by more than 50 % after one day and by more than 75 % after 28 days. Several factors may contribute to the massive loss of activity upon freezing. Low temperatures are able to cause the denaturation of enzymes even without freezing [240]. Also, the formation of ice crystals may result in a severe shift in pH (from 7.0 to 3.8 in a 100 mM phosphate buffer solution) and thereby cause the inactivation of β -galactosidase [241] which has limited stability in the acidic pH range [242].

The results of storage of HpE and HpENPs in the freezer are more inconsistent. After one day in the freezer, the microparticles show an enhancement in activity, whereas longer storage leads to a significant drop of activity. Extremely low temperatures could also affect the hydrogel's structure and swelling properties, thereby affecting the enzyme conformation and activity [243].

5.3.4. Further remarks

The presented study demonstrates the feasibility of producing hydrogel microparticles with embedded enzyme-conjugated nanoparticles and indicates the potential benefits and limitations of the method. Future studies should address the identified challenges in several areas.

The obtained results show that the encapsulation within hydrogel microparticles caused a significant loss in enzymatic activity. While this can potentially be compensated by improved reusability, it is still desirable to preserve maximum activity by optimizing the hydrogel content and photopolymerization process which have been identified as major contributors to activity loss. Further studies should address the possibility of a reduction in LAP concentration and UV exposure to reduce enzymatic inactivation through free radicals to a minimum. Other parameters to address are the type of photoinitiator and the PEG-DA chain length which may influence both the observed protective effect during polymerization and the cross-linking density of the resulting

polymer network. An increase in mesh size of the hydrogel can enhance activity by reducing mass transfer limitations [244]. This can also be achieved by producing smaller particles with a more favorable surface-area-to-volume ratio. Due to the enhanced production time for smaller particles, a trade-off is required between production throughput and optimization of the produced particles. Optimizing the production process can shift the balance in this trade-off. The microfluidic process could be improved and scaled up by optimizing flow rates and employing parallelized processes. The immobilization of beta-galactosidase on the nanoparticles could be switched to a single-step procedure by using different binding chemistry.

The performed storage studies indicated a slight superiority of ENPs over free enzymes regarding storage stability, mainly at room temperature. Future studies should address storage at elevated temperatures and at more adverse buffer conditions to identify use cases where hydrogel microparticles can demonstrate their full potential. Especially in buffers containing organic solvents, encapsulation in hydrogels has shown to be beneficial for enzyme stability [245]. For industrial processes, knowledge about the kinetics of the free and immobilized β -galactosidase is essential. Kinetic parameters can be evaluated using integrated reaction rate equations [102, 246]. In a previous study, we have already investigated the kinetics of β -galactosidase immobilized in 3D-printed composite hydrogels based on high internal phase emulsions [235].

A major aspect of encapsulating ENPs instead of the unbound enzyme inside hydrogel microparticles was not specifically addressed in the present study: the avoidance of leaching. Enzymes tend to leach from hydrogels over time depending on the size of the enzyme and the mesh size of the hydrogel network [244]. Attaching the enzyme to a nanoparticle sterically anchors the enzyme within the hydrogel and allows the use of hydrogels with a larger mesh size which reduces mass transfer limitations [244]. Future studies could investigate the correlations between nanoparticle and hydrogel mesh size and the resulting leaching behavior and activity.

The present study only investigated the conversion of the model substrate ONPG. One of the main “real-world” applications of β -galactosidase in food industry is the production of lactose-free milk [247, 248]. Future studies could implement the presented method and employ HpENPs in biocatalytic packed-bed reactors for the hydrolysis of lactose present in whey and milk. As an alternative approach, ENPs could be immobilized in 3D-printed, hydrogel-based bioreactors, as has already been demonstrated for β -galactosidase [235, 249] and other enzymes [245, 250].

5.4. Conclusion

β -galactosidase was conjugated onto polymer nanoparticles and subsequently encapsulated inside two types of hydrogel microparticles. Polymer nanoparticles were produced via aerosol thiol-ene photopolymerization and the reactive -SH groups on the surface of the nanoparticles were used for functionalization with biotin-maleimide. Streptavidin- β -galactosidase was then conjugated onto the biotin unit via affinity binding immobilization method. The enzyme-conjugated nanoparticles were encapsulated inside hydrogel microparticles using a microfluidic

device coupled with UV-LEDs. The size of the produced microparticles was 400-500 μm in diameter after swelling, depending on the nature of the hydrogel (PEG-DA or AcAm).

Our results demonstrate that the encapsulation within AcAm hydrogels resulted in particles with no relevant residual activity, whereas the PEG-DA microparticles preserved a residual activity of 15-25 %, compared to the amount of free unbound enzyme. The reduction in activity could mostly be attributed to enzymatic inactivation during the photopolymerization process which occurred due to the formation of free radicals from the photoinitiator exposed to UV-LEDs. The research highlighted in this paper contributed to the general understanding of activity behavior of β -galactosidase when exposed to a radical photopolymerization reaction for encapsulation. It is shown that UV light (and the heat from the UV lamp) does not significantly affect the activity of β -galactosidase in buffer solution. However, more detailed studies of effects caused by radicals on enzyme activity can improve the encapsulation process. Storage studies show a slight decline in activity over time for free unbound enzyme (94 % after 28 days) at room temperature, while the activity of nanoimmobilized enzyme increased to 115 %. All tested samples were stable at 8 $^{\circ}\text{C}$ and lost most of their activity when stored in a frozen state at -26 $^{\circ}\text{C}$, probably due to a pH shift induced by the employed phosphate buffer and other relevant factors. Encapsulating enzyme-conjugated nanoparticles inside hydrogel microparticles can enable the reusability, however, an improvement of the encapsulation technique is necessary to address the loss of enzymatic activity. Future studies should also address options to reduce the size of the hydrogel microparticles which might reduce mass-transfer limitations. Another focus is the systematic investigation of leaching of enzymes and ENPs and stability studies in harsher conditions e.g., at elevated temperatures and in organic solvents.

6. Aerosol photopolymerization reactor with LED light sources

6.1. Introduction

The work aimed to design and construct an improved, user-friendly and adaptable photoreactor for Aerosol Photopolymerization is presented in this section. The idea of the new generation of photoreactors was established to overcome the drawbacks of the previous system, improving the process control and making it safer and compact. The previous version of the Aerosol Photopolymerization setup included an aerosol generator, connected to the reaction tube, which was irradiated by two UV-fluorescent lamp arrays, and a collection chamber. The newly constructed *Photo-Capsule* introduced in this report has substituted the old irradiation source. The development of the new system consisted of four steps: design, construction of separate parts, assembly, launch. The CAD software was used to design individual parts of the reactor.

To establish homogeneous irradiation conditions, the light has to be delivered to the entire surface of the reaction tube. This specific requirement was the main idea behind the *Photo-Capsule*: a tube-in-tube setup with the light sources located in the circle around the reaction tube. Another important objective was to easily exchange the reaction tube; this determined the inner diameter of the *Photo-Capsule*. The length of the *Photo-Capsule* was chosen to coincide with the length of the reaction tube. The length of the reaction tube was chosen to comply with the residence time required for the aerosol to polymerize. **Figure 6. 1.** *A* shows the assembled *Photo-Capsule*

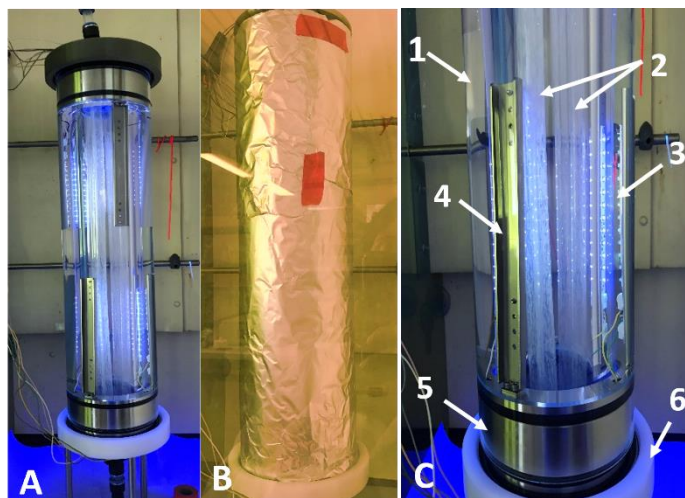


Figure 6. 1. *A*: the *Photo-Capsule* with the reaction tube inside, *B*: *Photo-Capsule* with Al-foil behind the protection shield. *C*: the *Photo-Capsule* bottom part: 1. outer tube, 2. reaction tubes, 3. LED PCBs, 4. LED PCBs' holders, 5. bottom lid, 6. bottom holder.

with the reaction tube; the blue light indicates that the *Photo-Capsule* is on. To redirect the scattered light towards the reaction tube and for the safety of the experimenter, the *Photo-Capsule* has to be covered in aluminum foil and placed behind the windows that block the UV-A irradiation (**Figure 6. 1. B**).

A closer look at the bottom part of the reactor is shown in **Figure 6. 1. C**. Here, the reaction tubes (2) are visible through the glass walls of the *Photo-Capsule* (1). Light-emitting diode printed circuit boards (LED PCBs) (3) designed by PESCHL are mounted onto the stainless steel frames (4). Three stainless steel frames with LED PCBs are mounted onto the bottom lid (5), supported by the bottom ring holder (6). Because the photoreactor is horizontally symmetrical, this description is genuine for the top part of the reactor as well. The LED PCBs are arranged in the interspace in between the glass walls of the *Photo-Capsule*, which is filled with a thermofluid. The design of the *Photo-Capsule* can be further optimized by silvering the outer wall with aluminum in order to improve its reflective properties.

6.2. Materials and Methods

6.2.1. *Photo-Capsule* design

Considerations. One of the most important aspects of building a reactor is selecting the appropriate proportions. This photoreactor was built according to the dimensions of the reaction tube of the old photoreactor. The dimensions of the reaction tube are directly linked to the residence time of aerosol droplets in the reaction tube, which is the irradiation time needed for the photopolymerization reaction to occur. The average residence time of the droplets in the photoreactor is calculated using the formula:

$$T_r = \frac{V}{C_t},$$

where T_r is the residence time of the aerosol, V is the volume of the reaction tube and C_t is the flow rate of the aerosol. The residence time of the aerosol particles calculated through the dimensions of the old photoreactor was 28 seconds. To coincide with the kinetics of the photopolymerization reaction, approximately the same residence time will be chosen for the *Photo-Capsule*. The optimal radiative surface of the new cylindrical photoreactor was calculated to be 450 mm in length and 80 mm in diameter in order to meet the requirements for the minimum residence time of the previously used photoreactor.

To irradiate the reaction tube from all angles a cylindrical shape of the *Photo-Capsule* was chosen. The replacement of the irradiation source of the old photoreactor (UV- fluorescent tubes) to the new irradiation source (UV-LEDs) was the main part of this chapter. LEDs have many advantages over fluorescent lamps. Advantages and disadvantages of LEDs and Fluorescent lamps are listed in **Table 6. 1**. For photopolymerization, LEDs are the favorable irradiation source

compared to fluorescent tubes, the main contribution being the tunable radiant flux and narrowband emission.

Design and Construction. The software used to design the separate parts of the Photoreactor and create an assembly simulation of a constructed photoreactor was Autodesk Inventor Professional 2018.

The LED stripes designed by PESCHL each contain twelve LED spots. The steel sheet frames were designed specifically for the Photo-Capsule to mount the LED stripes (**Figure 6. 2. A**). Sheet frame (1) is made of a stainless sheet and then bent on sides to prevent distortion of its vertical position. The frame is mounted onto the top or bottom lid of the Photo-Capsule (6) with appropriate screws. The LED stripe can be mounted onto the frame in four vertical positions, allowing an optimization of the irradiation conditions along the reaction tube. Each LED spot (3) with a 120° irradiation radius is located 5 mm away from the next one on the PCB (2). The LEDs are connected to the power supply through the connection wires (5). Temperature control is also provided within LED-PCBs.

Table 6. 1. Advantages and disadvantages of LEDs and Fluorescent tubes.

Light Source	Advantages	Disadvantages
LED	<ul style="list-style-type: none"> • produce less heat than other light sources • no warm-up time • durable • low maintenance • tunable radiant flux • long lifetime • high efficiency • up to 180° directional light 	<ul style="list-style-type: none"> • higher costs than other light sources • emits heat
Fluorescence lamp	<ul style="list-style-type: none"> • low cost • high efficiency • 360° directional light 	<ul style="list-style-type: none"> • fragile • requires warm-up time • difficulty in maintenance • emits heat • broad emission range • contains mercury-vapor • difficult to dispose of

The 3D - simulation of the partially disassembled reactor is shown in **Figure 6. 2. B**. Three LED stripes are located in the cylindrical reactor 120° away from each other (5) to deliver the light all through the surface of the reaction tube. All the scattered light is redirected onto the reactor due to the reflective surface of the outer glass tube (2) (currently, this is an aluminum foil cover). The

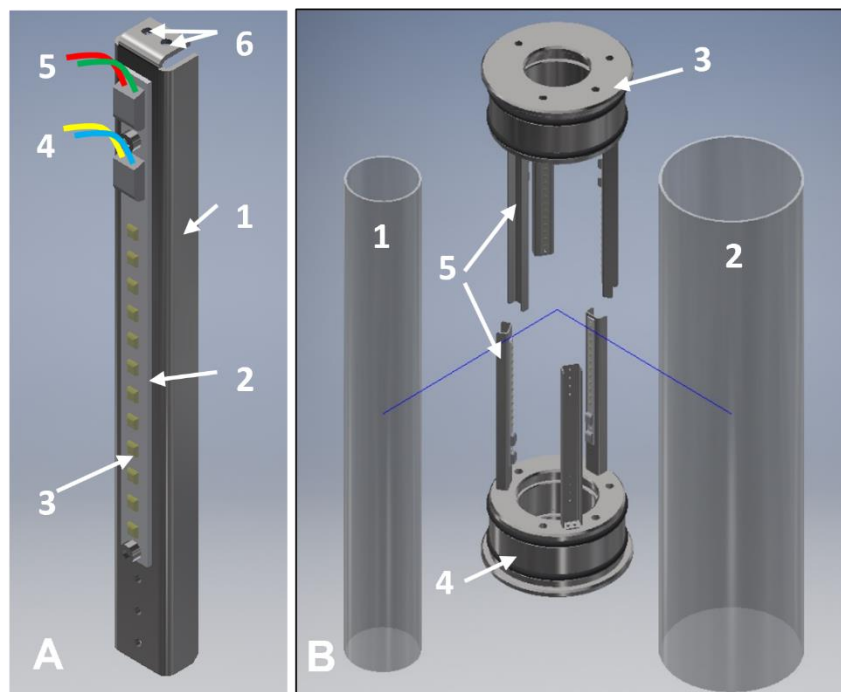


Figure 6. 2. *A: LED stripe mounted onto the steel sheet frame: 1. steel frame, 2. LED PCB, 3. LED spot, 4. LED temperature regulating connection, 5. LED connection wires, 6. connection to the lid. B: Scheme of the disassembled Photo-Capsule: 1. Inner glass tube, 2. outer glass tube, 3. top lid, 4. bottom lid, 5. LED PCB's frames.*

inner glass tube is made of DURAN® glass to pass the irradiation onto the reaction tube. The top (3) and bottom (4) lids are designed to fix the LED frames, pass the wiring through the reactor to the power supply, the oil inlet, and the outlet. The O-rings made of highly resistant material provide the secure connection of steel lids onto the glass walls.

Apart from the parts shown in **Figure 6. 2. B**, the Photo-Capsule also includes small connections (wiring connections, oil connections, screws, etc.) and sealings (o-rings, flat gaskets), top and bottom holders (for the positioning of the Photo-Capsule at a certain height), thermofluid (Trisco-UV5), a printed circuit board (PCB) for the cable connections and a power supply device.

6.2.2. Materials

LED lights. CUN66A1B high power UV LED lamps (from SeoulVioSys) provide high current operation and low thermal resistance (5.5°C/W). It is a lead-free and RoHS (Restriction of Hazardous Substances Directive) compliant product. These LEDs with 120° irradiation angle can be used for various purposes: UV curing, printing, coating, fluorescence photography, etc. With a peak wavelength at 365 nm, it is a perfect tool for photopolymerization. The radiant flux of each LED is 900 mW. The LEDs can operate in temperatures between -10°C and 85°C and stored in temperatures between -40°C and 100°C.

Stainless steel parts. Sheet metal parts, i.e. the LED frames were supplied by DORNHÖFER GmbH, the lids were supplied by Heavy Metal Engineering GmbH. All parts were designed on Autodesk (Fig. 3 and 4).

Glass parts. Glass walls (tubes) of the Photo-Capsule are made of the DURAN glass and provided by Peco Laborbedarf GmbH. The outer glass tube is 150 mm in diameter and 3 mm in thickness. The inner glass tube is 80 mm in diameter and 2,5 mm in thickness. Both tubes are of length 572 mm.

O-rings and sealings were purchased from Ludwig Meister GmbH, other connections were provided by PESCHL workshop. The top holder of the reactor was 3 D printed at the Institute of Process Engineering at KIT. The bottom holder was also provided by PESCHL.

Thermofluid. Trisco®UV5 was used as a thermal fluid for the thermal decoupling of LEDs in the Photo-Capsule. An optimal refractive index, high purity, excellent dielectric properties, and absence of corrosion are among the beneficial properties of Trisco®UV5 concerning the current application. This oil is made of low-viscous polydimethylsiloxane (PDMS) and provides high chemical resistance to sealings and other materials of the reactor. The refractive index of Trisco®UV5 at 25°C is 1,3960, the flashpoint is over 130°C, dropping point is below -80°C. Trisco®UV5 is mainly used for thermal decoupling in irradiation systems, modules, immersion lamp systems and photoreactors.

Spectroradiometry. UV-PAD-E (Opsytec Dr. Gröbel, Ettlingen, Germany) spectroradiometer with a dosimetry tool was employed to measure irradiance of the fluorescence tubes and UV-LED.

6.2.3. Chemicals

For aerosol photopolymerization reactions, the following chemicals were used: Trimethylolpropane triacrylate (TMPTA) contains 600 ppm monomethyl ether hydroquinone as an inhibitor, technical grade, Diphenyl(2,4,6-trimethylbenzoyl) phosphine oxide (TPO) 97%, trimethylolpropane tris(3-mercaptopropionate) (TRIS) $\geq 95\%$, (\pm)- α -Lipoic acid (α LA) $\geq 98.0\%$, Econix Silver Nanospheres PVP mean diameter 25 nm (AgNP powder) and ethanol ($\geq 99.9\%$ by GC), Lichrosolv®, gradient grade for the liquid chromatography, Supelco®. TMPTA, TRIS, TPO and α LA were purchased from Merck KGaA, AgNP powder was purchased from NanoComposix and ethanol was purchased from VWR International LLC.

Diphenyl(2,4,6-trimethylbenzoyl) phosphine oxide (TPO) was used as a photoinitiator during the photopolymerization reactions, due to its peak wavelength at 365 nm, which coincides with the wavelength of the CUN66A1B UV-LEDs used in the Photo-Capsule.

6.3. Results and Discussion

6.3.1. Technical characteristics

The flexible design of the Photo-Capsule allows the use of different lengths of reaction tubes. For example, in case the residence time must be decreased, the reaction tube length can be decreased as well; the outer and inner glass tubes can be exchanged for shorter tubes (between 572 and 185 mm). In addition, the location of the upper and bottom triplets of LEDs can be twisted along the Y-axis as shown in **Figure 6.3**. The linear (**Figure 6.3**. A1 and A2.) and angular (B1 and B2) alignments both have similar light distribution angles, although the angular alignment guarantees a more homogeneous irradiation distribution. The angular alignment also allows the intersection of the top and bottom parts (**Figure 6.3**. C) of the Photo-Capsule. This allows the utilization of shorter reaction tubes, provided glass walls of appropriate length are available.

Another benefit of using the newly constructed Photo-Capsule instead of the UV-Fluorescent tubes will be the opportunity to choose the irradiation intensity by toggling the LED PCBs. Advantages of LEDs over fluorescent lamps (see chapter 6. 2. 1, **Table 6. 1.**) are not the only benefits of using Photo-Capsule instead of the old photoreactor. The old photoreactor required more safety measures to protect the experimenter. During the reaction, the UV protection windows had to be installed due to the excess amounts of UV irradiation from the lamps. For the compact shape of the Photo-Capsule, no special safety measures are necessary, because all of the light irradiated by LEDs is confined within the reactor, due to the aluminum foil wrapping. Another considerable advantage of the Photo-Capsule is its cylindrical shape. When the reaction tube is

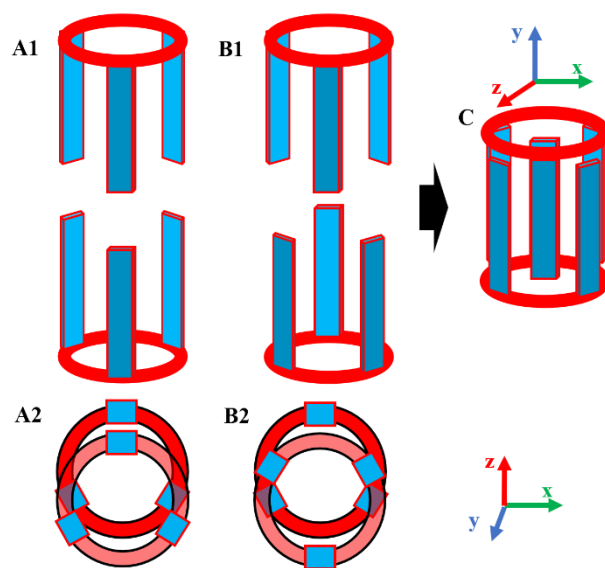


Figure 6.3. Schemes of LED locations within the Photo-Capsule. **A:** linear alignment, **B:** angular alignment, **C:** intersected angular alignment.

inserted into the Photo-Capsule it is positioned right in the middle of it; fixing the reactor to keep it in a vertical position is not necessary. The old photoreactor required additional maintenance to position the reaction tube on the correct height parallel to the UV-Fluorescent lamps. The fluorescent lamps must be always positioned right opposite each other at the same height. The reaction in both reactors flows in the exact same way. The nanoparticles produced by both reactors have a similar shape, low agglomeration and dispersity (see chapter 6.3.2).

The comparison of the irradiance spectra (measured using UV-Pad-E) of the old photoreactor and the *Photo-Capsule* are presented in **Figure 6. 4**. The spectrum shows the irradiance comparison of the two photoreactors. The green spectrum corresponds to measurements taken in the middle of the *Photo-Capsule*, and the blue spectrum corresponds to the measurements taken on the half-length between the two lamp sets each equipped with three UV-fluorescence tubes (T-15.C, Vilber Lourmat, $\lambda_{max} = 312$ nm, later referred to as UVF lamp set). This setup was used for the synthesis of nanoparticles via aerosol photopolymerization before the *Photo-Capsule* was designed.

Doses of irradiance of the UVF lamp set and the *Photo-Capsule* are presented in **Table 6.2.**, which shows that 99.8% of the light from the *Photo-Capsule* is registered in the UVA range. UVF lamp set, on the other hand, registers most of the light in both UVA and UVB and some fractions in UV-Vis and UVC. The results from the irradiance measurements demonstrate that the *Photo-Capsule* has a much higher radiant flux per unit area than the UVF lamp set.

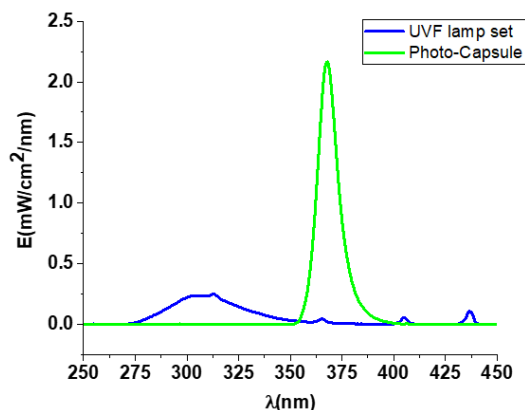


Figure 6. 4. The comparison of the irradiance spectra of the *Photo-Capsule* and the old photoreactor setup (right) consisting of two lamps with three UV-fluorescence tubes each facing each other.

Table 6.2. Doses of Irradiance of the UVF lamp sets and the Photo-Capsule.

Ultraviolet wavelength range (nm)	Irradiance (mW/cm ²)	
	UVF lamp set	Photo-Capsule
UV-Vis (400-480)	0.65	0.04
UVA (315-400)	4.11	28.44
UVB (280-315)	6.13	0
UVC (240-280)	0.18	0
Total (480-240)	11.07	28.48

6.3.2. Experimental performance

First reactions with the Photo-Capsule were carried out using four fluorinated ethylene propylene (FEP) reaction tubes of 62 cm active length, connected via tube fittings. The active volume of this reaction tube is 3812 cm³. The flow rate of the aerosol is 1,2 l/min. The residence time of the aerosol in the Photo-Capsule is roughly 19 seconds. Apart from the Photo-Capsule and the abovementioned reaction tube, aerosol generator TOPAS® ATM 220 and Durapore 0,1µm pore size, 47 mm diameter, PVDF collection membranes were parts of the Aerosol Photopolymerization setup. The Aerosol Photopolymerization process includes the preparation of a spray solution, which is then placed inside the aerosol generator. With the flow of nitrogen, the spray solution is atomized forming a droplet aerosol. The aerosol passes to the reaction tube and polymerizes due to the emitted irradiation of the Photo-Capsule, forming polymer nanoparticles. The nanoparticles are collected on the filter membranes, located in the outlet of the reaction tube. This process is well described in Chapter 3. Two spray solution recipes were tested with the new Aerosol Photopolymerization setup.

Recipe PC-1: 0,9536 g of TRIS, 0,7266 g of TMPTA, 0,0168 g of TPO were dissolved in 40 g of ethanol. The spray solution was stirred before the atomization. The individual spherical nanoparticles obtained from the photopolymerization of the aerosol droplets of this spray solution are shown on the Scanning Electron Microscopy (SEM) image in *Figure 6. 5. a*.

Recipe PC-2: 0,01g of Ag nanospheres, 10 mL of 10mM α-LA in ethanol, 0,7108 g of TMPTA, 0,9668 g of TRIS and 0,0177 of TPO were dispersed in 20 mL of ethanol. This dispersion was also stirred before and during the atomization to prevent the agglomeration of silver nanoparticles. The SEM image of the spherical and individual hybrid nanoparticles obtained from the reaction with this recipe is shown in *Figure 6. 5. a*. The silver nanoparticles are only visible via Transmission Electron Microscopy (TEM) as shown in *Figure 6. 5. a*.

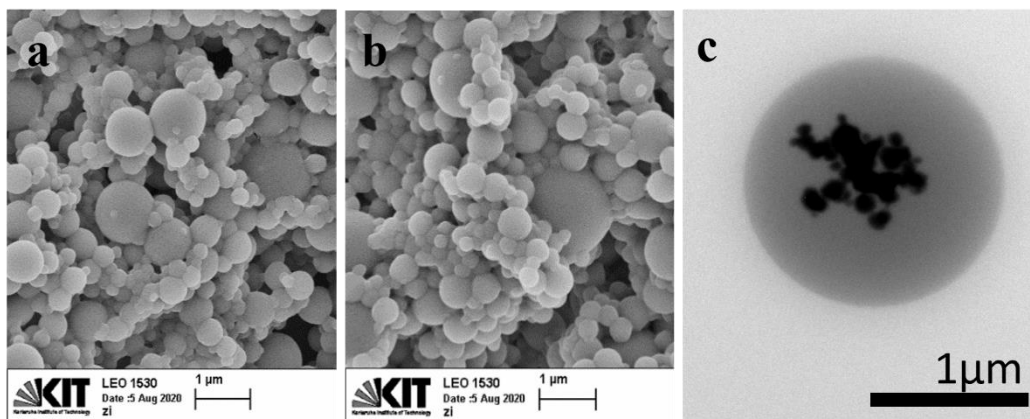


Figure 6. 5. Nanoparticles synthesized using Photo-Capsule: *a.* SEM image of polymeric nanoparticles from spray solution recipe PC-1, *b.* SEM image of silver nanoparticle hybrids, *c.* TEM image of silver nanoparticle hybrids from recipe PC-2

These experimental results shows a successful photopolymerization of the aerosol, therefore, fulfilling the main purpose of the Photo-Capsule as a part of the Aerosol Photopolymerization setup. The droplet aerosol can be polymerized and the nanoparticles obtained via this process are similar to those obtained from a previous Aerosol Photopolymerization Setup. However, the particles obtained from a new setup appear more individual, less aggregated than the particles from the previous setup (see chapter 3).

6.4. Conclusion

A new photoreactor for the Aerosol Photopolymerization setup was designed, constructed, assembled and launched in collaboration between KIT and PESCHL (as part of the Horizon 2020 “Photo-Emulsion” ITN project). The newly constructed *Photo-Capsule* is energy-efficient, compact, safe and of low maintenance. It was designed considering the residence time needed for the photochemical process, the irradiation distribution by LEDs and the reaction tube dimensions. Photo-Capsule has many advantages over the previous irradiation source (sets of UV-fluorescent lamps) including longer lifetime, transportation, no preheating time, high efficiency and tunability of light intensity. First experiments with the Photo-Capsule have shown that it can produce polymer nanoparticles with low agglomeration.

7. Conclusion and outlook

This thesis contributes to the research of aerosol photopolymerization and thiol-ene photopolymerization. One objective was focused on the application of thiol-ene chemistry to aerosol photopolymerization. A set of new monomer formulations that can produce spherical polymer nanoparticles with functional -SH groups on the surface was established. Furthermore, the findings of this objective were applied for the synthesis of spherical polymer nanocomposites by aerosol photopolymerization. A new biofunctionalization technique was introduced to conjugate various biomolecules on the surface of produced polymer nanocomposites. Another objective of the thesis was to use the thiol-functional polymer nanoparticles produced via aerosol photopolymerization from thiol-ene monomers for nanoimmobilization of enzymes. From another perspective, optimization of the aerosol photopolymerization process was attempted by designing a new photoreactor and introducing further steps into the process to narrow the size distribution of synthesized polymer nanoparticles.

The first part of this dissertation (Chapter 3) showed how polymer nanoparticles with reactive -SH groups can be produced from thiol and alkene monomers with aerosol photopolymerization. The combinations of various monomers of different functionalities were studied to obtain the formulations that can produce spherical and non-agglomerated cross-linked polymer nanoparticles. Combinations of trifunctional alkenes and trifunctional thiols work best in an equal stoichiometry of functional groups. The nanoparticles produced from several other monomer combinations are not as individual as nanoparticles from these combinations. The nanoparticles obtained from trithiol-triacrylate reactions contain no traces of unreacted ene groups, leading to the conclusion that all acrylate was consumed in cross-linking during photopolymerization. These polymers are a product of mixed-mode polymerization, where both the homopolymerization of the triacrylate and the heteropolymerization (or thiol-ene polymerization) of triacrylate and trithiol are underway. Polymer nanoparticles from triallyl and trithiol react only in thiol-ene photopolymerization and no homopolymerization of triallyl is underway. Infrared spectroscopy shows no trace of -SH groups in these nanoparticles. The size distribution of nanoparticles was also studied in this chapter. Increasing the concentration of solvent in relation to monomers lowers the viscosity of the spray solution, producing more volatile droplets. Subsequently, after the solvent evaporation droplets (afterward, polymer nanoparticles) of smaller size are obtained. The abundance of reactive -SH groups was detected in the polymer nanoparticles produced from triacrylate-trithiol and triacrylate-tetrathiol combinations using Elman's test. The products of this work can be adjusted for further applications in targeted drug delivery, biosensors, etc.

In the fourth chapter of this dissertation, the combination of aerosol photopolymerization and thiol-ene chemistry was applied to produce spherical hybrid particles with silver nanospheres inside polymer nanoparticles. Hybrid nanomaterials are systems that combine unique physical and

chemical properties of their single components and thus can be used for various applications. According to studies carried out in Chapter 3, aerosol thiol-ene photopolymerization provided an eco-efficient, easy, non-toxic method for the synthesis of spherical polymer nanoparticles. To produce hybrid materials, silver nanoparticles had to be stabilized to prevent their aggregation using different compounds and different qualities of the nanoparticles. After a successful stabilization, silver nanoparticles were well dispersed within the polymer matrix.

The obtained nanocomposites possess -SH groups on their surface and can, thus, be used in bioconjugation. A two-step bioconjugation process was developed to bind different types of biomolecules on the polymer nanoparticles' surface through a thiol-maleimide reaction. The reactivity of binding sites was successfully confirmed by using gold-tagged and fluorescence-labeled biomolecules. Nanoparticle hybrids produced in this study can find applications in cancer diagnostics and treatment, as well as many other areas of biomedicine and biosensors.

In Chapter 5 of this thesis, β -galactosidase was conjugated onto polymer nanoparticles produced following the method established in Chapter 3 and encapsulated inside two types of hydrogel microparticles. Biotin-maleimide was conjugated onto the surface of polymer nanoparticles, followed by conjugation of streptavidin- β -galactosidase onto the biotin unit via affinity binding immobilization. The enzyme-conjugated nanoparticles were encapsulated inside hydrogel microparticles using a microfluidic device coupled with UV devices. The results in this chapter demonstrated that the encapsulation of the PEG-based hydrogel microparticles preserved a residual activity of 15-25 % (free unbound enzyme 100%), compared to the other hydrogel (acrylamide-based), which lost activity entirely. Inactivation of enzyme is considered to have taken place during the photopolymerization process due to the formation of free radicals from the photoinitiator exposed to UV irradiation. A decline in activity over time for a free unbound enzyme (94 % after 28 days) at room temperature was observed, while the activity of nanoimmobilized enzyme increased to 115 %. All tested samples were stable at 8 °C and lost most of their activity when stored in a frozen state at -26 °C, presumably due to a pH shift induced by buffer and other relevant factors. Future studies should address options to reduce the size of the hydrogel microparticles which might reduce mass-transfer limitations, producing different PEG-based hydrogels to address the decrease in activity during encapsulation. Furthermore, leaching studies should be conducted to investigate the enzyme's stability within microparticles.

In Chapter 6, the presented work is still in progress of optimizing the aerosol photopolymerization setup by making it safer, compact and energy-efficient. A novel photoreactor (Photo-Capsule) for aerosol photopolymerization setup was designed, constructed, and assembled. The reactor is functional and can produce polymer nanoparticles through an efficient procedure compared to the method used in the previous three chapters. The most significant adjustment was made to the light source of the photoreactor, the UV-fluorescence tubes were replaced by UV-LED irradiation sources. The UV-LEDs offer several advantages over UV-fluorescent lamps, such as long lifetime, tunability, higher radiant flux per unit area. The Photo-Capsule was designed considering the residence time established after the use of the previous setup, the irradiation distribution by LEDs, and the reaction tube dimensions.

Bibliography

1. Rao, J.P. and K.E. Geckeler, *Polymer nanoparticles: Preparation techniques and size-control parameters*. Progress in Polymer Science, 2011. **36**(7): p. 887-913.
2. Bennet, D. and S. Kim, *Polymer nanoparticles for smart drug delivery*. Vol. 8. 2014: chapter.
3. Liu, Y., H. Miyoshi, and M. Nakamura, *Nanomedicine for drug delivery and imaging: A promising avenue for cancer therapy and diagnosis using targeted functional nanoparticles*. International Journal of Cancer, 2007. **120**(12): p. 2527-2537.
4. Chabner, B.A. and T.G. Roberts, *Chemotherapy and the war on cancer*. Nature Reviews Cancer, 2005. **5**(1): p. 65-72.
5. Feng, X., et al., *Conjugated Polymer Nanoparticles for Drug Delivery and Imaging*. ACS Applied Materials & Interfaces, 2010. **2**(8): p. 2429-2435.
6. Haag, R. and F. Kratz, *Polymer Therapeutics: Concepts and Applications*. Angewandte Chemie International Edition, 2006. **45**(8): p. 1198-1215.
7. Bhatt, R., et al., *Synthesis and in Vivo Antitumor Activity of Poly(L-glutamic acid) Conjugates of 20(S)-Camptothecin*. Journal of Medicinal Chemistry, 2003. **46**(1): p. 190-193.
8. Miele, E., et al., *Albumin-bound formulation of paclitaxel (Abraxane ABI-007) in the treatment of breast cancer*. International journal of nanomedicine, 2009. **4**: p. 99-105.
9. Cheon, J. and J.-H. Lee, *Synergistically Integrated Nanoparticles as Multimodal Probes for Nanobiotechnology*. Accounts of Chemical Research, 2008. **41**(12): p. 1630-1640.
10. Park, J.-H., et al., *Micellar Hybrid Nanoparticles for Simultaneous Magnetofluorescent Imaging and Drug Delivery*. Angewandte Chemie International Edition, 2008. **47**(38): p. 7284-7288.
11. Kim, J., et al., *Designed Fabrication of Multifunctional Magnetic Gold Nanoshells and Their Application to Magnetic Resonance Imaging and Photothermal Therapy*. Angewandte Chemie International Edition, 2006. **45**(46): p. 7754-7758.
12. Sailor, M.J. and J.-H. Park, *Hybrid Nanoparticles for Detection and Treatment of Cancer*. Advanced Materials, 2012. **24**(28): p. 3779-3802.
13. Cipolatti, E.P., et al., *Current status and trends in enzymatic nanoimmobilization*. Journal of Molecular Catalysis B: Enzymatic, 2014. **99**: p. 56-67.
14. Ansari, S.A. and Q. Husain, *Potential applications of enzymes immobilized on/in nano materials: A review*. Biotechnology Advances, 2012. **30**(3): p. 512-523.
15. Vert, M., et al., *Terminology for biorelated polymers and applications (IUPAC Recommendations 2012)*. Pure and Applied Chemistry, 2012. **84**(2): p. 377-410.
16. Lince, F., D.L. Marchisio, and A.A. Barresi, *Strategies to control the particle size distribution of poly-ε-caprolactone nanoparticles for pharmaceutical applications*. Journal of Colloid and Interface Science, 2008. **322**(2): p. 505-515.
17. Zielińska, A., et al., *Polymeric Nanoparticles: Production, Characterization, Toxicology and Ecotoxicology*. Molecules (Basel, Switzerland), 2020. **25**(16): p. 3731.
18. Chern, C.-S., *Principles and applications of emulsion polymerization*. 2008: John Wiley & Sons.
19. Asua, J.M., *Miniemulsion polymerization*. Progress in Polymer Science, 2002. **27**(7): p. 1283-1346.
20. Esen, C. and G. Schweiger, *Preparation of Monodisperse Polymer Particles by Photopolymerization*. Journal of Colloid and Interface Science, 1996. **179**(1): p. 276-280.
21. Vorderbruggen, M.A., K. Wu, and C.M. Breneman, *Use of Cationic Aerosol Photopolymerization To Form Silicone Microbeads in the Presence of Molecular Templates*. Chemistry of Materials, 1996. **8**(5): p. 1106-1111.

22. Akgün, E., J. Hubbuch, and M. Wörner, *Perspectives of aerosol-photopolymerization: Nanoscale polymer particles*. Chemical Engineering Science, 2013. **101**: p. 248-252.
23. Akgün, E., J. Hubbuch, and M. Wörner, *Perspectives of Aerosol-Photopolymerization: Nanostructured Polymeric Particles*. Macromolecular Materials and Engineering, 2014. **299**(11): p. 1316-1328.
24. Akgün, E., J. Hubbuch, and M. Wörner, *Perspectives of aerosol-photopolymerization: organic-inorganic hybrid nanoparticles*. Colloid and Polymer Science, 2014. **292**(5): p. 1241-1247.
25. Liu, D., et al., *The Smart Drug Delivery System and Its Clinical Potential*. Theranostics, 2016. **6**(9): p. 1306-1323.
26. Sinha, R., et al., *Nanotechnology in cancer therapeutics: bioconjugated nanoparticles for drug delivery*. Molecular Cancer Therapeutics, 2006. **5**(8): p. 1909.
27. Werengowska-Ciećwierz, K., et al., *The Chemistry of Bioconjugation in Nanoparticles-Based Drug Delivery System*. Advances in Condensed Matter Physics, 2015. **2015**: p. 198175.
28. Liu, Y., et al., *Thiol-ene click chemistry: a biocompatible way for orthogonal bioconjugation of colloidal nanoparticles*. Chemical Science, 2017. **8**(9): p. 6182-6187.
29. Akgün, E., et al., *Cationic Aerosol Photopolymerization*. Macromolecular Materials and Engineering, 2015. **300**(2): p. 136-139.
30. Lenggoro, I.W., et al., *Sizing of Colloidal Nanoparticles by Electrospray and Differential Mobility Analyzer Methods*. Langmuir, 2002. **18**(12): p. 4584-4591.
31. Gao, Z., E.A. Grulke, and A.K. Ray, *Synthesis of monodisperse polymer microspheres by photopolymerization of microdroplets*. Colloid and Polymer Science, 2007. **285**(8): p. 847-854.
32. Esen, C., T. Kaiser, and G. Schweiger, *Raman Investigation of Photopolymerization Reactions of Single Optically Levitated Microparticles*. Applied Spectroscopy, 1996. **50**(7): p. 823-828.
33. Roll, G., T. Kaiser, and G. Schweiger, *Optical trap sedimentation cell—a new technique for the sizing of microparticles*. Journal of Aerosol Science, 1996. **27**(1): p. 105-117.
34. Esen, C., et al., *Synthesis of spherical microcapsules by photopolymerization in aerosols*. Colloid and Polymer Science, 1997. **275**(2): p. 131-137.
35. Shaban, M., et al., *Facile synthesis of cauliflower-like hydrophobically modified polyacrylamide nanospheres by aerosol-photopolymerization*. European Polymer Journal, 2016. **83**: p. 323-336.
36. Nasri Lari, H., J. Chaouki, and J.R. Tavares, *Continuous aerosol photopolymerization to coat de-agglomerated nanoparticles*. Chemical Engineering Journal, 2020. **390**: p. 124526.
37. Poostforooshan, J., et al., *Synthesis of Spherical Carbon Nitride-Based Polymer Composites by Continuous Aerosol-Photopolymerization with Efficient Light Harvesting*. ACS Applied Materials & Interfaces, 2016. **8**(33): p. 21731-21741.
38. Sinha, A.K. and D. Equbal, *Thiol-Ene Reaction: Synthetic Aspects and Mechanistic Studies of an Anti-Markovnikov-Selective Hydrothiolation of Olefins*. Asian Journal of Organic Chemistry, 2019. **8**(1): p. 32-47.
39. Posner, T., *Beiträge zur Kenntniss der ungesättigten Verbindungen. II. Ueber die Addition von Mercaptanen an ungesättigte Kohlenwasserstoffe*. Berichte der deutschen chemischen Gesellschaft, 1905. **38**(1): p. 646-657.
40. Kade, M.J., D.J. Burke, and C.J. Hawker, *The power of thiol-ene chemistry*. Journal of Polymer Science Part A: Polymer Chemistry, 2010. **48**(4): p. 743-750.
41. Senyurt, A.F., et al., *Ternary Thiol-Ene/Acrylate Photopolymers: Effect of Acrylate Structure on Mechanical Properties*. Macromolecules, 2007. **40**(14): p. 4901-4909.
42. Gress, A., A. Völkel, and H. Schlaad, *Thio-click modification of poly [2-(3-butenyl)-2-oxazoline]*. Macromolecules, 2007. **40**(22): p. 7928-7933.

43. David, R.A. and J.A. Kornfield, *Facile, efficient routes to diverse protected thiols and to their deprotection and addition to create functional polymers by thiol–ene coupling*. *Macromolecules*, 2008. **41**(4): p. 1151-1161.
44. Lowe, A.B., *Thiol-ene “click” reactions and recent applications in polymer and materials synthesis*. *Polymer Chemistry*, 2010. **1**(1): p. 17-36.
45. Cramer, N.B. and C.N. Bowman, *Thiol–Ene Chemistry*. Vol. 1. 2017: Wiley-VCH Verlag GmbH & Co. KGaA Weinheim, Germany.
46. Hoyle, C.E. and C.N. Bowman, *Thiol–Ene Click Chemistry*. *Angewandte Chemie International Edition*, 2010. **49**(9): p. 1540-1573.
47. Nolan, M.D. and E.M. Scanlan, *Applications of Thiol-Ene Chemistry for Peptide Science*. *Frontiers in chemistry*, 2020. **8**: p. 583272-583272.
48. Scanlan, E.M., V. Corcé, and A. Malone, *Synthetic Applications of Intramolecular Thiol-Ene “Click” Reactions*. *Molecules*, 2014. **19**(11): p. 19137-19151.
49. Ravasco, J.M.J.M., et al., *Bioconjugation with Maleimides: A Useful Tool for Chemical Biology*. *Chemistry – A European Journal*, 2019. **25**(1): p. 43-59.
50. Stenzel, M.H., *Bioconjugation Using Thiols: Old Chemistry Rediscovered to Connect Polymers with Nature’s Building Blocks*. *ACS Macro Letters*, 2013. **2**(1): p. 14-18.
51. Cramer, N.B., et al., *Mechanism and Modeling of a Thiol–Ene Photopolymerization*. *Macromolecules*, 2003. **36**(12): p. 4631-4636.
52. Cramer, N.B. and C.N. Bowman, *Kinetics of thiol–ene and thiol–acrylate photopolymerizations with real-time fourier transform infrared*. *Journal of Polymer Science Part A: Polymer Chemistry*, 2001. **39**(19): p. 3311-3319.
53. Cramer, N.B., et al., *Thiol–Ene Photopolymerization Mechanism and Rate Limiting Step Changes for Various Vinyl Functional Group Chemistries*. *Macromolecules*, 2003. **36**(21): p. 7964-7969.
54. Jasinski, F., et al., *Light-Mediated Thiol–Ene Polymerization in Miniemulsion: A Fast Route to Semicrystalline Polysulfide Nanoparticles*. *ACS Macro Letters*, 2014. **3**(9): p. 958-962.
55. Luo, X., et al., *Graphene Oxide-Polymer Composite Langmuir Films Constructed by Interfacial Thiol-Ene Photopolymerization*. *Nanoscale Research Letters*, 2017. **12**(1): p. 99.
56. Çakmakçı, E., et al., *Flame retardant thiol–ene photocured coatings*. *Reactive and Functional Polymers*, 2011. **71**(1): p. 36-41.
57. Siebert, J.M., et al., *Towards copper-free nanocapsules obtained by orthogonal interfacial “click” polymerization in miniemulsion*. *Chemical Communications*, 2012. **48**(44): p. 5470-5472.
58. Quoc Le, C.M., M. Schmutz, and A. Chemtob, *Ab Initio Batch Emulsion Thiol–Ene Photopolymerization*. *Macromolecules*, 2020. **53**(7): p. 2369-2379.
59. Durham, O.Z., et al., *Radical Mediated Thiol-Ene Emulsion Polymerizations*. *Macromolecules*, 2017. **50**(3): p. 775-783.
60. Wang, C., et al., *Thiol-Michael addition miniemulsion polymerizations: functional nanoparticles and reactive latex films*. *Polymer Chemistry*, 2015. **6**(20): p. 3758-3763.
61. Nair, D.P., et al., *Two-Stage Reactive Polymer Network Forming Systems*. *Advanced Functional Materials*, 2012. **22**(7): p. 1502-1510.
62. Meroni, D. and S. Ardizzone, *Preparation and Application of Hybrid Nanomaterials*. *Nanomaterials*, 2018. **8**(11): p. 891.
63. Yin, P.T., et al., *Design, Synthesis, and Characterization of Graphene–Nanoparticle Hybrid Materials for Bioapplications*. *Chemical Reviews*, 2015. **115**(7): p. 2483-2531.
64. Mortera, R., et al., *Cell-induced intracellular controlled release of membrane impermeable cysteine from a mesoporous silica nanoparticle-based drug delivery system*. *Chemical Communications*, 2009(22): p. 3219-3221.

65. Rieter, W.J., et al., *Nanoscale Metal–Organic Frameworks as Potential Multimodal Contrast Enhancing Agents*. *Journal of the American Chemical Society*, 2006. **128**(28): p. 9024-9025.
66. Winey, K.I. and R.A. Vaia, *Polymer Nanocomposites*. *MRS Bulletin*, 2007. **32**(4): p. 314-322.
67. Pyun, J. and K. Matyjaszewski, *Synthesis of Nanocomposite Organic/Inorganic Hybrid Materials Using Controlled/"Living" Radical Polymerization*. *Chemistry of Materials*, 2001. **13**(10): p. 3436-3448.
68. Mai, Y.-W. and Z.-Z. Yu, *Polymer nanocomposites*. 2006.
69. Wilson, J.L., et al., *Synthesis and magnetic properties of polymer nanocomposites with embedded iron nanoparticles*. *Journal of Applied Physics*, 2004. **95**(3): p. 1439-1443.
70. Huang, X. and W.J. Brittain, *Synthesis and Characterization of PMMA Nanocomposites by Suspension and Emulsion Polymerization*. *Macromolecules*, 2001. **34**(10): p. 3255-3260.
71. Demir, M.M., et al., *PMMA/Zinc Oxide Nanocomposites Prepared by In-Situ Bulk Polymerization*. *Macromolecular Rapid Communications*, 2006. **27**(10): p. 763-770.
72. Fim, F.d.C., et al., *Polyethylene/graphite nanocomposites obtained by in situ polymerization*. *Journal of Polymer Science Part A: Polymer Chemistry*, 2010. **48**(3): p. 692-698.
73. Chugh, H., et al., *Role of gold and silver nanoparticles in cancer nano-medicine*. *Artificial Cells, Nanomedicine, and Biotechnology*, 2018. **46**(sup1): p. 1210-1220.
74. Cai, W., et al., *Applications of gold nanoparticles in cancer nanotechnology*. *Nanotechnology, science and applications*, 2008. **1**: p. 17-32.
75. Libutti, S., et al., *Results of a completed phase I clinical trial of CYT-6091: A pegylated colloidal gold-TNF nanomedicine*. *Journal of Clinical Oncology*, 2009. **27**(15_suppl): p. 3586-3586.
76. Anselmo, A.C. and S. Mitragotri, *Nanoparticles in the clinic: An update*. *Bioengineering & translational medicine*, 2019. **4**(3): p. e10143-e10143.
77. Jain, S., D.G. Hirst, and J.M. O'Sullivan, *Gold nanoparticles as novel agents for cancer therapy*. *The British Journal of Radiology*, 2012. **85**(1010): p. 101-113.
78. Zhang, Z., et al., *Near Infrared Laser-Induced Targeted Cancer Therapy Using Thermoresponsive Polymer Encapsulated Gold Nanorods*. *Journal of the American Chemical Society*, 2014. **136**(20): p. 7317-7326.
79. Abdel-Fattah, W.I. and G.W. Ali, *On the anti-cancer activities of silver nanoparticles*. *J Appl Biotechnol Bioeng*, 2018. **5**(2): p. 1-4.
80. Jeyaraj, M., et al., *Biogenic silver nanoparticles for cancer treatment: an experimental report*. *Colloids Surf B Biointerfaces*, 2013. **106**: p. 86-92.
81. Foldbjerg, R., D.A. Dang, and H. Autrup, *Cytotoxicity and genotoxicity of silver nanoparticles in the human lung cancer cell line, A549*. *Archives of Toxicology*, 2011. **85**(7): p. 743-750.
82. Lee, T.-W., S.-E. Lee, and Y.G. Jeong, *Highly Effective Electromagnetic Interference Shielding Materials based on Silver Nanowire/Cellulose Papers*. *ACS Applied Materials & Interfaces*, 2016. **8**(20): p. 13123-13132.
83. Sadasivuni, K.K., et al., *Silver Nanoparticles and Its Polymer Nanocomposites—Synthesis, Optimization, Biomedical Usage, and Its Various Applications*, in *Polymer Nanocomposites in Biomedical Engineering*, K.K. Sadasivuni, et al., Editors. 2019, Springer International Publishing: Cham. p. 331-373.
84. Verkhovskii, R., et al., *Physical properties and cytotoxicity of silver nanoparticles under different polymeric stabilizers*. *Heliyon*, 2019. **5**(3): p. e01305.
85. Hermanson, G.T., *Bioconjugate techniques*. 2013: Academic press.
86. Chen, W., et al., *Versatile synthesis of functional biodegradable polymers by combining ring-opening polymerization and postpolymerization modification via Michael-type addition reaction*. *Macromolecules*, 2010. **43**(1): p. 201-207.

87. Yhaya, F., et al., *RAFT polymerization of vinyl methacrylate and subsequent conjugation via enzymatic thiol-ene chemistry*. *Journal of Polymer Science Part A: Polymer Chemistry*, 2012. **50**(19): p. 4085-4093.
88. Jones, M.W., et al., *Phosphine-mediated one-pot thiol-ene "click" approach to polymer-protein conjugates*. *Chemical Communications*, 2009(35): p. 5272-5274.
89. Slavin, S., E. Khoshdel, and D.M. Haddleton, *Biological surface modification by 'thiol-ene' addition of polymers synthesised by catalytic chain transfer polymerisation (CCTP)*. *Polymer Chemistry*, 2012. **3**(6): p. 1461-1466.
90. Kow, S.C., et al., *Dicer-Labile PEG Conjugates for siRNA Delivery*. *Biomacromolecules*, 2011. **12**(12): p. 4301-4310.
91. Northrop, B.H., S.H. Frayne, and U. Choudhary, *Thiol-maleimide "click" chemistry: evaluating the influence of solvent, initiator, and thiol on the reaction mechanism, kinetics, and selectivity*. *Polymer Chemistry*, 2015. **6**(18): p. 3415-3430.
92. Hoyle, C.E., A.B. Lowe, and C.N. Bowman, *Thiol-click chemistry: a multifaceted toolbox for small molecule and polymer synthesis*. *Chemical Society Reviews*, 2010. **39**(4): p. 1355-1387.
93. Chan, J.W., et al., *Nucleophile-Initiated Thiol-Michael Reactions: Effect of Organocatalyst, Thiol, and Ene*. *Macromolecules*, 2010. **43**(15): p. 6381-6388.
94. Pounder, R.J., et al., *Metal free thiol-maleimide 'Click' reaction as a mild functionalisation strategy for degradable polymers*. *Chemical Communications*, 2008(41): p. 5158-5160.
95. Martínez-Jothar, L., et al., *Insights into maleimide-thiol conjugation chemistry: Conditions for efficient surface functionalization of nanoparticles for receptor targeting*. *Journal of Controlled Release*, 2018. **282**: p. 101-109.
96. Brena, B., P. González-Pombo, and F. Batista-Viera, *Immobilization of Enzymes: A Literature Survey*, in *Immobilization of Enzymes and Cells: Third Edition*, J.M. Guisan, Editor. 2013, Humana Press: Totowa, NJ. p. 15-31.
97. Cooper, G.M., *The cell: a molecular approach 2nd Edition*. 2000, National Center for Biotechnology Information's Bookshelf.
98. Brena, B.M. and F. Batista-Viera, *Immobilization of Enzymes*, in *Immobilization of Enzymes and Cells*, J.M. Guisan, Editor. 2006, Humana Press: Totowa, NJ. p. 15-30.
99. Tosa, T., et al., *Studies on continuous enzyme reactions. I. Screening of carriers for preparation of water-insoluble aminoacylase*. *Enzymologia*, 1966. **31**(4): p. 214-24.
100. Bickerstaff, G.F., *Immobilization of enzymes and cells*, in *Immobilization of enzymes and cells*. 1997, Springer. p. 1-11.
101. Mohamad, N.R., et al., *An overview of technologies for immobilization of enzymes and surface analysis techniques for immobilized enzymes*. *Biotechnology & Biotechnological Equipment*, 2015. **29**(2): p. 205-220.
102. Goldstein, L., *[29] Kinetic behavior of immobilized enzyme systems*, in *Methods in Enzymology*. 1976, Academic Press. p. 397-443.
103. Selvarajan, E., et al., *Nanoimmobilization of β -Galactosidase for Lactose-Free Product Development*, in *Nanoscience and Biotechnology for Environmental Applications*, K.M. Gothandam, et al., Editors. 2019, Springer International Publishing: Cham. p. 199-223.
104. Tanriseven, A. and Ş. Doğan, *A novel method for the immobilization of β -galactosidase*. *Process Biochemistry*, 2002. **38**(1): p. 27-30.
105. Panesar, P.S., S. Kumari, and R. Panesar, *Potential applications of immobilized β -galactosidase in food processing industries*. *Enzyme research*, 2010. **2010**.
106. Ateş, S. and Ü. Mehmetoğlu, *A new method for immobilization of β -galactosidase and its utilization in a plug flow reactor*. *Process Biochemistry*, 1997. **32**(5): p. 433-436.

107. Kurokawa, Y., K. Suzuki, and Y. Tamai, *Adsorption and enzyme (β -galactosidase and α -chymotrypsin): Immobilization properties of gel fiber prepared by the gel formation of cellulose acetate and titanium iso-propoxide*. *Biotechnology and Bioengineering*, 1998. **59**(5): p. 651-656.
108. Sheu, D.-C., C.-I. Huang, and K.-J. Duan, *Production of isomaltooligosaccharides by α -glucosidase immobilized in chitosan beads and by polyethyleneimine-glutaraldehyde treated mycelia of *Aspergillus carbonarius**. *Biotechnology Techniques*, 1997. **11**(5): p. 287-291.
109. Carpio, C., et al., *Bone-bound enzymes for food industry application*. *Food Chemistry*, 2000. **68**(4): p. 403-409.
110. Jia, H., G. Zhu, and P. Wang, *Catalytic behaviors of enzymes attached to nanoparticles: the effect of particle mobility*. *Biotechnology and Bioengineering*, 2003. **84**(4): p. 406-414.
111. Wu, Z., et al., *Improving the properties of β -galactosidase from *Aspergillus oryzae* via encapsulation in aggregated silica nanoparticles*. *New Journal of Chemistry*, 2013. **37**(11): p. 3793-3797.
112. Verma, M.L., et al., *Immobilization of β -d-galactosidase from *Kluyveromyces lactis* on functionalized silicon dioxide nanoparticles: Characterization and lactose hydrolysis*. *International Journal of Biological Macromolecules*, 2012. **50**(2): p. 432-437.
113. Selvarajan, E., et al., *Immobilization of β -galactosidase from *Lactobacillus plantarum* HF571129 on ZnO nanoparticles: characterization and lactose hydrolysis*. *Bioprocess and Biosystems Engineering*, 2015. **38**(9): p. 1655-1669.
114. Wang, Z.-G., et al., *Enzyme immobilization on electrospun polymer nanofibers: An overview*. *Journal of Molecular Catalysis B: Enzymatic*, 2009. **56**(4): p. 189-195.
115. Pan, C., et al., *Novel and efficient method for immobilization and stabilization of β -d-galactosidase by covalent attachment onto magnetic Fe₃O₄-chitosan nanoparticles*. *Journal of Molecular Catalysis B: Enzymatic*, 2009. **61**(3): p. 208-215.
116. Park, T.G. and A.S. Hoffman, *Immobilization and characterization of β -galactosidase in thermally reversible hydrogel beads*. *Journal of Biomedical Materials Research*, 1990. **24**(1): p. 21-38.
117. Facin, B.R., et al., *Immobilization and controlled release of β -galactosidase from chitosan-grafted hydrogels*. *Food Chemistry*, 2015. **179**: p. 44-51.
118. Grosová, Z., et al., *Entrapment of β -galactosidase in polyvinylalcohol hydrogel*. *Biotechnology Letters*, 2008. **30**(4): p. 763-767.
119. Cargnin, M.A., et al., *Pinus residue/pectin-based composite hydrogels for the immobilization of β -D-galactosidase*. *International Journal of Biological Macromolecules*, 2020. **149**: p. 773-782.
120. Elaissari, A., *Colloidal polymers: synthesis and characterization*. Vol. 115. 2003: CRC press.
121. Christopher, G.F. and S.L. Anna, *Microfluidic methods for generating continuous droplet streams*. *Journal of Physics D: Applied Physics*, 2007. **40**(19): p. R319.
122. Serra, C.A. and Z. Chang, *Microfluidic-Assisted Synthesis of Polymer Particles*. *Chemical Engineering & Technology*, 2008. **31**(8): p. 1099-1115.
123. Wang, J.-T., J. Wang, and J.-J. Han, *Fabrication of Advanced Particles and Particle-Based Materials Assisted by Droplet-Based Microfluidics*. *Small*, 2011. **7**(13): p. 1728-1754.
124. Engl, W., R. Backov, and P. Panizza, *Controlled production of emulsions and particles by milli- and microfluidic techniques*. *Current Opinion in Colloid & Interface Science*, 2008. **13**(4): p. 206-216.
125. Shum, H.C., et al., *Droplet Microfluidics for Fabrication of Non-Spherical Particles*. *Macromolecular Rapid Communications*, 2010. **31**(2): p. 108-118.
126. Yu, W., et al., *Preparation and Deep Characterization of Composite/Hybrid Multi-Scale and Multi-Domain Polymeric Microparticles*. *Materials*, 2019. **12**(23): p. 3921.
127. Xia, B., et al., *Cytocompatible cell encapsulation via hydrogel photopolymerization in microfluidic emulsion droplets*. *Biomicrofluidics*, 2017. **11**(4): p. 044102.

128. Zhang, Z., et al., *Encapsulation of lactase (β -galactosidase) into κ -carrageenan-based hydrogel beads: Impact of environmental conditions on enzyme activity*. Food Chemistry, 2016. **200**: p. 69-75.
129. Pessi, J., et al., *Microfluidics-assisted engineering of polymeric microcapsules with high encapsulation efficiency for protein drug delivery*. International Journal of Pharmaceutics, 2014. **472**(1): p. 82-87.
130. Zhang, H., et al., *Fabrication of a Multifunctional Nano-in-micro Drug Delivery Platform by Microfluidic Templated Encapsulation of Porous Silicon in Polymer Matrix*. Advanced Materials, 2014. **26**(26): p. 4497-4503.
131. Ain, Q.U., et al., *Enhanced mechanical properties and biocompatibility of novel hydroxyapatite/TOPAS hybrid composite for bone tissue engineering applications*. Materials Science and Engineering: C, 2017. **75**: p. 807-815.
132. Peters, M., et al., *PPV-Based Conjugated Polymer Nanoparticles as a Versatile Bioimaging Probe: A Closer Look at the Inherent Optical Properties and Nanoparticle–Cell Interactions*. Biomacromolecules, 2016. **17**(8): p. 2562-2571.
133. Jiang, Y. and K. Pu, *Multimodal Biophotonics of Semiconducting Polymer Nanoparticles*. Accounts of Chemical Research, 2018. **51**(8): p. 1840-1849.
134. Yin, J. and B. Deng, *Polymer-matrix nanocomposite membranes for water treatment*. Journal of Membrane Science, 2015. **479**: p. 256-275.
135. Kim, J. and B. Van der Bruggen, *The use of nanoparticles in polymeric and ceramic membrane structures: Review of manufacturing procedures and performance improvement for water treatment*. Environmental Pollution, 2010. **158**(7): p. 2335-2349.
136. Pradhan, N., et al., *Facets of nanotechnology as seen in food processing, packaging, and preservation industry*. BioMed research international, 2015. **2015**.
137. Singh, T., et al., *Application of nanotechnology in food science: perception and overview*. Frontiers in microbiology, 2017. **8**: p. 1501.
138. Venier-Julienne, M.C. and J.P. Benoît, *Preparation, purification and morphology of polymeric nanoparticles as drug carriers*. Pharmaceutica Acta Helvetiae, 1996. **71**(2): p. 121-128.
139. Song, C., et al., *Formulation and characterization of biodegradable nanoparticles for intravascular local drug delivery*. Journal of Controlled Release, 1997. **43**(2-3): p. 197-212.
140. Jeong, Y.-I., et al., *Preparation of poly(DL-lactide-co-glycolide) nanoparticles without surfactant*. Journal of Applied Polymer Science, 2001. **80**(12): p. 2228-2236.
141. Yordanov, G.G. and C.D. Dushkin, *Preparation of poly (butylcyanoacrylate) drug carriers by nanoprecipitation using a pre-synthesized polymer and different colloidal stabilizers*. Colloid and Polymer Science, 2010. **288**(9): p. 1019-1026.
142. Allémann, E., R. Gurny, and E. Doelker, *Preparation of aqueous polymeric nanodispersions by a reversible salting-out process: influence of process parameters on particle size*. International journal of pharmaceutics, 1992. **87**(1-3): p. 247-253.
143. Cheng, X., et al., *Preparation of SiO₂/PMMA composite particles via conventional emulsion polymerization*. Journal of Polymer Science Part A: Polymer Chemistry, 2006. **44**(12): p. 3807-3816.
144. Bardajee, G.R., et al., *Synthesis, characterization, and energy transfer studies of dye-labeled poly(butyl methacrylate) latex particles prepared by miniemulsion polymerization*. Polymer, 2007. **48**(20): p. 5839-5849.
145. Jang, J., J. Bae, and S. Ko, *Synthesis and curing of poly(glycidyl methacrylate) nanoparticles*. Journal of Polymer Science Part A: Polymer Chemistry, 2005. **43**(11): p. 2258-2265.
146. Pappas, S.P., *Radiation curing: science and technology*. 2013: Springer Science & Business Media.

147. Biskos, G., et al., *Generation and Sizing of Particles for Aerosol-Based Nanotechnology*. KONA Powder and Particle Journal, 2008. **26**: p. 13-35.
148. Akgün, E., *Nanoscale Polymeric Particles Via Aerosol-Photopolymerization*. 2015.
149. Bazzano, M., et al., *Nano-structured polymeric microparticles produced via cationic aerosol photopolymerization*. Journal of Photochemistry and Photobiology A: Chemistry, 2017. **346**: p. 364-371.
150. Bazzano, M., et al., *A molecular dynamics approach to nanostructuring of particles produced via aerosol cationic photopolymerization*. Chemical Engineering Science, 2019. **195**: p. 1021-1027.
151. Hoelscher, F., et al., *In Vitro Degradation and Cytotoxicity Response of Biobased Nanoparticles Prepared by Thiol-ene Polymerization in Miniemulsion*. Journal of Polymers and the Environment, 2021.
152. Yaşar, M., et al., *Polymeric nanoparticles for selective protein recognition by using thiol-ene miniemulsion photopolymerization*. Journal of Biomaterials Science, Polymer Edition, 2020. **31**(16): p. 2044-2059.
153. Lee, T.Y., et al., *Thiol–Ene Photopolymerization Kinetics of Vinyl Acrylate/Multifunctional Thiol Mixtures*. Macromolecules, 2004. **37**(10): p. 3606-3613.
154. Le, C.M.Q., et al., *Droplet nucleation in miniemulsion thiol–ene step photopolymerization*. Polymer Chemistry, 2021. **12**(14): p. 2084-2094.
155. Jasinski, F., et al., *Thiol–Ene Linear Step-Growth Photopolymerization in Miniemulsion: Fast Rates, Redox-Responsive Particles, and Semicrystalline Films*. Macromolecules, 2016. **49**(4): p. 1143-1153.
156. Chiou, B.-S., R.J. English, and S.A. Khan, *Rheology and Photo-Cross-Linking of Thiol–Ene Polymers*. Macromolecules, 1996. **29**(16): p. 5368-5374.
157. Northrop, B.H. and R.N. Coffey, *Thiol–Ene Click Chemistry: Computational and Kinetic Analysis of the Influence of Alkene Functionality*. Journal of the American Chemical Society, 2012. **134**(33): p. 13804-13817.
158. Landfester, K., *The Generation of Nanoparticles in Miniemulsions*. Advanced Materials, 2001. **13**(10): p. 765-768.
159. Landfester, K., *Miniemulsion Polymerization and the Structure of Polymer and Hybrid Nanoparticles*. Angewandte Chemie International Edition, 2009. **48**(25): p. 4488-4507.
160. Li, M., et al., *Preparation of Polyurethane/Acrylic Hybrid Nanoparticles via a Miniemulsion Polymerization Process*. Macromolecules, 2005. **38**(10): p. 4183-4192.
161. Matsumoto, A., et al., *Comparison of Gelation in the Free-Radical Polymerization of Triallyl Isocyanurate and its Isomer Triallyl Cyanurate*. Journal of Macromolecular Science: Part A - Chemistry, 1989. **26**(9): p. 1279-1289.
162. Jansen, J.F.G.A., et al., *Fast Monomers: Factors Affecting the Inherent Reactivity of Acrylate Monomers in Photoinitiated Acrylate Polymerization*. Macromolecules, 2003. **36**(11): p. 3861-3873.
163. Salinas, C.N. and K.S. Anseth, *Mixed Mode Thiol–Acrylate Photopolymerizations for the Synthesis of PEG–Peptide Hydrogels*. Macromolecules, 2008. **41**(16): p. 6019-6026.
164. Giannakitsas, I., *Mixed mode polymerization*. 1999: Illinois Institute of Technology.
165. Kharissova, O.V., et al., *The greener synthesis of nanoparticles*. Trends in Biotechnology, 2013. **31**(4): p. 240-248.
166. Singh, P., et al., *Biological Synthesis of Nanoparticles from Plants and Microorganisms*. Trends in Biotechnology, 2016. **34**(7): p. 588-599.
167. Duan, H., D. Wang, and Y. Li, *Green chemistry for nanoparticle synthesis*. Chemical Society Reviews, 2015. **44**(16): p. 5778-5792.

168. Kango, S., et al., *Surface modification of inorganic nanoparticles for development of organic–inorganic nanocomposites—A review*. Progress in Polymer Science, 2013. **38**(8): p. 1232-1261.
169. Garnweitner, G., et al., *Large-Scale Synthesis of Organophilic Zirconia Nanoparticles and their Application in Organic–Inorganic Nanocomposites for Efficient Volume Holography*. Small, 2007. **3**(9): p. 1626-1632.
170. Anžlovar, A., Z.C. Orel, and M. Žigon, *Poly(methyl methacrylate) composites prepared by in situ polymerization using organophilic nano-to-submicrometer zinc oxide particles*. European Polymer Journal, 2010. **46**(6): p. 1216-1224.
171. Shim, J.-W., et al., *Zinc oxide/polymethylmethacrylate composite microspheres by in situ suspension polymerization and their morphological study*. Colloids and Surfaces A: Physicochemical and Engineering Aspects, 2002. **207**(1): p. 105-111.
172. Camargo, P.H.C., K.G. Satyanarayana, and F. Wypych, *Nanocomposites: synthesis, structure, properties and new application opportunities*. Materials Research, 2009. **12**(1): p. 1-39.
173. Hoyle, C.E., T.Y. Lee, and T. Roper, *Thiol–enes: Chemistry of the past with promise for the future*. Journal of Polymer Science Part A: Polymer Chemistry, 2004. **42**(21): p. 5301-5338.
174. O'Brien, A.K., N.B. Cramer, and C.N. Bowman, *Oxygen inhibition in thiol–acrylate photopolymerizations*. Journal of Polymer Science Part A: Polymer Chemistry, 2006. **44**(6): p. 2007-2014.
175. Roper, T.M., et al., *Photopolymerization of pigmented thiol–ene systems*. Polymer, 2004. **45**(9): p. 2921-2929.
176. Lillie, L.M., W.B. Tolman, and T.M. Reineke, *Degradable and renewably-sourced poly (ester-thioethers) by photo-initiated thiol–ene polymerization*. Polymer Chemistry, 2018. **9**(23): p. 3272-3278.
177. Machado, T.O., C. Sayer, and P.H.H. Araujo, *Thiol-ene polymerisation: A promising technique to obtain novel biomaterials*. European Polymer Journal, 2017. **86**: p. 200-215.
178. Suvarli, N., et al., *Thiol-Functional Polymer Nanoparticles via Aerosol Photopolymerization*. Polymers, 2021. **13**(24): p. 4363.
179. Weber, P.C., et al., *Structural origins of high-affinity biotin binding to streptavidin*. Science, 1989. **243**(4887): p. 85.
180. Banerjee, H.N. and M. Verma, *Application of Nanotechnology in Cancer*. Technology in Cancer Research & Treatment, 2008. **7**(2): p. 149-154.
181. Jiang, Y., et al., *Influencing Selectivity to Cancer Cells with Mixed Nanoparticles Prepared from Albumin–Polymer Conjugates and Block Copolymers*. Bioconjugate Chemistry, 2017. **28**(4): p. 979-985.
182. Vekariya, K.K., J. Kaur, and K. Tikoo, *ER α signaling imparts chemotherapeutic selectivity to selenium nanoparticles in breast cancer*. Nanomedicine: Nanotechnology, Biology and Medicine, 2012. **8**(7): p. 1125-1132.
183. Ahmad, M.Z., et al., *Nanometric gold in cancer nanotechnology: current status and future prospect*. Journal of Pharmacy and Pharmacology, 2012. **65**(5): p. 634-651.
184. Heath, J.R. and M.E. Davis, *Nanotechnology and cancer*. Annual review of medicine, 2008. **59**: p. 251-265.
185. Ong, C., et al., *Silver nanoparticles in cancer: therapeutic efficacy and toxicity*. Curr Med Chem, 2013. **20**(6): p. 772-81.
186. van der Meel, R., et al., *Smart cancer nanomedicine*. Nature Nanotechnology, 2019. **14**(11): p. 1007-1017.
187. Mansoori, G.A., K.S. Brandenburg, and A. Shakeri-Zadeh, *A Comparative Study of Two Folate-Conjugated Gold Nanoparticles for Cancer Nanotechnology Applications*. Cancers, 2010. **2**(4): p. 1911-1928.

188. Stranik, O., et al., *Bioanalytics using single plasmonic nanostructures*. SPIE BiOS. Vol. 8595. 2013: SPIE.
189. Singh, P., et al., *Gold Nanoparticles in Diagnostics and Therapeutics for Human Cancer*. Int J Mol Sci, 2018. **19**(7).
190. Lee, K.-S. and M.A. El-Sayed, *Gold and Silver Nanoparticles in Sensing and Imaging: Sensitivity of Plasmon Response to Size, Shape, and Metal Composition*. The Journal of Physical Chemistry B, 2006. **110**(39): p. 19220-19225.
191. De Matteis, V., et al., *Silver Nanoparticles: Synthetic Routes, In Vitro Toxicity and Theranostic Applications for Cancer Disease*. Nanomaterials, 2018. **8**(5): p. 319.
192. Homan, K., et al., *Silver nanosystems for photoacoustic imaging and image-guided therapy*. Journal of Biomedical Optics, 2010. **15**(2): p. 021316.
193. Jun, B.H., et al., *Multifunctional silver-embedded magnetic nanoparticles as SERS nanoprobe and their applications*. Small, 2010. **6**(1): p. 119-25.
194. Dathe, A., et al. *Plasmonic nanoparticles sensors utilizing hybrid modes, electrical excitation, and anisotropic particles*. in *Biosensing and Nanomedicine VIII*. 2015. International Society for Optics and Photonics.
195. Winther, J.R. and C. Thorpe, *Quantification of thiols and disulfides*. Biochimica et biophysica acta, 2014. **1840**(2): p. 838-846.
196. Kvítek, L., et al., *Effect of Surfactants and Polymers on Stability and Antibacterial Activity of Silver Nanoparticles (NPs)*. The Journal of Physical Chemistry C, 2008. **112**(15): p. 5825-5834.
197. Badawy, A.M.E., et al., *Impact of Environmental Conditions (pH, Ionic Strength, and Electrolyte Type) on the Surface Charge and Aggregation of Silver Nanoparticles Suspensions*. Environmental Science & Technology, 2010. **44**(4): p. 1260-1266.
198. El Badawy, A.M., et al., *The impact of stabilization mechanism on the aggregation kinetics of silver nanoparticles*. Science of The Total Environment, 2012. **429**: p. 325-331.
199. Cotton, G., et al., *Efficacy and safety of alpha lipoic acid-capped silver nanoparticles for oral applications*. RSC advances, 2019. **9**(12): p. 6973-6985.
200. Pfirman, A., *The fabrication and study of Silver nanoparticle structures*. 2013.
201. Guzmán-Soto, I., et al., *Lipoic acid capped silver nanoparticles: a facile route to covalent protein capping and oxidative stability within biological systems*. RSC Advances, 2020. **10**(54): p. 32953-32958.
202. Quaroni, L. and G. Chumanov, *Preparation of Polymer-Coated Functionalized Silver Nanoparticles*. Journal of the American Chemical Society, 1999. **121**(45): p. 10642-10643.
203. Cheng, X., et al., *Size-controlled silver nanoparticles stabilized on thiol-functionalized MIL-53(Al) frameworks*. Nanoscale, 2015. **7**(21): p. 9738-9745.
204. Schmid, A., et al., *Industrial biocatalysis today and tomorrow*. Nature, 2001. **409**(6817): p. 258-268.
205. Vellard, M., *The enzyme as drug: application of enzymes as pharmaceuticals*. Current Opinion in Biotechnology, 2003. **14**(4): p. 444-450.
206. Kuraishi, C., K. Yamazaki, and Y. Susa, *Transglutaminase: its utilization in the food industry*. Food reviews international, 2001. **17**(2): p. 221-246.
207. Lei, X. and C. Stahl, *Biotechnological development of effective phytases for mineral nutrition and environmental protection*. Applied Microbiology and Biotechnology, 2001. **57**(4): p. 474-481.
208. Bisgaard-Frantzen, H., et al., *Development of industrially important α -amylases*. Journal of Applied Glycoscience, 1999. **46**(2): p. 199-206.
209. Doshi, R. and V. Shelke, *Enzymes in textile industry-An environment-friendly approach*. 2001.
210. Hemalatha, T., et al., *Enzymes in clinical medicine: an overview*. 2013.

211. Chapman, J., A.E. Ismail, and C.Z. Dinu, *Industrial Applications of Enzymes: Recent Advances, Techniques, and Outlooks*. Catalysts, 2018. **8**(6): p. 238.
212. Shukla, T.P. and L.E. Wierzbicki, *Beta-galactosidase technology: A solution to the lactose problem*. C R C Critical Reviews in Food Technology, 1975. **5**(3): p. 325-356.
213. Nguyen, V.D., et al., *Immobilization of β -galactosidase on chitosan-coated magnetic nanoparticles and its application for synthesis of lactulose-based galactooligosaccharides*. Process Biochemistry, 2019. **84**: p. 30-38.
214. Datta, S., L.R. Christena, and Y.R.S. Rajaram, *Enzyme immobilization: an overview on techniques and support materials*. 3 Biotech, 2013. **3**(1): p. 1-9.
215. Roy, I. and M.N. Gupta, *Bioaffinity Immobilization*, in *Immobilization of Enzymes and Cells*, J.M. Guisan, Editor. 2006, Humana Press: Totowa, NJ. p. 107-116.
216. Park, S., et al., *Wood mimetic hydrogel beads for enzyme immobilization*. Carbohydrate Polymers, 2015. **115**: p. 223-229.
217. Betigeri, S.S. and S.H. Neau, *Immobilization of lipase using hydrophilic polymers in the form of hydrogel beads*. Biomaterials, 2002. **23**(17): p. 3627-3636.
218. Lee, Y., et al., *Preparation of interpenetrating polymer network composed of poly (ethylene glycol) and poly (acrylamide) hydrogels as a support of enzyme immobilization*. Polymers for Advanced Technologies, 2008. **19**(7): p. 852-858.
219. Johnson, A.K., et al., *Novel method for immobilization of enzymes to magnetic nanoparticles*. Journal of Nanoparticle Research, 2008. **10**(6): p. 1009-1025.
220. Ureta, M.M., et al., *Recent advances in β -galactosidase and fructosyltransferase immobilization technology*. Critical Reviews in Food Science and Nutrition, 2021. **61**(16): p. 2659-2690.
221. Souza, C.J.F., et al., *Immobilization of β -galactosidase by complexation: Effect of interaction on the properties of the enzyme*. International Journal of Biological Macromolecules, 2019. **122**: p. 594-602.
222. Kim, J., J.W. Grate, and P. Wang, *Nanostructures for enzyme stabilization*. Chemical Engineering Science, 2006. **61**(3): p. 1017-1026.
223. Kouassi, G.K., J. Irudayaraj, and G. McCarty, *Examination of Cholesterol oxidase attachment to magnetic nanoparticles*. Journal of Nanobiotechnology, 2005. **3**(1): p. 1.
224. Villalonga, R., et al., *Supramolecular assembly of β -cyclodextrin-modified gold nanoparticles and Cu, Zn-superoxide dismutase on catalase*. Journal of Molecular Catalysis B: Enzymatic, 2005. **35**(4): p. 79-85.
225. Bang, S.H., et al., *Evaluation of whole lysosomal enzymes directly immobilized on titanium (IV) oxide used in the development of antimicrobial agents*. Enzyme and Microbial Technology, 2011. **49**(3): p. 260-265.
226. Klein, M.P., et al., *Effect of the Support Size on the Properties of β -Galactosidase Immobilized on Chitosan: Advantages and Disadvantages of Macro and Nanoparticles*. Biomacromolecules, 2012. **13**(8): p. 2456-2464.
227. Valério, A., et al., *Kinetic Study of Candida antarctica Lipase B Immobilization Using Poly(Methyl Methacrylate) Nanoparticles Obtained by Miniemulsion Polymerization as Support*. Applied Biochemistry and Biotechnology, 2015. **175**(6): p. 2961-2971.
228. Suvarli, N., et al., *Synthesis of Spherical Nanoparticle Hybrids via Aerosol Thiol-Ene Photopolymerization and Their Bioconjugation*. Nanomaterials, 2022. **12**(3): p. 577.
229. West, J.L. and J.A. Hubbell, *Photopolymerized hydrogel materials for drug delivery applications*. Reactive Polymers, 1995. **25**(2): p. 139-147.
230. Serra, C., et al., *A Predictive Approach of the Influence of the Operating Parameters on the Size of Polymer Particles Synthesized in a Simplified Microfluidic System*. Langmuir, 2007. **23**(14): p. 7745-7750.

231. Dang, T.-D., et al., *Preparation of monodisperse PEG hydrogel microparticles using a microfluidic flow-focusing device*. *Journal of Industrial and Engineering Chemistry*, 2012. **18**(4): p. 1308-1313.
232. Riddles, P.W., R.L. Blakeley, and B. Zerner, *Ellman's reagent: 5,5'-dithiobis(2-nitrobenzoic acid)—a reexamination*. *Analytical Biochemistry*, 1979. **94**(1): p. 75-81.
233. Walt, D.R. and V.I. Agayn, *The chemistry of enzyme and protein immobilization with glutaraldehyde*. *TrAC Trends in Analytical Chemistry*, 1994. **13**(10): p. 425-430.
234. N. Suvarli, M.F., I. Perner-Nochta, J. Hubbuch, M. Wörner, *Synthesis of spherical nanoparticle hybrids via aerosol thiol-ene photopolymerization and their bioconjugation*, in *Nanoscale*. 2021.
235. Wenger, L., et al., *3D-Printable and Enzymatically Active Composite Materials Based on Hydrogel-Filled High Internal Phase Emulsions*. *Frontiers in Bioengineering and Biotechnology*, 2020. **8**(713).
236. Dumitru, I.F. and M.T. Nechifor, *Decrease in yeast glucose-6-phosphate dehydrogenase activity due to oxygen free radicals*. *International Journal of Biochemistry*, 1994. **26**(2): p. 229-233.
237. Wang, W., *Instability, stabilization, and formulation of liquid protein pharmaceuticals*. *International Journal of Pharmaceutics*, 1999. **185**(2): p. 129-188.
238. Mateo, C., et al., *Improvement of enzyme activity, stability and selectivity via immobilization techniques*. *Enzyme and Microbial Technology*, 2007. **40**(6): p. 1451-1463.
239. Fumio, U., et al., *Swelling and mechanical properties of poly(vinyl alcohol) hydrogels*. *International Journal of Pharmaceutics*, 1990. **58**(2): p. 135-142.
240. Hatley, R.H.M. and F. Franks, *The cold-induced denaturation of lactate dehydrogenase at sub-zero temperatures in the absence of perturbants*. *FEBS Letters*, 1989. **257**(1): p. 171-173.
241. Pikal-Cleland, K.A., et al., *Protein Denaturation during Freezing and Thawing in Phosphate Buffer Systems: Monomeric and Tetrameric β -Galactosidase*. *Archives of Biochemistry and Biophysics*, 2000. **384**(2): p. 398-406.
242. Ustok, F.I., C. Tari, and S. Harsa, *Biochemical and thermal properties of β -galactosidase enzymes produced by artisanal yoghurt cultures*. *Food Chemistry*, 2010. **119**(3): p. 1114-1120.
243. Morelle, X.P., et al., *Highly Stretchable and Tough Hydrogels below Water Freezing Temperature*. *Advanced Materials*, 2018. **30**(35): p. 1801541.
244. Jang, E., et al., *Fabrication of poly(ethylene glycol)-based hydrogels entrapping enzyme-immobilized silica nanoparticles*. *Polymers for Advanced Technologies*, 2010. **21**(7): p. 476-482.
245. Maier, M., et al., *On-Demand Production of Flow-Reactor Cartridges by 3D Printing of Thermostable Enzymes*. *Angewandte Chemie International Edition*, 2018. **57**(19): p. 5539-5543.
246. Carrara, C.R. and A.C. Rubiolo, *Determination of kinetics parameters for free and immobilized β -galactosidase*. *Process Biochemistry*, 1996. **31**(3): p. 243-248.
247. Lartillot, S., *Immobilization of lactase on silica gel: Study of lactose hydrolysis using the immobilized material*. *Biochemical Education*, 1993. **21**(3): p. 157-159.
248. Haider, T. and Q. Husain, *Preparation of lactose-free milk by using salt-fractionated almond (*Amygdalus communis*) β -galactosidase*. *Journal of the Science of Food and Agriculture*, 2007. **87**(7): p. 1278-1283.
249. Radtke, C.P., N. Hillebrandt, and J. Hubbuch, *The Biomaker: an entry-level bioprinting device for biotechnological applications*. *Journal of Chemical Technology & Biotechnology*, 2018. **93**(3): p. 792-799.
250. Peng, M., et al., *3D-Printed Phenacrylate Decarboxylase Flow Reactors for the Chemoenzymatic Synthesis of 4-Hydroxystilbene*. *Chemistry (Weinheim an der Bergstrasse, Germany)*, 2019. **25**(70): p. 15998-16001.

Abbreviations

SEM	Scanning Electron Microscopy
TEM	Transmission Electron Microscopy
NMR	Nuclear Magnetic Resonance
FTIR	Fourier-transform Infrared
mM	millimoles
UV	Ultraviolet
LED	Light-emitting Diode
PEG-DA	Poly(ethylene glycol) Diacrylate
CAD	Computer-aided Design
MRI	Magnetic Resonance Imaging
CT	Computed X-ray Tomography
IUPAC	International Union of Pure and Applied Chemistry
RES	Reticulo-endothelial system
XeCl	xenon chloride
MMA	methyl methacrylate
PMNC	polymer matrix nanocomposites
ZnO	zinc oxide
TiO ₂	titanium oxide
ONPG	ortho-nitrophenyl- β -galactoside
Fe ₃ O ₄	iron oxide (II, III)
APP	aerosol photopolymerization
DAA	diallyl adipate
TEG-DVE	tri(ethylene glycol) divinyl ether
TMPTA	trimethylolpropane triacrylate
NPG	neopentyl glycol diacrylate
TATT	1,3,5-triallyl-1,3,5-triazin-2,4,6-(1H,3H,5H)-trion
Trithiol	trimethylolpropane tris (3-mercaptopropionate)
TMPIC	tris(2-(3-mercaptopropionyloxy)ethyl) isocyanurate
Dithiol	ethylenbis(3-mercaptopropionat)
Tetrathiol	pentaerythrit-tetrakis-(3-mercaptopropionat)
MMP(MT-2MP)	2-methyl-4'-(methylthio)-2 morpholinopropiophenone
DTNB	5,5'-dithiobis(2-nitrobenzoic acid)
FEP	fluorinated ethylene propylene
PVDF	polyvinylidene fluoride
AcO	acetone
MeCN	acetonitrile
ATR-FTIR	Attenuated Total Reflectance Fourier-transform infrared

LSPR	Localized Surface Plasmon Resonance
AgINK	Silver nanoparticles in ink
Ag25nm	dried silver nanospheres 25 nm in diameter
Ag50nm	dried silver nanospheres 50 nm in diameter
α -LA	$\pm\alpha$ -Lipoic acid
MUL	11-Mercapto-1-undecanol
Au@Mal	gold-maleimide conjugate
Au@Strep	gold-streptavidin conjugate
425-St	Atto 425-Streptavidin
b-M	biotin-maleimide
i-FM	iFluor-maleimide
AgNPs	Silver nanoparticles
EtOH	Ethanol
PBS	phosphate buffered saline
PVP	poly(vinyl pyrrolidone)
HMPs	hydrogel microparticles
ENPs	enzyme-conjugated polymer nanoparticles
AcAm	acrylamide
PEG	Poly(ethylene glycol)
E	free unbound enzyme – streptavidin- β -galactosidase
β -gal	β -Galactosidase from <i>Aspergillus oryzae</i>
ONP	2-nitrophenol
BisAc	N, N'-methylene bis(acrylamide)
LAP	lithium-phenyl-2,4,6-trimethylbenzoylphosphinate
H _p ENPs	enzyme-conjugated polymer nanoparticles encapsulated in PEG-based hydrogel microparticles
H _A ENPs	enzyme-conjugated polymer nanoparticles encapsulated in AcAm-based hydrogel microparticles
H _p E	unbound enzyme encapsulated in PEG-based hydrogel microparticles
H _A E	unbound enzyme encapsulated in AcAm-based hydrogel microparticles
PCB	printed circuit board
TPO	diphenyl(2,4,6-trimethylbenzoyl) phosphine oxide
UVF	Ultraviolet fluorescence

Appendix A. Supplementary data for Chapter 3

I. Nuclear Magnetic Resonance

Experimental. Solid state ^{13}C magic angle spinning (MAS) NMR was carried out with solid polymer nanoparticles in Bruker double channel 4 mm probe with a spinning frequency of 12 kHz using Bruker Avance 400 NMR spectrometer ($B_0 = 9.4$ T (Larmor frequency $\nu_0(^{13}\text{C}) = 100.63$ MHz and $\nu_0(^1\text{H}) = 400.17$ MHz). ^{13}C Single Pulse MAS NMR experiments were performed with a $\pi/4$ pulse duration of 2.9 microseconds and a 60 seconds recycling delay; these recording conditions ensure the quantitative determination of the proportions of the different carbon species. Typically, 1800 scans were recorded. ^{13}C CPMAS NMR experiments were acquired using a ramp for Hartmann-Hahn matching with a 5 seconds recycling delay and a contact time of 2 milliseconds. The radiofrequency field strength used for ^1H decoupling was set to 69 kHz. Chemical shifts reported relative to tetramethylsilane (TMS).

Results. The solid state ^{13}C NMR spectra of TMPTA homopolymer and Trithiol-TMPTA heteropolymer and Trithiol-TATT heteropolymer nanoparticles (**Figure S1**) show that thorough cross-linking of TMPTA took place in the Trithiol-TMPTA heteropolymer. TMPTA homopolymer still shows a peak of carbons of unreacted double bonds at 129.51 ppm. The peak of carbons located near the free -SH groups was not identified due to the broad peak and overlap at 20-42 ppm range. The polymer from Trithiol and TATT produces polymer with unreacted double bonds at δ 149.92 ppm. The following data corresponds to the ^{13}C NMR spectra in **Figure S1**.

Product of aerosol photopolymerization of TMPTA: Solid state ^{13}C NMR (400 MHz), δ 7.65, 18.87, 24.36, 41.64, 66.37, 129.51, 165.87, 174.42.

Product of aerosol photopolymerization of Trithiol and TMPTA: Solid state ^{13}C NMR (400 MHz), δ 8.24, 20.52, 27.15, 34.48, 41.58, 64.56, 171.81.

Product of aerosol photopolymerization of Trithiol and TATT: Solid state ^{13}C NMR (400 MHz), δ 8.28, 28.92, 35.60, 42.67, 65.63, 149.92, 172.01.

II. Fourier Transform Infrared Spectroscopy

Presence of -SH groups in Trithiol, M1, P1 and P5 were measured using a Fourier transform infrared spectrometry utilizing attenuated total reflectance (FTIR-ATR, Equinox 55, Bruker Optics), and the spectra are presented in **Figure S2**. The spectra of M1 and P1 are combined with offset to show the presence of -SH groups on P1 and absence in M1. The spectrum of Trithiol is combined with the spectrum of P5 to show absence of -SH groups in P5. In general, detection of -SH groups is not completely reliable in this case, due to very weak absorption of -SH stretching mode even in the sample of Trithiol.

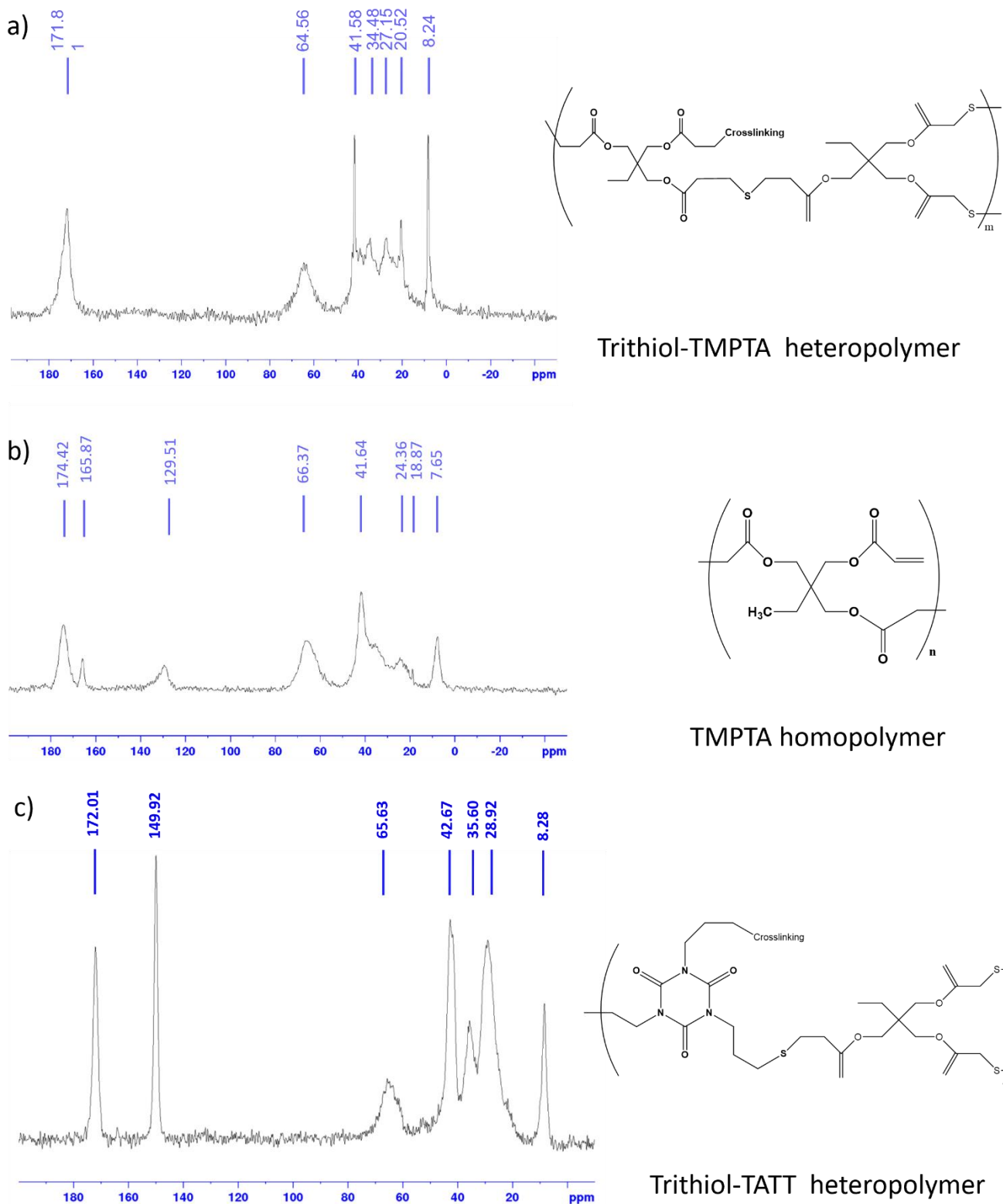


Figure S1. Solid State ^{13}C NMR spectra of a) Trithiol-TMPTA heteropolymer, b) TMPTA homopolymer, c) Trithiol-TATT heteropolymer nanoparticles. Possible structures of the polymers are presented on the right side of the corresponding spectrum.

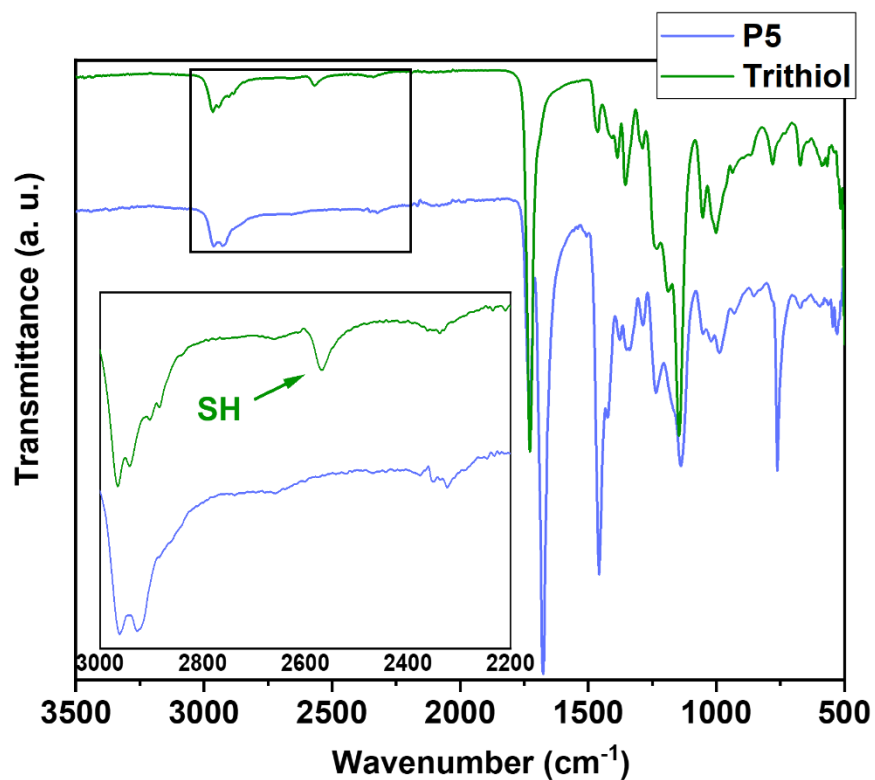
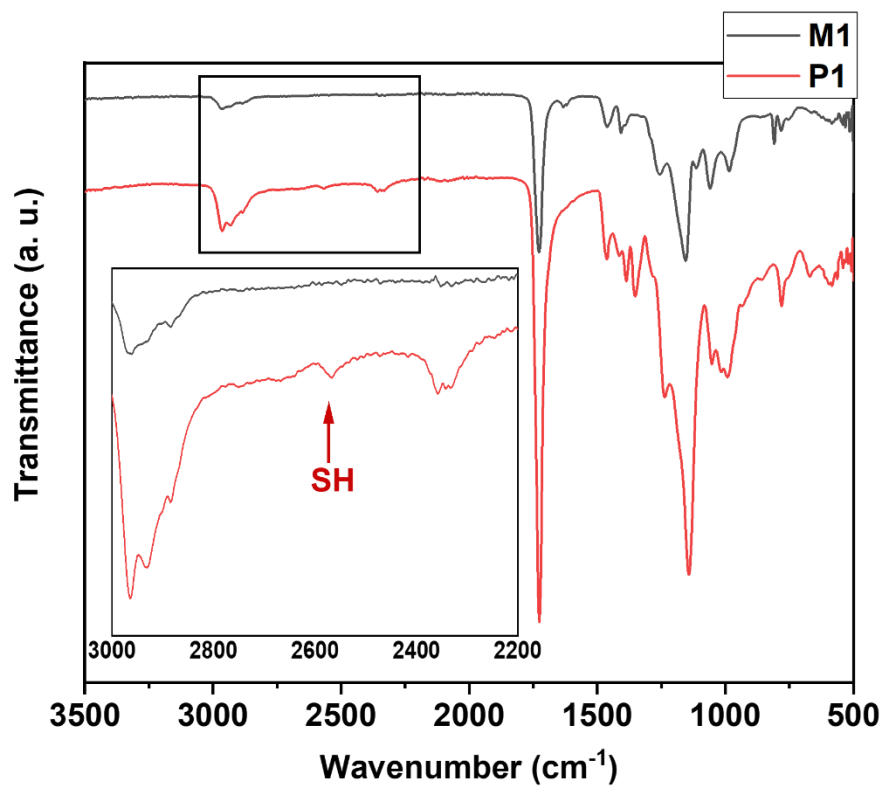


Figure S2. FTIR spectra of the TMPTA homopolymer (M1), Trithiol-TMPTA heteropolymer (P1), Trithiol-TATT heteropolymer (P5) nanoparticles and Trithiol monomer. The spectra are offset to show the presence of -SH groups in Trithiol and P1 nanoparticles and their absence in M1 and P5.

III. Aerosol photopolymerization of acrylates and thiol-ene monomers.

The formulations of other spray solutions of thiol-ene monomer combinations are presented in **Table SI**. The parameters are chosen to be comparable with experiments described in the main part: solvent ratio is 1:1 to the ratio of combined monomers, the quantity of the photoinitiator corresponding to 1wt% of combined monomers. TMPTA and NPG are the only alkene monomers among the tested alkenes that produce polymer nanoparticles via aerosol photopolymerization (M1, M2). The homopolymer nanoparticles of TMPTA and NPG are presented in **Figure S3**.

Table SI. Formulations of spray solutions used in aerosol photopolymerization, presenting monomers, their quantities and the employed solvent.

Spray solution	Thiol	Thiol (mM)	Alkene	Alkene (mM)	Solvent
M1	-	-	TMPTA	33.7	EtOH
M2	-	-	NPG	47.1	EtOH
P16	TMPIC	12.1	TMPTA	12.1	MeCN
P17	TMPIC	12.1	TEG-DVE	18.1	MeCN
P18	TMPIC	11.6	DAA	17.3	MeCN
P19	TMPIC	11.8	NPG	17.8	MeCN
P20	Trithiol	15.7	TMPTA	12.6	EtOH
P21	Trithiol	13.0	TMPTA	16.3	EtOH
P22	Dithiol	24.7	TATT	16.5	EtOH

Several thiol-ene monomers produced individual polymer nanoparticles in aerosol photopolymerization reaction, whereas some others produced aggregated materials (**Figure S4**). During this research it was supposed that AcO affected the properties of the nanoparticles, i.e., may cause increased agglomeration. In the main text of this paper, we described that some thiol-ene combinations were dissolved in AcO to ensure homogeneous spray formulations. To test, whether the change of solvent (from AcO to MeCN) affects the degree of agglomeration of polymer nanoparticles, combinations of TMPIC with alkene monomers were also combined with MeCN in spray solution formulations. The SEM images of produced nanoparticles (P16-P19) revealed no significant difference to SEM images of P5-P9. This evinces that AcO did not cause the agglomeration of nanoparticles in combinations P8 and P9. The nanoparticles from the combination of TMPIC and TMPTA are individual in every used solvent (P6 and P16).

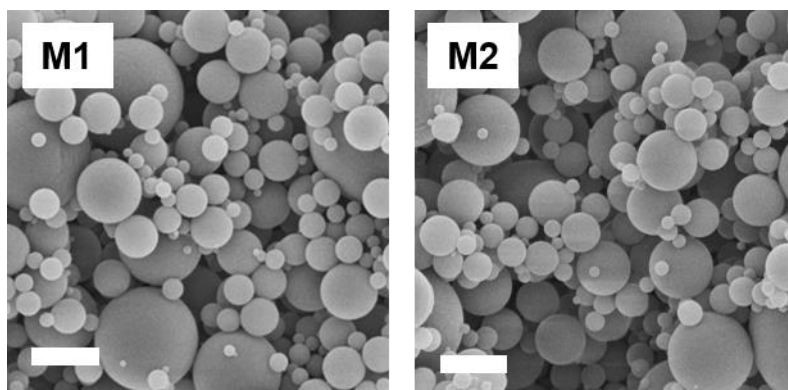


Figure S3. SEM images of homopolymer nanoparticles produced via APP of TMPTA (left) and NPG (right).

Aerosol photopolymerization of thiol-ene monomers with unequal stoichiometric ratios of functional groups was carried out as well (P20 and P21). Ratios of TMPTA and Trithiol were shifted in favor of Trithiol (P20) and TMPTA (P21). Polymer nanoparticles in P20 start to form agglomerates when the ratio of functional groups changes from 1:1 to 5:4 (with 25% increase in favor of Trithiol in sample P20). When the ratio of thiol is increased to 50%, a premature polymerization reaction takes place inside the aerosol generator and no polymer nanoparticles could be collected on the filter membranes. An increase in thiol amount in the aerosol photopolymerization reaction with TMPTA leads to agglomeration; the reason for this behavior can be the presence of more unreacted thiol groups in the polymer nanoparticles after the APP process triggering post polymerization reactions.

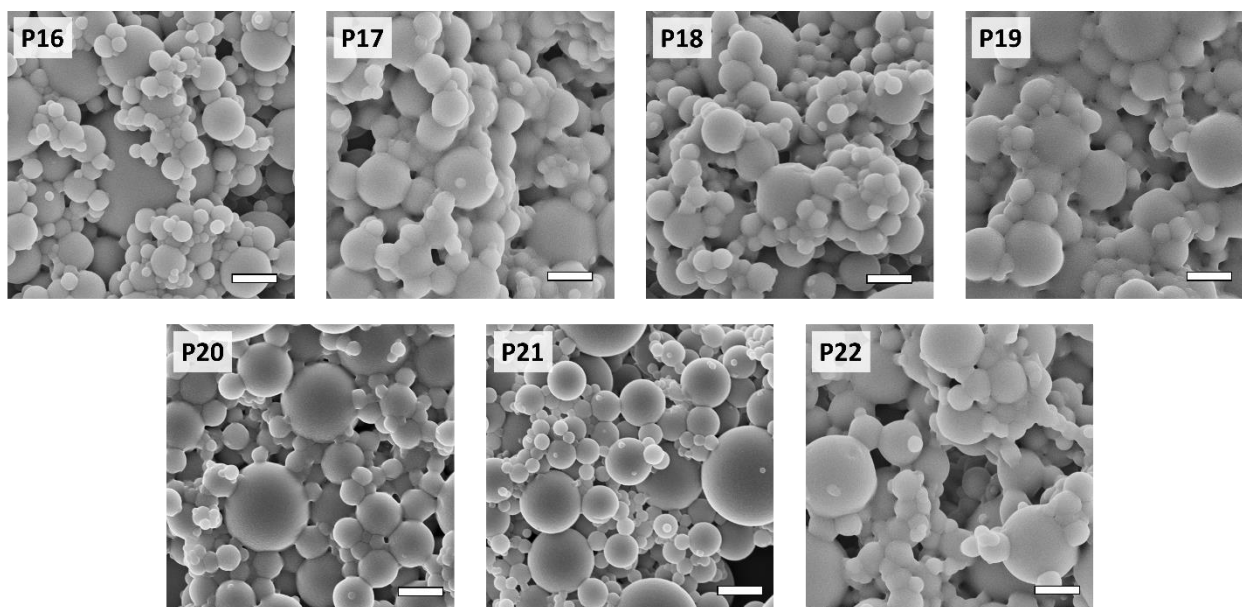


Figure S4. SEM images of polymer nanoparticles produced via aerosol thiol-ene photopolymerization. The nomenclature on the top left of each micrograph corresponds to spray solution formulations in Table I. Scalebar - 1 μ m.

When the balance of ratio of monomers is shifted towards TMPTA in the APP, polymer nanoparticles appear individual (P21).

Dithiol did not form polymer nanoparticles with TEG-DVE and DAA, however a premature polymerization reaction takes place in combinations of Dithiol with TMPTA and NPG starting inside the aerosol generator. Polymer nanoparticles cannot be produced from combination of Dithiol and DAA and TEG-DVE via APP, although an oily material is collected. In fact, the thiol-ene photopolymerization reaction may occur within a few seconds [54, 155]. Nevertheless, the reactivity of alkenes in the thiol-ene photopolymerization depends on the chemical structure of the alkene and has to be considered [157].

The combination of Dithiol and TATT (P22) produced a small amount of collected product before the premature polymerization occurred in the aerosol generator after 45 minutes of atomization. Dithiol and TATT combination resulted in formation of polymer nanoparticles which show significant agglomeration (P22). We expect that cross-linking takes place between the nanoparticles on the filter membrane after the aerosol photopolymerization reaction is finished or during sample preparation for SEM analysis.

Appendix B. Supplementary data for Chapter 4

1. TEM image of the polymer nanoparticle composites.

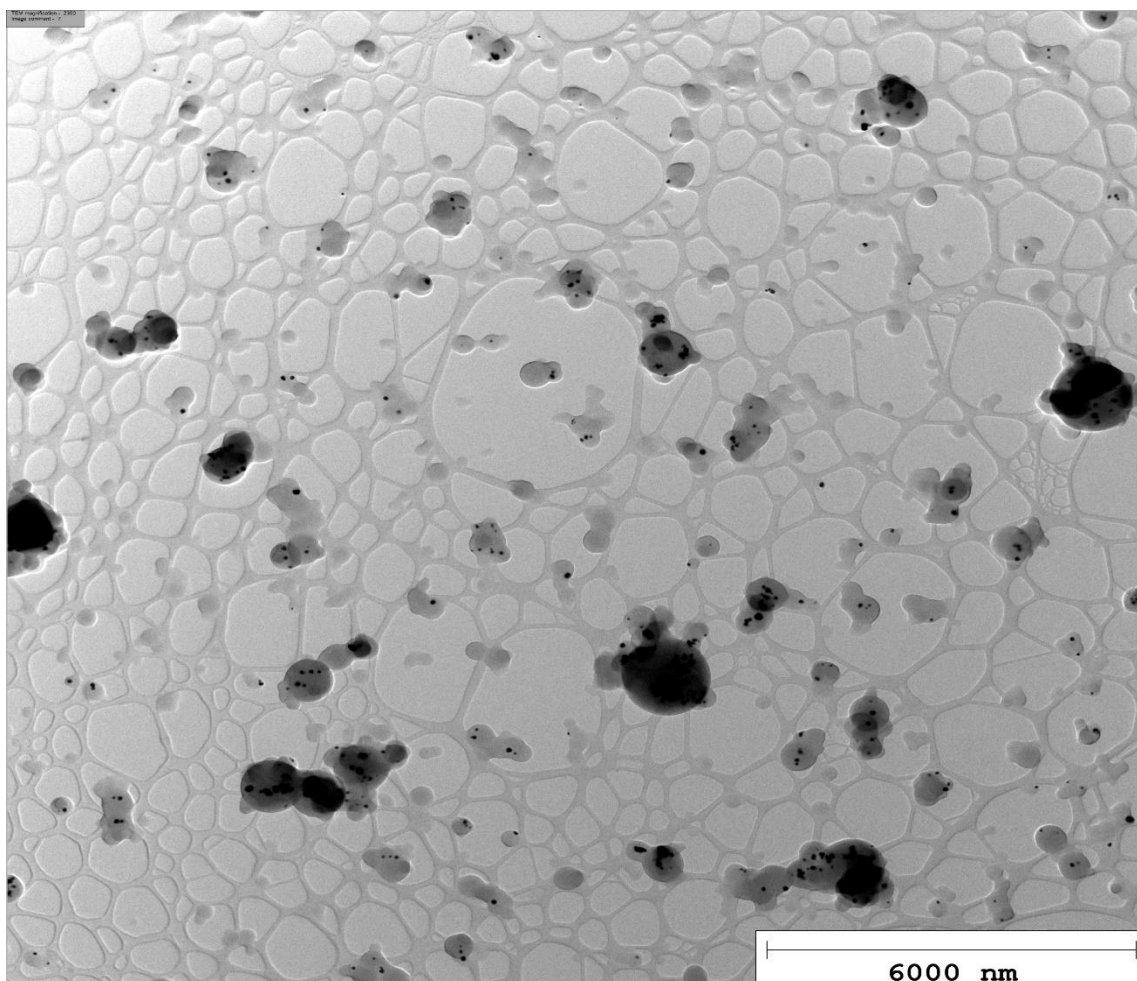


Figure S4.7. TEM image of NC-8 polymer nanoparticle hybrids on a lower magnification.

2. Size Distributions.

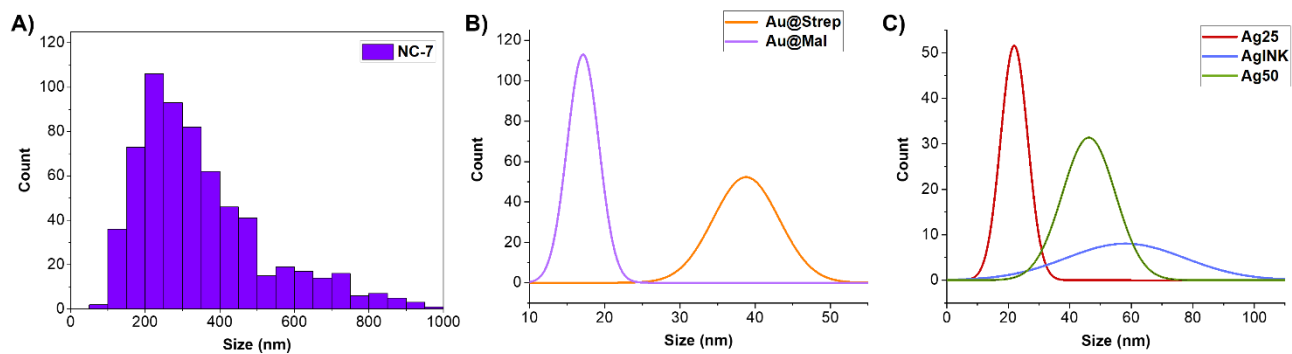


Figure S4.8. Size distributions of **A)** polymer nanoparticle composites NC-7, **B)** Au@Strep and Au@Mal nanoparticles and **C)** Ag25, AgINK and Ag50 nanoparticles, as determined using image analysis of SEM and TEM micrographs.